DISTRIBUTED COOPERATIVE COMMUNICATION IN LARGE-SCALE WIRELESS NETWORKS

A Dissertation

Presented to the Faculty of the Graduate School

of Cornell University

in Partial Fulfillment of the Requirements for the Degree of

Doctor of Philosophy

by

Birsen Sirkeci

August 2006

DISTRIBUTED COOPERATIVE COMMUNICATION IN LARGE-SCALE WIRELESS NETWORKS

Birsen Sirkeci, Ph.D.

Cornell University 2006

Cooperative communication employs distributed transmission resources at the physical layer as a single radio with spatial diversity in order to increase the performance of wireless networks. However, node cooperation entails large communication overhead, and distributed protocols that eliminate or reduce the communication overhead are desirable. This dissertation proposes distributed cooperative schemes for wireless ad hoc networks and develops new methods to analyze their performance.

First, we study the behavior of distributed cooperative transmission in wireless networks for both point-to-point and broadcasting scenarios. In particular, we analyze the effect of critical network parameters on the number of nodes reached by cooperative transmission. We show that there exists a phase transition in the network behavior: if the decoding threshold is below a critical value, the message is delivered to the intended recipient(s). Otherwise, only a fraction of the nodes is reached. Our approach is based on the idea of continuum approximation, which yields closed-form expressions that are accurate when the network density is high.

We next study the optimal power allocation problem for the cooperative broadcast in dense large-scale networks. The transmission order (schedule) and the transmission powers of the relays are designed so that the message reaches the

entire network with the minimum possible total power consumption. In general, finding the best scheduling in cooperative broadcast is known to be an NP-complete problem. We show that the optimal scheduling problem can be solved for dense networks, which can be expressed as a continuum of nodes.

Finally, we study the design of distributed space-time codes for cooperative communication. With few exceptions, most of the literature on the subject proposes coding rules such that either inter-node communication or a central control unit is required for code assignment. We introduce novel randomized strategies that decentralize the transmission of a space time code from a set of distributed relays. Our simple idea is to let each node transmit an independent random linear combination of the codewords that would have been transmitted by all the elements of a multi-antenna system. We show that the proposed scheme achieves the optimal diversity order.

Biographical Sketch

Birsen Sirkeci was born in 1976 in Konya, Turkey. She received her B.Sc. degrees in Electrical and Electronics Engineering and Mathematics in 1998 from Middle East Technical University (METU), Ankara, Turkey. She received her M.Sc. degree in Electrical and Computer Engineering from Northeastern University, Boston, MA, in 2001. She worked as a DSP engineer at Aware Inc, Bedford, MA during 2000-2002. She decided to go back to academic life and she joined Cornell University, Ithaca, NY to pursue PhD in Electrical and Computer Engineering. After four years, she graduated in August 2006.

Her research interests lie mainly in the field of digital signal processing and communications. In particular, she is interested in cooperative transmission in wireless ad-hoc networks and distributed protocols. She received the Fred Ellersick Award for the best unclassified paper in MILCOM 2005 with her co-authors.

To my parents.

Acknowledgements

I am glad to have the chance to thank everybody who supported me during my PhD. First of all, I would like to express my sincere gratitude to my advisor, Prof. Anna Scaglione. I am deeply impressed by her enthusiasm, dynamism, out-of-the-box thinking and motivation for research. It was a great pleasure to work under her supervision.

I would like to thank Prof. Lang Tong not only for being in my thesis committee but also for his kindness and guidance. I am grateful to Prof. Toby Berger for accepting to serve in my thesis committee. He has been an idol for many students including me. I would also like to thank Prof. Stephen Wicker for accepting to attend my thesis defense.

The research that was part of this dissertation was supported by National Science Foundation under grant ITR CCR - 0428427 and in part by Office of Naval Research (ONR) under the contract N00014-00-1-0564.

Many friends and colleagues have made my stay at Cornell enjoyable. I would like to thank all the former and present members of CRISP. Especially, Azadeh, Peter, Matt and Ercan for sharing many laughs, hours of conversations, and for making the office a pleasant place. I would also like to thank ACSP members Vidyut, Chris, Min, Qing, Ting, Zhiyu, Youngchul, Parv for accepting me as their

honorary group member. My special thanks go to Azadeh, Vidyut, Yelda and Yesim for being there whenever I most needed.

My best attempts to thank my husband Gökhan Mergen would not be sufficient. I probably would not survive the PhD without his love, encouragement and support. He has also been a great colleague with whom I had the privilege to discuss research.

Last but not least, I would like to thank my parents and my brother for their endless love and support. I hope I make them proud.

Table of Contents

1 Introduction **1**
- 1.1 Cooperative communication . . . 1
- 1.2 Dissertation Outline . . . 4
- 1.3 Multi-Stage Cooperative Transmission . . . 4
- 1.4 Analysis of Multi-Stage Cooperative Transmission for a Single Source-Destination Pair . . . 7
- 1.5 Analysis of Multi-Stage Cooperative Broadcast . . . 9
- 1.6 Optimal Power Allocation for Cooperative Broadcast . . . 12
- 1.7 Randomized Space-Time Coding for Cooperative Communication . 14
- 1.8 Related Work . . . 17

2 Asymptotic Analysis of Cooperative Transmission for a Single Source-Destination Pair **20**
- 2.1 Organization . . . 20
- 2.2 System Model . . . 21
  - 2.2.1 Transmission Protocol . . . 21
  - 2.2.2 Reception Model . . . 22
- 2.3 Network with the Deterministic Channel Model . . . 23
  - 2.3.1 Random Network . . . 24
  - 2.3.2 Continuum of Nodes . . . 25
  - 2.3.3 An Approximation of the Continuum . . . 26
- 2.4 Random Channel Model . . . 32
- 2.5 Simulations . . . 37
- 2.A Proof of Lemma 1 . . . 43

3 Asymptotic Analysis of Multi- Stage Cooperative Broadcast **46**
- 3.1 Organization . . . 46
- 3.2 Network Behavior Under Deterministic Channel Model . . . 46
  - 3.2.1 Random Network . . . 47
  - 3.2.2 Continuum Network . . . 48
  - 3.2.3 Explicit Characterization of Level Sets . . . 50
  - 3.2.4 Effect of Multihop Diversity . . . 54
- 3.3 Derivation of Equivalent Channel Model for Fading Channels . . . 55

3.3.1 Transmitted and Received Signals for Non-orthogonal Transmissions . . . 57
3.3.2 Asymptotic Channel Distribution . . . 58
3.3.3 Orthogonal Transmissions over Fading Channels . . . 60
3.4 Network Behavior with Random Channels . . . 62
3.4.1 Random Network . . . 62
3.4.2 Continuum Network . . . 64
3.4.3 Behavior of Continuum Network with Orthogonal Channels 66
3.4.4 Behavior of Continuum Network with Non-orthogonal Channels . . . 68
3.4.5 Comparison between non-orthogonal and orthogonal cooperative broadcast . . . 71
3.4.6 Multihop diversity under fading channels . . . 73
3.4.7 Extensions to correlated fading . . . 73
3.5 Simulation Results . . . 78
3.5.1 Deterministic Channel Model . . . 78
3.5.2 Random Channel Model . . . 81
3.A Proof of Theorem 5 . . . 86
3.B Proof of Theorem 7 . . . 93
3.C Proof of Theorem 10 . . . 96

4 Power Efficiency of Cooperative Broadcast in Dense Wireless Networks 98
4.1 Organization . . . 98
4.2 System Model . . . 99
4.2.1 Reception Model . . . 99
4.3 Power Allocation for OCB: Problem Formulation . . . 101
4.3.1 Further Results on the Best Scheduling for Cooperative Broadcast . . . 103
4.4 Optimum Cooperative Broadcast in Dense Networks . . . 105
4.5 Cooperative Broadcast with Uniform Power Allocation . . . 112
4.5.1 Previous work and its comparison to OCB . . . 112
4.5.2 Double-Threshold Cooperative Broadcast (DTCB) . . . 115
4.6 Cooperative versus noncooperative Broadcast . . . 116
4.6.1 Noncooperative multihop broadcast . . . 117
4.6.2 Direct transmission . . . 118
4.6.3 Power efficiency of DTCB for $\ell(r) = 1/r^2$ . . . 118
4.7 Simulations . . . 120
4.A Proof of Lemma 7 . . . 125
4.B Proof of Lemma 8 . . . 126
4.C Proof of Theorem 13 . . . 127

5 Randomized Space-Time Coding for Distributed Cooperative Communication 129
5.1 Organization . . . 129
5.2 System Model and the Proposed Protocol . . . 130
5.2.1 Proposed Diversity Scheme . . . 132
5.2.2 Performance Metrics . . . 135
5.3 Design and Analysis of Randomized Space-time Codes . . . 136
5.3.1 Exact Characterization of the Diversity Order . . . 136
5.3.2 Upper Bound to the Probability of Error . . . 141
5.3.3 Diversity Order for Randomized Space-time Codes with Power Constraint . . . 142
5.4 Specific Designs and Their Performance . . . 144
5.4.1 Complex Gaussian distribution . . . 145
5.4.2 Real Gaussian distribution . . . 146
5.4.3 Uniform phase distribution . . . 147
5.4.4 Uniform distribution on a hypersphere . . . 149
5.5 Antenna Selection and Discrete Randomization Matrix . . . 150
5.6 Simulations & Numerical Evaluations . . . 153
5.A Proof of Lemma 11 . . . 159
5.B Proof of Theorem 14 . . . 160
5.C Proof of Theorem 15 . . . 162
5.D Proof of Theorem 16 . . . 164
5.E Proof of Theorem 17 . . . 167

6 Conclusion 168

Bibliography 170

List of Tables

2.1 Step-size convergence - Mean values 38
2.2 Step-size convergence - Standard Deviation 38
2.3 The ratio $|\mathcal{S}_k|/\rho W r_k$ averaged over different realizations 39

3.1 The ratio of expected number of nodes in each level to the approximate number of nodes, $\frac{|S_k|}{\pi\rho(a_k - a_{k-1})}$ 79
3.2 The ratio of expected radius of each level disc to approximate radius, $\frac{R_k}{\sqrt{a_k}}$ 79

List of Figures

1.1 The relay Channel 2
1.2 Non-Cooperative versus Cooperative Broadcast 5
1.3 Cooperative transmissions (k'th level is the group of nodes that participate in the k'th hop transmissions.) 8
1.4 (a) Transmissions propagate. (b) Transmissions die off. 9
1.5 (a) Transmissions propagate. (b) Transmissions die off. Nodes belonging to different levels are represented with different symbols. The nodes that did not receive/retransmit the source message are shown with dots. 12

2.1 (a) Random network; (b)-(c) continuum approximations. 23
2.2 $h(x)$ vs. x for two cases that $h'(0) > 1$ and $h'(0) < 1$. 28
2.3 $h(x)$ vs. x for $h'(0) > 1$. 30
2.4 r_∞ vs. the effective threshold $\beta = \tau/\bar{P}_r$ ($W = 1$). 32
2.5 Transmissions become a travelling wave. 35
2.6 Transmissions die out. 35
2.7 A realization of the random network 39
2.8 The expected $\tilde{r}_{10}$ vs. W 40
2.9 Probability of reaching the destination vs. τ 41
2.10 Travelling wave behavior 41
2.11 Transmissions die out 42

3.1 Illustration of $f(x, p)$. 50
3.2 (a) Transmissions propagate. (b) Transmissions die off. Notice that the scale of (a) and (b) are vastly different. 53
3.3 The reception models for random fading corresponding to orthogonal and non-orthogonal relay transmission. 56
3.4 The parameters are $\tau = 1.5, P_s = 5, \bar{P}_r = 1, d_0 = 1, \Sigma = 1$. The transmissions continue. 67
3.5 The parameters are $\tau = 2.5, P_s = 3.5, \bar{P}_r = 1, d_0 = 0.5, \Sigma = 1$. The transmissions die out. 68
3.6 Transmissions continue. The parameters are $\tau = 1, P_s = 10, \bar{P}_r = 1, M = 2, d_0 = 1, \Sigma = \frac{1}{M}\mathbf{I}$, where $\mathbf{I}$ is the identity matrix. 69
3.7 Transmissions die out. The parameters are $\tau = 3, P_s = 10, \bar{P}_r = 1, M = 2, d_0 = 1, \Sigma = \frac{1}{M}\mathbf{I}$, where $\mathbf{I}$ is the identity matrix. 70

3.8 Wideband orthogonal vs. narrowband non-orthogonal: the upper, rectangular shaped levels are the orthogonal, the lower wave-like levels are non-orthogonal. The parameters are $\tau = 1, P_s = 5, \bar{P}_r = 1, M = 1, d_0 = 1, \Sigma = 1$. 72
3.9 Narrowband non-orthogonal transmissions: $\tau = 1, P_s = 5, \bar{P}_r = 1, M = 1, d_0 = 1, \Sigma = 1$. Three different scenarios: (i) straight line $m = 3$, (ii) dotted line $m = 2$ (iii) dashed line $m = 1$. Note that first level curve $P_1(r)$ is the same for $m = 1, 2, 3$ and the second level curve $P_2(r)$ is the same for $m = 2, 3$. 74
3.10 First level nodes for the correlated fading model (dark regions) . . 75
3.11 Probability of number of nodes that transmit in a 1000 node network, $\rho = 1$, $P_r = 1$. Note that the scales for both horizontal and vertical axis are different. 80
3.12 Expected number of nodes that transmits vs P_s 81
3.13 Random Network Realization vs Continuum Approx. 82
3.14 Transmissions continue 84
3.15 Transmissions die out 84
3.16 Transmissions continue 85
3.17 Transmissions die out 85
3.18 Illustration of $\ell_N(x, 0, 0, 0)$ as a function of x. 89

4.1 Network topologies for which the optimal scheduling is trivial . . . 103
4.2 Continuum approximation of dense networks 105
4.3 Network topologies for which the optimal power allocation scheme assigns equal powers to nodes belonging to the same level. 106
4.4 Continuum approximation of dense networks-linear configurations . 109
4.5 Optimal power density - circular network 110
4.6 Double-Threshold Uniform Power Allocation: the shaded regions correspond to the active portions of the levels 116
4.7 Noncooperative multihop broadcast: shaded area = $\frac{r^2\sqrt{3}}{4}$ 117
4.8 Percentage of the nodes reached by the source 120
4.9 Total power consumption 121
4.10 The critical power per node required to cover an area $A = 20m^2$, where $P_s = \tau$, $m = 1$. 122
4.11 Total power spent to cover an area A by both optimal and suboptimal cooperative broadcasting schemes. The node density is $\rho = 20$.123
4.12 Total power spent to cover an area A. The node density is $\rho = 20$ and decoding threshold is $\tau = 1$. For cooperative broadcast, $P_s = 1.5$.123
4.13 Cooperative versus noncooperative under fixed number of hops. Cooperative scheme with $K = \infty$ and $m = 1$. 124
4.14 Derivation of $H(r, u)$. 128

5.1 Two phase cooperative communication. 130

5.2 Average Probability of Error versus SNR (dB), L = 2: N=2 (upper-left); N=3 (upper-right); N=4 (lower-left); N=10 (lower-right). For $N = 2$, the upper bounds to the average probability of error are drawn for each of the schemes with dotted curves. 156
5.3 Average Probability of Error versus SNR (dB), L = 2: N=2 (upper-left); N=3 (upper-right); N=4 (lower-left); N=10 (lower-right). . . 157
5.4 Average error probability behavior w.r.t. N 158

Chapter 1

Introduction

1.1 Cooperative communication

Increased demands for high-data rates and advances in VLSI technology have made wireless communication an active research field in the last decades. Researchers have studied various issues that limits the performance of wireless channels such as interference, fading and resource allocation. In wireless communications, a breakthrough is the innovation of multi-antenna systems, which received considerable attention not only from researchers but also from technology developers. It is currently well-established that utilizing multi-antennas dramatically improves the performance of wireless channels.

In ad hoc networks, the users are constrained in the complexity of their hardware and in their size. Hence, it might not be practical to use multiple-antennas for certain applications. For such scenarios, cooperative communication, a spatial diversity method, is proposed as an alternative to multi-antennas [1–3]. The idea is to allow users to cooperate in transmitting and/or receiving at the physical layer. The collection of cooperating nodes is also called a *virtual multi-antenna system.*

Cooperative communication can be applied in a wide variety of wireless networks including sensor networks, cellular networks and ad hoc networks.

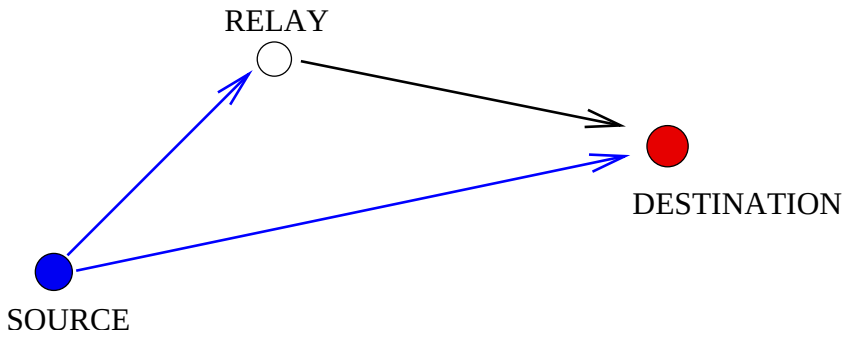

Figure 1.1: The relay Channel

One of the motivations behind cooperative communication is the information theoretic work on the relay channel by Cover and El Gamal [4] (see Fig. 1.1). Cover and El Gamal introduced new schemes to increase the source-destination communication rate with the help of a relay. The information theoretic capacity of the relay channel is still unknown. However, numerous practical schemes have been shown to improve the achievable rate. In the following, we present cooperation methods that are proposed previously for the single relay system [3]. The received signal is processed and forwarded by the relay and the destination efficiently combines the received signals from the relay and the source.

- *Amplify and forward:* The relay node transmits the received signal after scaling it to its power level. Main advantage of amplify-and-forward strategy is its simplicity. On the other hand, performance is limited since the noise at the relay is also amplified and forwarded to the destination.

- *Decode and forward:* The relay node decodes, re-encodes and forwards the message to the destination. The performance of decode-and-forward strategy

is limited by the source-relay link. If source-relay channel performs well, decode-and-forward strategy is optimal, *i.e.,* it achieves the capacity of the relay channel [5]. In this case, the relay channel is similar to a 2x1 multiple-input single-output (MISO) channel.

- *Compress and forward:* The relay sends a compressed version of the received signal. Compression is done using Wyner-Ziv source coding. Compress-and-forward strategy is optimal when the relay-destination channel performs well, and in this scenario, the relay channel is similar to a 1x2 single-input multiple-output (SIMO) channel. The main drawback of the compress-and-forward strategy is its complexity.

There are many other relaying strategies, which are extended versions of the above; namely, partial decode-and-forward, dynamic decode-and-forward, estimate-and-forward, bursty amplify-and-forward, selective relaying, relaying with feedback, etc. Coded cooperation is another scheme proposed for multi-user scenarios [1, 6, 7], *i.e.,* the case where the relay node also wants its own data to be transmitted to the destination. In this case, the source and relay act as partners for each other.

A challenging problem is the design and analysis of protocols for networks with multiple relays. In cooperative networks, if peer-to-peer communications are utilized, the overhead introduced in the system might detract from the gains obtained via cooperation. This overhead becomes more significant for large networks. Therefore, it is crucial to design distributed protocols which reduce the overhead and eliminate the need of internode communication. Most of previous analyses of cooperation protocols considered single- or two-hop communications. The analysis of networks with multiple cooperating nodes is a very challenging problem, and

the results obtained for such networks are mostly in the asymptotes such as low SNR, high SNR, infinite node, etc [8, 9].

1.2 Dissertation Outline

We first introduce a simple multi-stage transmission scheme for multiple cooperating nodes and analyze its performance as a function of the network parameters. In Chapter 2, the analysis is done for a network with single source-destination pair. We extend the cooperative scheme proposed to broadcasting scenario and analyze its performance in Chapter 3. In Chapter 4, we study the optimal power allocation problem for cooperative broadcast, and also compare the performance of our distributed protocol with the optimal and non-cooperative schemes. In Chapter 5, we introduce a randomized strategy which is a feasible solution for the code allocation problem for distributed space-time coding.

In this thesis we only consider a single-shot communication for a given source. A network with multiple sources is considerably more complicated than this one; other issues such as collisions, acknowledgements, end-to-end rate control, etc. have to be addressed. Our aim is to understand the single-shot cooperative communication thoroughly before it can be incorporated into a network setting.

1.3 Multi-Stage Cooperative Transmission

An important property of the wireless medium is that the transmitted packets are heard not only by their intended recipients but also by other neighboring nodes. While such unintended receptions are harmful when there is a single intended recipient, they may be *exploited* in broadcast mode. Moreover, "*collisions*"

between different transmitting nodes, which hinder point-to-point communication, may actually be *beneficial*, when the transmitting nodes are broadcasting the same message.

In Chapters 2 and 3, we analyze the transmission dynamics of a *cooperative transmission protocol*, in which nodes sequentially transmit the same message in large groups to increase the received power. Here, we take the view that the group transmissions (hence, the *intentional* collisions) are actually beneficial, since they increase the received power and the transmission range. This approach is in contrast with the traditional network layer flooding that treats each link individually and attempts to eliminate collisions as much as possible. Compared to multi-hop broadcast, cooperative broadcast results in more rapid message propagation with fewer number of steps (Fig. 1.2).

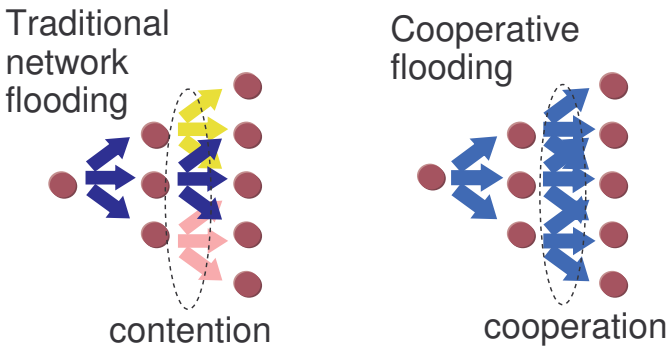

Figure 1.2: Non-Cooperative versus Cooperative Broadcast

In the considered setup, a source node initiates the transmission session by sending a packet. Every cooperating node who can hear the source with sufficient signal-to-noise ratio (SNR), decodes and retransmits the same packet. A training preamble in the message helps nodes to detect the packet's presence, estimate the received power and synchronize the retransmissions. The retransmissions are

done *simultaneously*, even though they may not be symbol synchronized. The first group excites a second group of nodes and the retransmissions continue until every node who hears the others with sufficient SNR, retransmits once. The subsequent groups of nodes that are activated are referred to as *levels*.

The nodes use a simple SNR threshold criterion to decide if they are going to retransmit or not, *i.e.,* every node monitors its received SNR and decodes and retransmits if its SNR exceeds a certain pre-determined threshold. In this way, the network can operate in a distributed fashion, since the nodes only use the locally available received SNR information to make transmission decisions. We assume that appropriate channel coding is used so that the decoding and retransmissions are correct as long as the received SNR is above the threshold.

The network performance crucially depends on the threshold. One would like to make it as low as possible to maximize the number of nodes who participate in transmission. On the other hand, a low threshold means decreased packet data rate; nodes are required to decode with lower SNR. Inherently, there exists a trade-off between the packet data rate and the number of participants in each transmission.

In our analysis, we consider two different models for receptions. The first one, which we call the *deterministic model*, assumes that the power of simultaneously transmitted packets is equal to the sum of individual powers. This model is valid if the relays transmit in orthogonal channels, as in FDMA or CDMA, or if the relays use orthogonal space-time codes as considered in [10] [1]. In case of orthogonal channels, a large bandwidth is required, *i.e.,* the network should operate in the

[1] In Chapter 5, we propose randomized space-time codes which provide diversity gains in a distributed and efficient way. The deterministic channel model is also valid if the relays utilize randomized orthogonal space-time codes.

wideband regime. In our second setup, we derive and consider a *random channel model* applicable for narrowband communication. Here, the impulse response of the channel with multiple transmitters is modelled as a Gaussian random vector. This model takes into account the effects of channel fading, time differences between simultaneous transmissions and random phases.

In order to obtain explicit results, we consider random networks and their *continuum asymptote*. For the random network, the node locations are assumed to be randomly and uniformly distributed. A continuum model is obtained from the random network by letting the number of nodes go to infinity while the total relay power is fixed. The continuum approach was previously used in different contexts in [11,12]. By numerical evaluation, it is shown that the continuum model provides reasonably accurate performance estimates for dense random networks.

1.4 Analysis of Multi-Stage Cooperative Transmission for a Single Source-Destination Pair

In Chapter 2, we study the dynamics of a multi-hop network with *cooperative transmissions* for a single source-destination pair, which is helped by relays located in a *strip* joining the source and the destination (see Fig. 1.3). In the considered cooperative protocol, the source node starts the delivery by transmitting a packet. The relays within the strip who hear the packet decode and retransmit the same packet *simultaneously*. Then, a second level of nodes receive the packet, decode and retransmit simultaneously. The retransmissions continue until every relay in the strip, who receives previous levels' transmission with sufficient SNR, retransmits once.

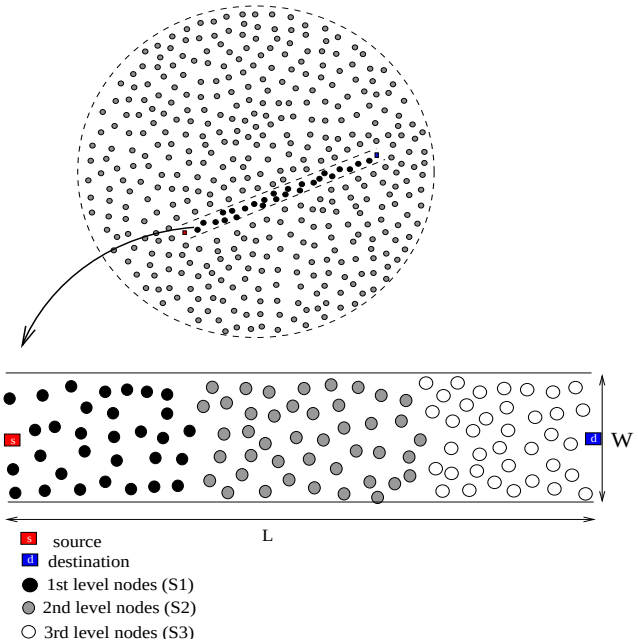

Figure 1.3: Cooperative transmissions (k'th level is the group of nodes that participate in the k'th hop transmissions.)

We analyze the network behavior as a function of the SNR threshold and the source/relay powers. We identify two different *regimes* of operation. If the threshold is above a *critical value* (*i.e.,* high data rate), then the transmissions die off eventually, and the data is not delivered to a destination far away. Otherwise (low data rate), the packet moves with uniform steps after a transient period, and gets delivered regardless of how far the destination is. Fig. 1.4 depicts these two regimes.

The continuum model is used to obtain expressions for the step size (*i.e.,* the length of each hop), and to characterize the effect of network parameters on the delivery dynamics. Using a *deterministic channel model*, it is shown that the critical SNR threshold is

$$\mathrm{SNR}_c = (\pi \ln 2) P_r \rho,$$

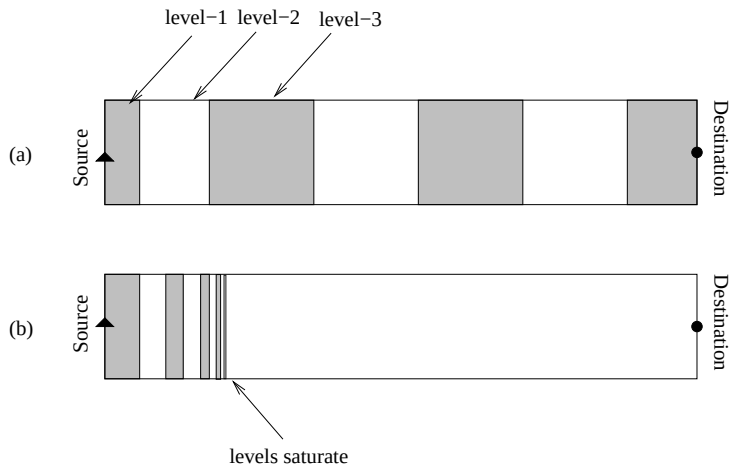

Figure 1.4: (a) Transmissions propagate. (b) Transmissions die off.

where P_r is the relay transmit power, ρ is the relay density [node/area]; the channel noise is of unit power. For networks with *Rayleigh distributed* channels, an upper bound to the critical threshold is provided.

1.5 Analysis of Multi-Stage Cooperative Broadcast

In distributed ad hoc networks, most network protocols require multicast or broadcast of certain control messages. These messages generally constitute a significant portion of network traffic, and they may cause performance bottlenecks. Several authors have studied how to optimally transmit broadcast information to minimize the total number of transmissions or the energy consumption in large wireless networks (*e.g.,* see [13, 14]).

In Chapter 3, we analyze the transmission dynamics of a simple cooperation protocol for broadcast over multiple stages of relays. The objective of cooperative broadcast is to deliver the source message to the whole network. However, this goal may or may not be achieved depending on certain network parameters such as the source/relay transmission powers and the decoding threshold. We analyze the ef-

fect of these parameters on the number of nodes reached by cooperative broadcast. In particular, we show that there exists a *phase transition* in the network behavior: if the decoding threshold is below a *critical value*, the message is delivered to the whole network. Otherwise, only a fraction of the nodes is reached proportional to the source transmit power.

The two regimes above and below the critical threshold are depicted in Fig. 1.5. Here, after the source transmission, other nodes in the network transmit in levels. The levels move outward as the transmissions continue. In Fig. 1.5(a), the number of simultaneously transmitting nodes grows at each stage, and the packet is distributed to the whole network in growing steps. On the other hand, in Fig. 1.5(b), the number of transmitting nodes diminishes in time, and the transmissions die out. We would like to note that the full-broadcast behavior is obtained at the cost of reduced SNR threshold, which results in a reduced communication rate in order to avoid erroneous decoding.

Using the deterministic channel model with squared path-loss model, in the continuum limit, we provide a complete characterization of the broadcast levels, the total area reached by broadcast, and the critical threshold. In particular, for the deterministic model the critical threshold is shown to be equal to

$$\mathrm{SNR}_c = (\pi \ln 2) P_r \rho,$$

where P_r is the relay transmit power, ρ is the relay density [node/area], and the channel noise is of unit power. It is worth noting that the phase transition behavior and critical threshold under broadcasting is similar to network behavior of single source-destination transmission.

We further consider the case that the relays exploit the received signal not only from their immediate neighbors (i.e. the previous level), but from m previous levels

that repeated the same source message. The importance of using transmissions coming from multiple hops was recognized by [15–17]. Following the terminology in [15], we shall call this *multi-hop diversity*. In the case of m-level multihop diversity, it is shown that the phase transition occurs at the critical threshold $\mathrm{SNR}_c = [\pi \ln(m+1)] P_r \rho$.

In the second part of Chapter 3, we derive equivalent channel models for networks with channel fading. Both orthogonal and non-orthogonal relay transmissions are considered. The network behavior is characterized in the continuum limit by the solution of a nonlinear deterministic dynamical system. Furthermore, an upper bound on the critical threshold is found for the non-orthogonal case. For both the deterministic and random channel models, it is shown by simulations that the continuum model provides reasonably accurate performance estimates for dense random networks.

Using the continuum model for orthogonal and non-orthogonal relay channels, we analyze the speed of propagation under these two scenarios. More specifically, we fix the duration of the source message, and compare the number of hops necessary to reach a given distance from the source. Interestingly, our results indicate that the speed of propagation in the high-density network with the narrowband non-orthogonal scheme is faster than that of the wideband orthogonal scheme. Although this appears highly non-intuitive, we reason , in the first system, that there is a possibility that the signals may add up constructively. In the asymptotic regime, a fraction of the nodes will receive a signal power equal to the power that would have been obtained if the transmitters were *beamforming* towards these fortunate destinations. Obviously, the orthogonal transmission scheme does not enable beamforming gains for any of the users. The nodes that do receive with

beamforming gain grow as the groups expand in size, creating a positive feedback effect that explains why the non-orthogonal scheme outperforms the orthogonal one. In the literature, there are other examples where channel randomization improves the system performance such as the opportunistic communication method proposed in [18].

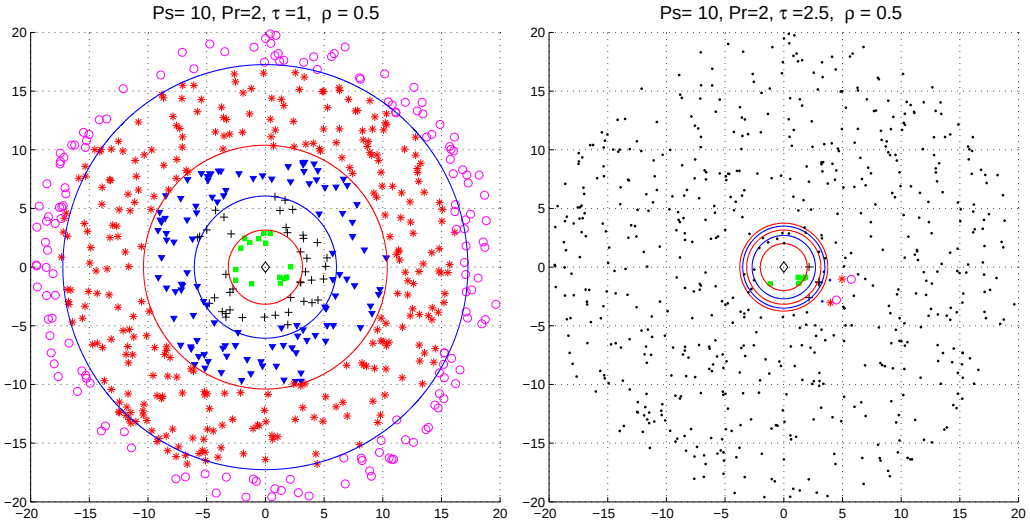

(a) (b)

Figure 1.5: (a) Transmissions propagate. (b) Transmissions die off. Nodes belonging to different levels are represented with different symbols. The nodes that did not receive/retransmit the source message are shown with dots.

1.6 Optimal Power Allocation for Cooperative Broadcast

The aim of cooperative broadcast is to deliver a source message to a wireless network by means of collaborating nodes. The energy efficiency of cooperative transmission has been studied extensively and the advantages of cooperation over direct and multi-hop transmissions have been shown under several different proto-

cols [1–3,10,15–17,19–23]. Cooperative transmission enhances the energy efficiency either by providing diversity or by increasing the received SNR.

In Chapter 4, we study the power efficiency of cooperative broadcasting in dense networks. Both optimal and suboptimal schemes are studied. Furthermore, we compare the cooperative broadcast with traditional noncooperative schemes.

In the optimal cooperative broadcasting (OCB), the nodes utilize *all* the previous receptions [16,19,20]. In addition, the nodes transmit based on predetermined schedule and power allocation policy such that total power consumption of the network is minimized. In [16, 19, 20], it was shown that for a given transmission schedule, the optimal power allocation can be formulated as a constrained optimization problem which can be solved in polynomial time by utilizing linear programming tools. On the other hand, the authors showed also that finding the optimal scheduling that leads to the minimum total power consumption is an NP-complete problem and thus, it is not computationally tractable. Both works proposed heuristic methods to determine the optimal schedule.

In the first part of Chapter 4, we study the OCB for dense networks. First, we study specific network topologies and channel models for which we are able to show that the optimal scheduling is resolved in polynomial time. Then, we extend the analysis to dense networks. In particular, for dense large-scale networks, we approximate the optimal schedule with the schedule that allows the nodes to transmit in the order of their distances from the source node. This approximation becomes exact in the asymptote as the node density increases, which we will refer to as the *continuum network*. Under the continuum model, we are able to show that the optimal power density is given by the solution of a *Volterra equation* with parameters that depend on the network topology and the channel gains. In

addition, for specific path loss models and topologies we are able to find closed form expressions for the optimal power density $p(r)$. For example, for a disc network with radius R and the source node located at the center, under the pathloss model $\ell(r) = 1/(1 + r^2)$, we show that the optimal relay power density is $O(1/\ln(r))$ which amounts to total minimal power expenditure of $O(R^2/\ln(R))$ for large R. There are two interesting conclusions that can be drawn from our analysis: (i) as the network density increases, the scheduling problem tends to be *trivial*; (ii) at an appropriate distance from the source, the power density is a very slowly varying function of the distance that can be well approximated by a uniform power density.

In the second part of Chapter 4, we design and analyze low-complexity distributed cooperative broadcasting schemes and compare their power efficiency with both the optimal and the noncooperative multihop broadcast. The proposed schemes utilize a simple uniform power control policy. Part of the results are based on our previous work in [24]. Finally, we conclude that dense cooperative networks can bring considerable advantages in terms of power efficiency relative to the commonly employed multihop architecture.

1.7 Randomized Space-Time Coding for Cooperative Communication

In the case of multiple relays, several methods have been proposed for forwarding the common message by the relays, from the simple repetition, to space-time coding [10], to more idealistic approaches derived from the information theoretic framework established by Cover & El Gamal [4]. In general, space-time coding is superior to repetition, since it provides diversity without a significant loss in

spectral efficiency [25].

A major challenge in distributed cooperative transmissions is to find a way to coordinate the relay transmissions without requiring extra control information overhead, which would reduce part of the gain. The coding rule applied by each of the cooperating nodes should, therefore, be identical and independent from node to node. However, most of the distributed space-time codes in the literature do not focus on this issue, see e.g. [10, 26–32]. In these schemes, each node emulates a specific array element of a multiple-antenna system; in practice, the implementation requires a centralized code allocation procedure. In addition, in large-scale distributed wireless networks, the set of cooperating nodes is unknown or random in most scenarios. For example, in networks with a single source-destination pair and multiple cooperating relays, the set of nodes that is responsible for retransmission is random due to the error-free decoding constraint. The randomness in the cooperating set may be due to fading, mobility, node failure, expired battery life, or the occurrence of a possible sleep state. In this context, designing codes that provide diversity gains even when the number of cooperating nodes is unknown or random is another issue to address in cooperative networks.

The contribution of Chapter 5 is a novel design of a simple methodology to decentralize the relay transmissions and yet obtain diversity and coding gains analogous to those that can be attained using a multi-antenna systems. Our idea is to let each relay transmit an independent, random linear combination of the columns of a space-time code matrix which has a fixed size L, irrespective of the number of cooperative nodes N. Special cases of the proposed scheme include: i) each node emulates one randomly selected antenna; ii) each node transmits the superposition of all antennas with random phases; iii) each node transmits the superposition of

all antennas with random gains and phases. We refer to our scheme as *randomized space-time coding* (RSTC). RSTC entails the specification of a space-time code of size L, and an $L \times N$ random matrix $\boldsymbol{\mathcal{R}}$, whose columns are independent. The purpose of randomization, as mentioned before, is to eliminate the need for a centralized code (or *antenna*) allocation procedure. Random linear mapping has also been considered in the context of network coding [33, 34].

In order to analyze the performance of the proposed scheme, we express the diversity of the randomized space-time codes as the order of the probability of deep fade event [35] (see Section 5.3.1). The analysis in Section 5.3.1 provides the diversity order of any given arbitrary randomization procedure. However, the results are expressed as non-trivial functions of the statistics of $\boldsymbol{\mathcal{R}}$ and, thus, do not lead directly to constructive designs. To provide design guidelines, we resort to a Chernoff bound on the decoding error probability that allows us to derive sufficient conditions under which full diversity is achieved. In our study, we consider random coefficients drawn from both continuous and discrete distributions. For the case of continuous complex coefficients, we provide designs that achieve full diversity under the condition $N \neq L$, where N is the number of active transmitters and L is the number of antennas in the underlying space-time code. We show that, despite the code randomization, the proposed scheme achieves full diversity (N) if $N < L$, and the diversity order L is achieved for $N > L$. Interestingly, for $N = L$ we show that the proposed scheme exhibits a fractional diversity (for example, for $N = L = 2$, the diversity order of the scheme with randomly selected phases is 1.5). For the case of discrete valued random matrices, we observe a multi-slope behavior in the average probability of error for sufficiently large number of nodes ($N > 10$) (see also [36]).

1.8 Related Work

Cooperative protocols can be categorized according to the number of relays for which they are designed. The papers [1–3, 28, 37] investigate the spatial diversity in cooperative networks with a few number of nodes. More specifically, [3] develops low complexity cooperation protocols exploiting the spatial diversity. In [1], cooperative transmissions are considered for improving the uplink capacity. In both [1] and [3], a network with two sources and a single destination is considered. It is also assumed that the nodes are both sources and relays at the same time, and each node has an orthogonal channel assigned exclusively. It is worth noting that the channel assignment to different nodes in most proposed methods usually requires a central control unit.

Most of the protocols for multiple relays are generally extensions of designs for a few number of nodes. The extension is done by using relays in parallel (*i.e.,* multiple relays transmit simultaneously in groups—*e.g.,* [10,30,31,38]), or in series (*i.e.,* relays transmit sequentially—*e.g.,* [15,39]), or a combination of these two (*e.g.,* [40]). In [15, 39], four different network models are considered, which are grouped according to relay processing (amplifying or decoding) and signal reception model (from all previously transmitted terminals or from the immediate terminal). In [40], authors derive symbol error probability expressions, valid under high SNR, for networks with parallel, serial, and also combined configurations. Both [16, 20] investigate the energy efficiency of cooperative transmissions over multi-hop networks for different setups. In [9] and [5], the authors consider the channel capacity with multiple relays.

Another related scheme is *Opportunistic Large Arrays* proposed in [17], which relies on a distributed rule, referred to as the *integrate and fire model*, to syn-

chronize the nodes. In this method, the nodes select a firing time based on the energy accumulated at the receiver. The nodes emit their decision at the firing times, which are decided in a distributed fashion. This scheme has low complexity compared to the centralized cooperative schemes, and it eliminates the problem of scheduling transmissions; however, it cannot guarantee diversity gains since the transmitted signals can overlap in time, and it requires non-negligible bandwidth overhead (see [17] for details).

In a recent work on cooperative transmission [41], the authors show that there exists a critical rate C such that the outage probability of every receiver converges to zero, for rates below C, as the number of nodes goes to infinity. The analysis is done under a sum power constraint and also independent and identically distributed channel gains. Interesting phase transitions also arise in applications of percolation theory such as the connectivity analysis of random networks [42, 43].

Other approaches that apply to a decentralized scenario are in [44] and [17]. In [44], the authors propose a protocol where the relay nodes transmit with a randomly chosen delay. Hence, further diversity is obtained by intentionally creating a frequency selective channel. Note that this scheme may not provide diversity gains due to the possibility that each node may choose to use the same delay. In fact, our analysis in Section 5.5 provides the performance of a class of forwarding strategies which includes the random delay scheme in [44] as a special case (see also Example 3). In [17], the nodes regenerate the signal at time instants that depend on the energy accumulated per symbol. The decentralized policy produces diversity only if the delays can be resolved at the receiver, which in general requires a large bandwidth.

Other works that address the need for distributed implementation at cooperat-

ing nodes are [10,45–48]. In [10], the authors propose orthogonal space-time codes, which may become impractical for large number of nodes. In [45], the authors propose a filtering approach that does not require the knowledge of the number of cooperating nodes in order to achieve maximum diversity. The scheme proposed in [46], has the closest formulation to ours, since each node transmits the product of a space-time code matrix with a pre-assigned vector-code. As a result, this scheme does not require the knowledge of the number of cooperating nodes that are active, but it still requires a preliminary code allocation phase. In one way or another, most of these schemes become impractical in a self-organized networks with a large and/or random number of nodes.

Another linear relaying technique is amplify-and-forward. The schemes in [47, 49] are alternatives to the amplify-and-forward strategy. The authors propose diversity achieving methods that are based on linear mapping of the received message at each relay. Our focus in this thesis is, however, on decode and forward strategies.

Chapter 2

Asymptotic Analysis of Cooperative Transmission for a Single Source-Destination Pair

2.1 Organization

The organization of the chapter is as follows. In the next section, the transmission protocol is specified, the deterministic and random channel models are introduced. The network with the deterministic channel model is analyzed in Section 2.3. The network with the random channel model is investigated in Section 2.4. In Section 4.7, we provide simulation results for random networks, and check the accuracy of continuum approximation.

2.2 System Model

2.2.1 Transmission Protocol

Consider a multi-hop ad-hoc network formed by a set of nodes randomly distributed in a geographical region. Suppose that a node (= source node) aims to send a packet to another node (= destination node) with the help of other nodes. Consider the *strip* of length L and width W joining the source and the destination (Fig. 1.3). The nodes within this strip serve as relays from the source to the destination.

The cooperation protocol is such that the source node initiates the delivery by transmitting a packet. The nodes that receive the packet with sufficient SNR and lie within the designated strip decode, and retransmit the same packet *simultaneously* (these are called *level-1* nodes; see Fig. 1.3). Then, a second set of nodes (*i.e., level-2* nodes) within the strip receive the packet, and retransmit simultaneously. The retransmissions continue until every node in the strip who successfully receives the packet retransmits once. The level-3, level-4, $\cdots$ nodes are defined similarly. We would like to emphasize that relays do *not* transmit the same packet more than once. Also note that the transmitted packets are channel-coded with an appropriate rate such that the nodes with sufficient receive SNR can decode the packet without errors.

For the protocol to work properly, it is assumed that every node knows its geographical location. Furthermore, every transmitted packet includes information about the coordinates of the strip. So, the nodes can tell whether they are in the strip or not after receiving a packet.

2.2.2 Reception Model

As mentioned earlier, we analyze the network behavior under two different reception models: (i) deterministic channel model, (ii) random channel model. Let the source transmit with power P_s, and the relays transmit with power P_r. We consider path-loss attenuation with exponent 2, *i.e.,* every transmission with power P is received with power $\frac{P}{d^2}$ at distance d. We will consider two different models for the received power of simultaneously transmitted signals. In the first one, it is assumed that if a set of relay nodes (say, level-m nodes= $\mathcal{L}_m$) transmit simultaneously, then node j receives with power

$$Power = \sum_{i \in \mathcal{L}_m} \frac{P_r}{d_{ij}^2}, \tag{2.1}$$

where d_{ij} is the distance between the i'th and j'th nodes. This will be called the *deterministic channel model* in the following. The received power in (4.1) can be achieved under many scenarios; for example, the nodes in a given level transmit in orthogonal channels as in TDMA, FDMA or CDMA.

The squared-distance attenuation model P/d^2 comes from the free-space attenuation of electromagnetic waves, and it does *not* hold when d is very small (see near-field vs. far-field attenuation in [50]). This issue has been recognized by several researchers (*e.g.,* [42,51]). One possible solution is to consider constant power for the near-field $d \leq d_0$ for some d_0, *i.e.,* to replace $1/d^2$ by

$$\ell(d) := \begin{cases} 1/d^2 & d_0 \leq d \\ 1/d_0^2 & 0 \leq d \leq d_0. \end{cases}$$

Another simplistic assumption the model (4.1) makes is that the power of the simultaneously transmitted packets is equal to the sum of the powers. If the simultaneous transmissions are not in orthogonal dimensions, the cumulative power of transmitted packets depends on the relative delays and phases of individual

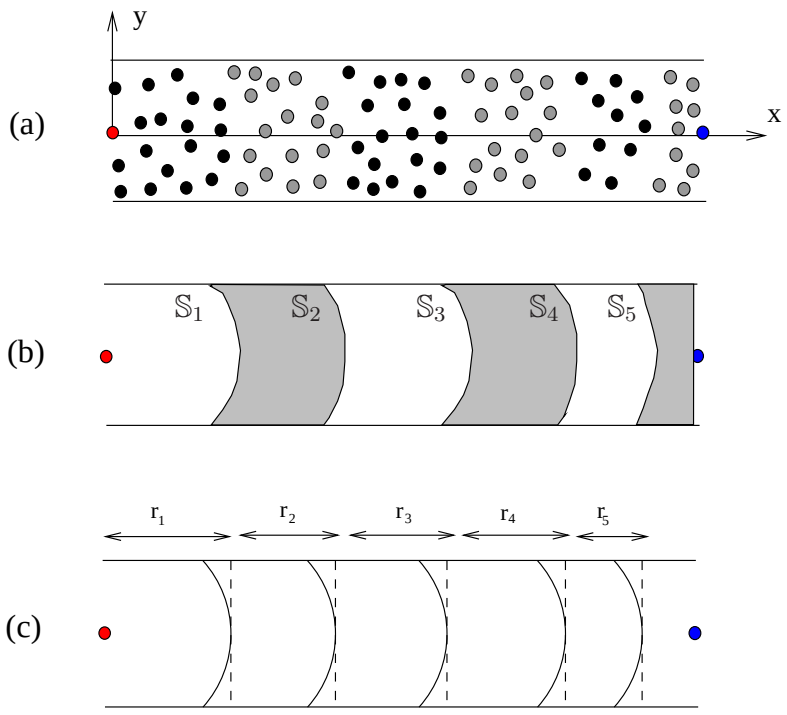

Figure 2.1: (a) Random network; (b)-(c) continuum approximations.

overlapping signals. In literature, random addition of multiple signal paths is generally modelled as *Rayleigh fading* [35]. This motivates us to replace (4.1) with

$$Power = \gamma \sum_{i \in \mathcal{L}_m} P_r \ell(d_{ij}), \tag{2.2}$$

where γ is a unit-mean exponential random variable (it is well known that squared Rayleigh is the exponential distribution). This will be called the *random channel model*. In the following we will consider the deterministic model besides the random one, since it is tractable, and provides intuition about the system.

2.3 Network with the Deterministic Channel Model

In this section we analyze the propagation of the source packet using the deterministic reception model. We consider two models for the network topology: randomly

distributed nodes and a continuum of nodes. The continuum model is obtained from the random one as the node density goes to infinity.

2.3.1 Random Network

Suppose that the source and destination locations are fixed at the two opposite ends of the strip as shown in Fig. 1.3. Let N relay nodes be uniformly and randomly distributed in the strip. Consider the coordinate axes shown in Fig. 2.1a, where the source is located at the origin.

Let $\mathcal{S} = \{(x_i, y_i) : i = 1 \dots N\}$ be the set of relay locations. The locations of level-1 nodes are denoted by the set

$$\mathcal{S}_1 = \{(x, y) \in \mathcal{S} : \frac{P_s}{x^2 + y^2} \geq \tau\}, \tag{2.3}$$

where τ is the *minimum signal power* required for successful reception of a packet. Under the assumption that the channel noise is of unit power, τ is equal to the previously mentioned SNR threshold. Locations of the level-k nodes for $k \geq 2$ are given recursively by

$$\mathcal{S}_k = \{(x, y) \in \mathcal{S} \setminus \bigcup_{i=1}^{k-1} \mathcal{S}_i : \sum_{(x',y') \in \mathcal{S}_{k-1}} \frac{P_r}{(x' - x)^2 + (y' - y)^2} \geq \tau\}. \tag{2.4}$$

An important question in the considered cooperative protocol is that "Under what conditions does the packet reach to the destination?" Second, how do the network parameters such as P_s, P_r, τ affect the delivery behavior? To be able to answer such questions, we need to understand how the sets $\mathcal{S}_1, \mathcal{S}_2, \cdots$ evolve as the packet moves forward within the strip. For this purpose we will consider the continuum model described next.

2.3.2 Continuum of Nodes

Let $\mathbb{S} := \{(x, y) : |y| \leq W/2,\ 0 \leq x \leq L\}$ denote the strip. Let $\rho = N/\text{Area}(\mathbb{S})$ be the density [node/unit area] of relays within the strip. In the continuum model we are interested in the high density asymptote. That is, the number of relay nodes N goes to infinity, while W, L and the *total relay power* $P_r N$ are fixed. This implies that the *relay power per unit area*

$$\bar{P}_r := \frac{P_r N}{\text{Area}(\mathbb{S})} = P_r \rho$$

is also fixed, and $P_r = \bar{P}_r/\rho$.

In this regime the level-1 nodes become dense in the set

$$\mathbb{S}_1 := \{(x, y) \in \mathbb{S} : \frac{P_s}{x^2 + y^2} \geq \tau\}$$

(this is the intersection of the strip with the circle $x^2+y^2 \leq P_s/\tau$). Moreover, as the network density goes to infinity, every infinitesimal area $dxdy$ in $\mathbb{S}_1$ contains $\rho dxdy$ nodes each with power P_r. The total transmission power is $P_r \rho dxdy = \bar{P}_r dxdy$. Hence, the level-2 nodes become dense in the set

$$\mathbb{S}_2 = \{(x, y) \in \mathbb{S} \setminus \mathbb{S}_1 : \iint_{\mathbb{S}_1} \frac{\bar{P}_r}{(x' - x)^2 + (y' - y)^2} dx'dy' \geq \tau\} \tag{2.5}$$

(see Fig. 2.1b). By recursion, it is seen that the level-k nodes, $k \geq 2$, become dense in

$$\mathbb{S}_k = \{(x, y) \in \mathbb{S} \setminus \bigcup_{i=1}^{k-1} \mathbb{S}_i : \iint_{\mathbb{S}_{k-1}} \frac{\bar{P}_r}{(x' - x)^2 + (y' - y)^2} dx'dy' \geq \tau\}. \tag{2.6}$$

The sets $\mathbb{S}_1, \mathbb{S}_2, \cdots$ specify the continuum model. A relation between the random network and the continuum model is provided by the following theorem.

Theorem 1 *Let $\bar{P}_r, W, L$ be fixed, and*

$$P_r = \frac{\bar{P}_r}{\rho}, \quad \rho = \frac{N}{WL}$$

be a function of N. For all $k \in \{1, 2, \cdots\}$ and any open set $\mathbb{D} \subset \mathbb{S}$, the number of level-$k$ nodes in $\mathbb{D}$ scales as $\rho Area(\mathbb{D} \cap \mathbb{S}_k)$, i.e.,

$$\frac{|\mathbb{D} \cap \mathcal{S}_k|}{\rho Area(\mathbb{D} \cap \mathbb{S}_k)} \xrightarrow{\text{p}} 1, \quad as\ N \to \infty, \tag{2.7}$$

where $\xrightarrow{\text{p}}$ denotes convergence in probability.

An extended version of this proof is given for the broadcast scenario in Chapter 3 (Theorem 5). Here, we only summarize its main ideas.

Sketch of the proof: i) Partition the strip into rectangles of appropriate size, which shrink as $N \to \infty$.

ii) Show that every rectangle of size $\Delta x \Delta y$ has $(\rho \pm \epsilon N)\Delta x \Delta y$ nodes with high probability for large N by using the uniform law of large numbers (the Vapnik-Chervonenkis Theorem).

iii) Show that the summation in $\mathcal{S}_k$ converges to the corresponding integral in $\mathbb{S}_k$ as $N \to \infty$.

iv) Combine parts ii) and iii) to obtain (2.7). ■

2.3.3 An Approximation of the Continuum

The regions $\mathbb{S}_1, \mathbb{S}_2, \cdots$ can be specified by their boundary curves as shown in Fig. 2.1b. These curves, however, can only be computed numerically (*i.e.,* they are non-linear without closed form expressions). To gain more insights about propagation in cooperative networks, we will approximate the boundaries by *straight lines*. This approximation is expected to be accurate especially when W is small. Through simulations, we will observe that such an approximation gives reasonable accurate estimates of network behavior.

The $\mathbb{S}_1$ is approximated by the rectangle $\tilde{\mathbb{S}}_1$ with coordinates $0 \leq x \leq \sqrt{P_s/\tau}$,

$|y| \leq W$. Let r_1 denote $\sqrt{P_s/\tau}$ (see Fig. 2.1c). Assuming that the level-1 set is $\tilde{\mathbb{S}}_1$, a new $\mathbb{S}_2$ can be computed from (2.5) by replacing $\mathbb{S}_1$ with $\tilde{\mathbb{S}}_1$. This again, however, gives a non-linear boundary. To compensate this, let $r_2 > 0$ be the unique real number satisfying

$$\iint_{\tilde{\mathbb{S}}_1} \frac{\bar{P}_r}{(x-(r_1+r_2))^2+y^2} dxdy = \tau \tag{2.8}$$

(*i.e.*, $x = r_1 + r_2$ is the boundary of the new $\mathbb{S}_2$ at $y = 0$). By applying a change of variables, (2.8) can be equivalently expressed as

$$\int_{-W/2}^{W/2} \int_{r_2}^{r_2+r_1} \frac{\bar{P}_r}{x^2+y^2} dxdy = \int_{r_2}^{r_2+r_1} \frac{2\bar{P}_r}{x} \arctan(\frac{W}{2x}) dx = \tau. \tag{2.9}$$

Now, we again approximate the curved region $\mathbb{S}_2$ by a rectangle $\tilde{\mathbb{S}}_2$ with coordinates $r_1 \leq x \leq r_1 + r_2,\ |y| \leq W$. Recursively, $r_3, r_4, \cdots$ is defined by the relation $r_{k+1} = h(r_k)$, where $h(x)$ for $x > 0$ is defined as the unique solution of

$$\int_{h(x)}^{h(x)+x} \frac{2\bar{P}_r}{u} \arctan(\frac{W}{2u}) du = \tau. \tag{2.10}$$

We call r_k the *step-size* of level-k.

The following lemma summarizes our findings about $h(x)$.

Lemma 1 *i) The function h is well-defined. That is, for every $x > 0$, the solution of (2.10) with respect to $h(x)$ exists, and is unique. By continuity, $h(0) := \lim_{x \downarrow 0} h(x) = 0$.*

ii) The function h is increasing and concave.

iii) $h'(0) = 1/(e^{\tau/\pi \bar{P}_r} - 1)$.

iv) When $h'(0) > 1$, then h has a unique positive fixed point $h(x) = x$. When $h'(0) < 1$, the only non-negative fixed point of h is at $x = 0$ (see Fig. 2.2).

Proof See the Appendix 2.A.

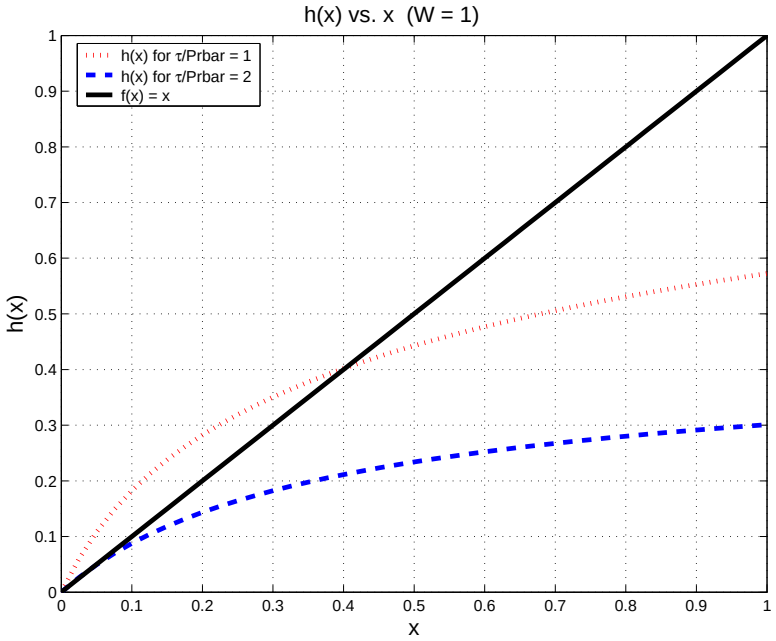

Figure 2.2: $h(x)$ vs. x for two cases that $h'(0) > 1$ and $h'(0) < 1$.

The network behavior is determined by the summation $\sum_{k=1}^{\infty} r_k$. When this sum is *infinite*, then the source message reaches the destination regardless of how far the destination is. However, if the summation is *finite*, then the message does not reach the destination when the source and the destination are too far (*i.e.*, $L > \sum_{k=1}^{\infty} r_k$). The following theorem characterizes the limiting behavior of the step-size r_k and the summation $\sum_{k=1}^{\infty} r_k$ as a function of network parameters.

Theorem 2 *The network presents the following dichotomy:*

i) If $\tau > (\pi \ln 2)\bar{P}_r$, *then the transmissions die out and only a finite portion of the network is reached, i.e.,* $\lim_{k\to\infty} r_k = 0$ *and*

$$\sum_{k=1}^{\infty} r_k \leq r_1 \frac{e^{\tau/\pi\bar{P}_r} - 1}{e^{\tau/\pi\bar{P}_r} - 2} < \infty. \tag{2.11}$$

ii) If $\tau < (\pi \ln 2)\bar{P}_r$, *then the transmissions reach a steady state with the limiting step size* $\lim_k r_k = r_\infty > 0$, *where* r_∞ *is the unique positive fixed point of* h,

i.e.,

$$\int_{r_\infty}^{2r_\infty} \frac{2\bar{P}_r}{u} \arctan(\frac{W}{2u})du = \tau. \tag{2.12}$$

Proof i) Since the h is concave, the line tangent to the graph of h at $x = 0$ stays above, *i.e.,*

$$h(x) \leq h'(0)x, \quad \forall x \geq 0.$$

Our claim is

$$r_{k+1} \leq (h'(0))^k r_1, \quad \forall k \geq 0. \tag{2.13}$$

This can be seen by induction. For $k = 0$, the statement is clearly true. Assume that $r_k \leq (h'(0))^{k-1} r_1$ holds. Then,

$$r_{k+1} = h(r_k) \leq h'(0) r_k \leq (h'(0))^k r_1,$$

as it was claimed.

Using the part iii) of the previous lemma, notice that $h'(0) < 1$ if and only if $\tau > (\pi \ln 2)\bar{P}_r$. Under this condition, sum (2.13) over k to get

$$\begin{aligned} \sum_{k=1}^{\infty} r_k &\leq r_1 \sum_{k=0}^{\infty} (h'(0))^k \\ &= r_1 \frac{1}{1 - h'(0)} \\ &= r_1 \frac{e^{\tau/\pi\bar{P}_r} - 1}{e^{\tau/\pi\bar{P}_r} - 2} \end{aligned}$$

Since the series is summable, r_k necessarily converges to zero as $k \to \infty$. This finishes part i).

ii) The relation $r_{k+1} = h(r_k)$ defines a one-dimensional dynamical system. The convergence of such systems can be established by analyzing their phase trajectories [52]. That is, consider Fig. 2.3. When the system starts from an initial condition below the fixed point of h, then r_k monotonically increases to $h(x) = x$

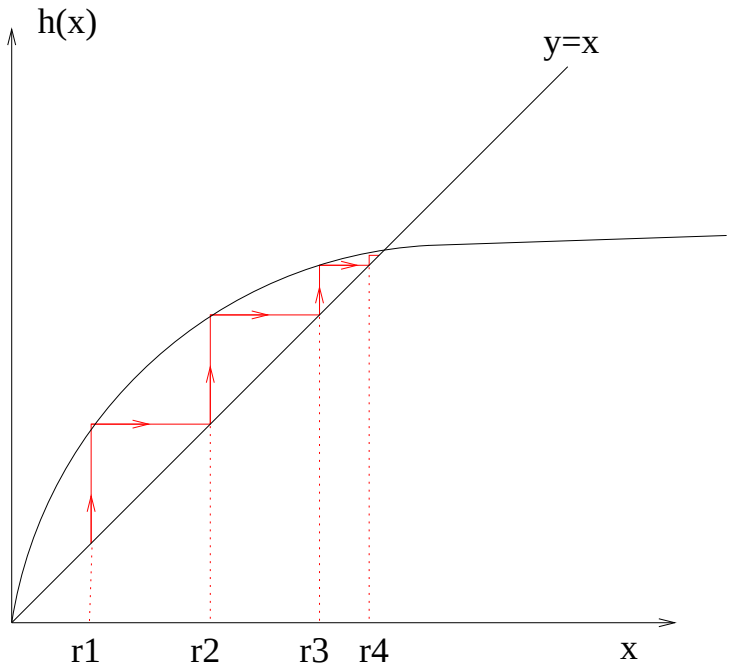

Figure 2.3: $h(x)$ vs. x for $h'(0) > 1$.

since h is increasing and concave. Similarly, when r_1 is above $x = h(x)$, then r_k monotonically decreases towards the fixed point. The convergence of r_k to the fixed point is determined by the slope of h at the fixed point; if $|h'(x)| < 1$ at $x = h(x)$, then r_k converges to the fixed point [52, Sec. 1.4]. By taking the derivative of (2.10) with respect to x and substituting $h(x) = x$, we get

$$h'(x) = \frac{\arctan(\frac{1}{4x})}{2\arctan(\frac{1}{2x}) - \arctan(\frac{1}{4x})}, \quad \text{at } x = h(x).$$

Notice that $h'(x) < 1$ if and only if

$$\arctan(\frac{1}{4x}) < 2\arctan(\frac{1}{2x}) - \arctan(\frac{1}{4x}) \quad \Leftrightarrow \quad \arctan(\frac{1}{4x}) < \arctan(\frac{1}{2x}), \quad (2.14)$$

which is true for $x > 0$. Part ii) follows.

Interestingly, the results of the above theorem are independent of the initial condition r_1. The limiting step size r_∞ does not have a closed-form expression,

but the following theorem gives a characterization of it, and provides tight upper and lower bounds.

Theorem 3 *Consider the regime* $\tau < (\pi \ln 2)\bar{P}_r$.

i) The limiting step size r_∞ *is solely determined by* W *and the* effective-threshold $\beta := \frac{\tau}{\bar{P}_r}$.

ii) The r_∞ *is linear in* W. *That is, let* r_∞^* *be the limiting step size for* $W = 1$, *then* $r_\infty = W r_\infty^*$.

iii) The r_∞ *satisfies*

$$\frac{W(\pi \ln 2 - \beta)}{4} \leq r_\infty \leq \frac{W}{2\beta}. \tag{2.15}$$

Proof Part i) is trivial.

From the definition of r_∞^* we know that r_∞^* is the unique positive number satisfying

$$\int_{r_\infty^*}^{2r_\infty^*} \frac{2}{u} \arctan(\frac{1}{2u}) du = \frac{\tau}{\bar{P}_r}. \tag{2.16}$$

Next, consider r_∞ for an arbitrary W. Apply change of variables $v = u/W$ in (2.12) to get

$$\int_{\frac{r_\infty}{W}}^{\frac{2r_\infty}{W}} \frac{2}{v} \arctan(\frac{1}{2v}) dv = \frac{\tau}{\bar{P}_r}. \tag{2.17}$$

Since r_∞^* is the unique number satisfying this equation, $r_\infty^* = r_\infty/W$. This gives ii).

It is well known that

$$\frac{\pi}{2} - \frac{1}{z} \leq \arctan(z) \leq z. \tag{2.18}$$

These inequalities are tight in two extremes, *i.e.,* $\arctan(z) \approx z$ for $z \approx 0$, and $\arctan(z) \approx \frac{\pi}{2} - \frac{1}{z}$ for $z \to \infty$. Substitute (2.18) into (2.12) to get (2.15).

Fig. 2.4 shows how the bounds in (2.15) compare with the actual r_∞. It is seen from the figure that the bounds become almost exact at the extreme values $\beta \approx \pi \ln 2$ and $\beta \approx 0$.

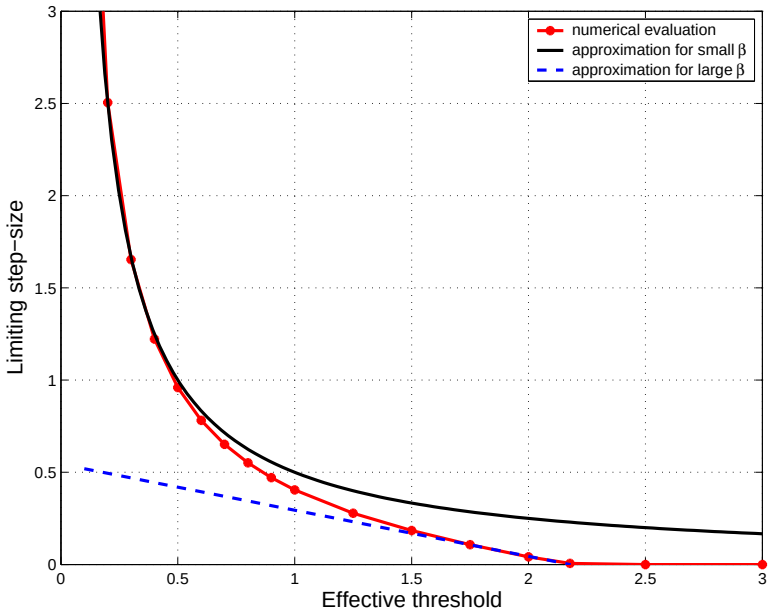

Figure 2.4: r_∞ vs. the effective threshold $\beta = \tau/\bar{P}_r$ $(W = 1)$.

2.4 Random Channel Model

In this section, we provide an analysis of the cooperative network with the random channel model (Eqn. 4.2). In case of random channels, one can define the network with random topology, and obtain the continuum model in the limit as $N \to \infty$. Nevertheless, this process is quite similar to what is done in the previous section. Therefore, we shall discuss the continuum model directly.

Suppose that there exists a continuum of nodes over strip $\mathbb{S} = \{(x, y) : |y| \leq W/2, 0 \leq x \leq L\}$. The source is located at the origin, and transmits with power P_s. If the channels were deterministic, a node at location (x, y) would receive the

source transmission with power $\sigma_0^2(x,y) := P_s\ell(x,y)$, where

$$\ell(x,y) = \begin{cases} 1/(x^2+y^2) & (x^2+y^2) \geq d_0^2 \\ 1/d_0^2 & 0 \leq (x^2+y^2) \leq d_0^2. \end{cases}$$

is the path-loss function. However, the actual reception power $\gamma\sigma_0^2(x,y)$ is random, where γ is a unit-mean exponential random variable. A node at location (x,y) receives the source transmission successfully with probability

$$\begin{aligned} P_1(x,y) &= \Pr\{Power \geq \tau\} \\ &= \Pr\{\gamma \geq \tau/\sigma_0^2(x,y)\} = e^{-\tau/\sigma_0^2(x,y)}. \end{aligned}$$

This is also the probability that a node at (x,y) joins level-1.

Informally speaking, in an infinitesimal interval $dudv$ at location (u,v) there are $\rho P_1(u,v)dudv$ level-1 nodes. Each such node transmits with power P_r. The sum of signal powers at location (x,y) due to level-1 transmissions is

$$\sigma_1^2(x,y) = \iint_{\mathbb{S}} \underbrace{P_r\rho}_{=\bar{P}_r} P_1(u,v)\ell(x-u,y-v)dudv.$$

A node at (x,y) receives the level-1 transmission successfully with probability $e^{-\tau/\sigma_1^2(x,y)}$. The probability that a node at (x,y) joins level-2 is

$$\begin{aligned} P_2(x,y) &= \Pr\{\text{receives from level-1, does not receive from the source}\} \\ &= e^{-\tau/\sigma_1^2(x,y)}(1 - e^{-\tau/\sigma_0^2(x,y)}). \end{aligned}$$

What's done so far can be generalized as follows.

Definition Let $P_k(x,y)$ denote the probability that a node at location (x,y) joins level-k, and $\sigma_k^2(x,y)$ be the sum of signal powers from level-k at location (x,y). For $k = 1, 2, 3, \cdots$, the equations

$$P_k(x,y) = e^{-\tau/\sigma_{k-1}^2(x,y)} \prod_{n=0}^{k-2} (1 - e^{-\tau/\sigma_n^2(x,y)}), \tag{2.19}$$

$$\sigma_k^2(x,y) = \iint_{\mathbb{S}} \bar{P}_r P_k(u,v)\ell(x-u,y-v)dudv. \tag{2.20}$$

with the initial condition $\sigma_0^2(x,y) = P_s\ell(x,y)$ specify the *continuum model* for networks with random channels.

The functions P_k, σ_k^2 define a non-linear dynamical system which evolves with k. Analytical solution of the system appears to be a highly non-trivial problem. In order to gain intuition we evaluated (2.19) and (2.20) numerically for large L. Similar to the case of deterministic channels, it is observed that there exists a critical threshold τ^*. For $\tau > \tau^*$, the transmissions eventually die out, *i.e.,*

$$\sup_{\{x\geq 0,\ |y|\leq W/2\}} P_k(x,y) \to 0 \quad \text{as} \quad k\to\infty.$$

Otherwise, for $\tau < \tau^*$, the transmissions look like a *travelling wave* along the x-direction as $k\to\infty$, *i.e.,* there exists a function $P(\cdot,\cdot)$ and a period $T > 0$ such that

$$P_k(x,y) \approx P(x - Tk, y), \quad \forall x, y \quad \text{as} \quad k\to\infty.$$

The critical threshold τ^* appears to be close to the previous threshold $(\pi \ln 2)\bar{P}_r$. See Figs. 2.5 and 2.6.

We have the following result which gives a sufficient condition for the transmissions to die out as $k\to\infty$.

Theorem 4 *Consider the strip* $\mathbb{S} = \{(x,y) : x \geq 0, |y| \leq W/2\}$ *with* $L = \infty$. *If* $\tau > \left(\frac{4We^{-1}}{d_0}\right)\bar{P}_r$, *then the transmissions eventually die out, i.e.,*

$$\sup_{(x,y)\in\mathbb{S}} P_k(x,y) \to 0, \quad \text{as} \quad k\to\infty. \tag{2.21}$$

Proof We will first upper bound the $\sigma_k^2(x,y)$. First notice that $\ell(x,y) \leq \ell(x,0)$,

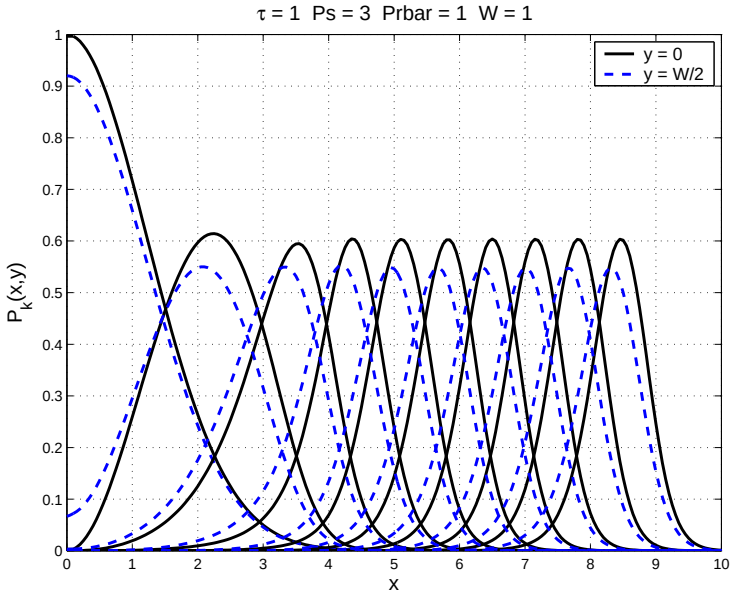

Figure 2.5: Transmissions become a travelling wave.

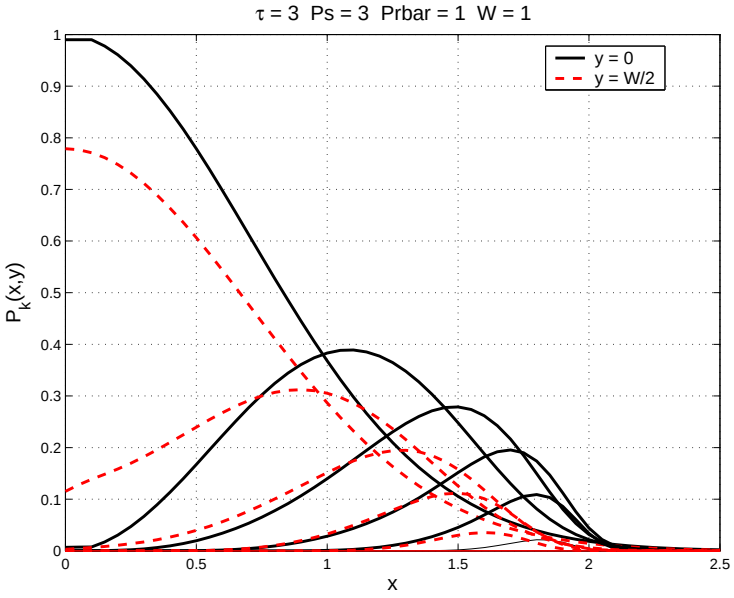

Figure 2.6: Transmissions die out.

$\forall x, y$. Using (2.20),

$$\begin{aligned}
\sigma_k^2(x,y) &\leq \iint_{\mathbb{S}} \bar{P}_r \left(\sup_{(u,v)\in\mathbb{S}} P_k(u,v) \right) \ell(x-u,0) du dv \\
&= \bar{P}_r \sup_{(u,v)\in\mathbb{S}} P_k(u,v) \int_0^L \int_{-W/2}^{W/2} \ell(x-u,0) dv du \\
&\leq \bar{P}_r \sup_{(u,v)\in\mathbb{S}} P_k(u,v) \int_{-\infty}^{\infty} \int_{-W/2}^{W/2} \ell(x-u,0) dv du \\
&= \bar{P}_r \sup_{(u,v)\in\mathbb{S}} P_k(u,v) \frac{4W}{d_0}, \qquad (2.22)
\end{aligned}$$

where (2.22) directly follows from the definition of g. Also, using (2.19) we can derive an upper bound for $P_{k+1}(x,y)$ in terms of $\sigma_k^2(x,y)$:

$$\begin{aligned}
P_{k+1}(x,y) &\leq e^{-\tau/\sigma_k^2(x,y)} \\
&\leq e^{-\tau/\sup_{(x,y)\in\mathbb{S}} \sigma_k^2(x,y)}, \qquad (2.23)
\end{aligned}$$

where the second inequality is because $e^{-\tau/x}$ is an increasing function of x.

Let $M_k = \sup_{(x,y)\in\mathbb{S}} P_k(x,y)$. Combining (2.22) and (2.23), we have the relation

$$M_{k+1} \leq e^{-\beta/M_k}, \qquad k = 1, 2, \cdots, \qquad (2.24)$$

where $\beta = \frac{\tau d_0}{4WP_r}$. The initial condition is that

$$\begin{aligned}
M_1 &= \sup_{(x,y)\in\mathbb{S}} P_1(x,y) \\
&= \sup_{(x,y)\in\mathbb{S}} e^{-\tau/\sigma_0^2(x,y)} \\
&= e^{-\tau/\sup_{(x,y)\in\mathbb{S}} \sigma_0^2(x,y)} \\
&= e^{-\tau d_0^2/P_s},
\end{aligned}$$

where we only used the definitions of $P_1(x,y), \sigma_0^2(x,y)$.

Next, we will show that any sequence $M_1, M_2, \cdots$ satisfying (2.24) converges to zero. To this end, consider a sequence $L_1, L_2, \cdots$ satisfying $L_{k+1} = e^{-\beta/L_k}$ with

the initial condition $L_1 = M_1$. We will first argue that $M_k \leq L_k, \quad \forall k$. This can be easily proved by induction:

i) $M_1 \leq L_1$ by the definition of L_1.

ii) Assume that $M_k \leq L_k$ for some k. Then,

$$M_{k+1} \leq e^{-\beta/M_k} \leq e^{-\beta/L_k} = L_{k+1},$$

because the function $e^{-\beta/x}$ is increasing in x.

Second, we will observe that $L_k \to 0$ as $k \to \infty$ if

$$1 > \frac{1}{\beta e} \quad \Leftrightarrow \quad \tau > \left(\frac{4We^{-1}}{d_0}\right)\bar{P}_r.$$

Observe that

$$\frac{L_{k+1}}{L_k} \leq \sup_{x \geq 0} \frac{e^{-\beta/x}}{x} = \frac{1}{\beta e}; \tag{2.25}$$

by differentiation it can be seen that the function $\frac{e^{-\beta/x}}{x}$ is maximized at $x = \beta$. Eqn. (2.25) shows that $L_{k+1} \leq \frac{L_1}{(\beta e)^k} \to 0$. The theorem follows.

2.5 Simulations

In this section we check the accuracy of continuum approximations in predicting the behavior of the random network. We first focus on the deterministic channel model. Then, the random channel model is discussed.

In Section 2.3, the boundaries between levels are approximated by straight lines. Under this approximation, we came to the conclusion that the signal flows in fixed steps after a transient period. First, we validate the fact that the flow is in approximately constant steps. Let $\tilde{r}_k$ denote the distance between nodes that are farthest to the source in level-k and in level-$(k-1)$ in the *random* network. To obtain a single number, we consider $\tilde{r}_k$ averaged over different realizations of

Table 2.1: Step-size convergence - Mean values

k	1	2	3	4	5	6	7
$\rho = 1$	10.69	6.15	5.02	4.52	4.59	4.49	4.47
$\rho = 5$	11.08	6.27	5.25	5.06	4.94	4.80	4.78
$\rho = 10$	11.13	6.33	5.35	5.02	4.99	4.92	4.90
$\rho = \infty$	11.18	6.35	5.38	5.09	5.01	4.97	4.96

Table 2.2: Step-size convergence - Standard Deviation

k	1	2	3	4	5	6	7
$\rho = 1$	0.48	1.30	1.37	1.29	1.32	1.38	1.59
$\rho = 5$	0.10	0.47	0.57	0.49	0.58	0.48	0.49
$\rho = 10$	0.05	0.32	0.31	0.35	0.36	0.30	0.36

the network. In Table 2.1, we show averaged $\tilde{r}_k$ for $\rho = 1, 5, 10$ over 100 random networks. The standard deviations are given in Table 2.2. The continuum result r_k is displayed under $\rho = \infty$ ($W = 2$, $L = 45$, $\tau = 0.2$, $\bar{P}_r = 1$, $P_s = 25$). The limiting step-size is $r_\infty = 4.96$. We see that continuum analysis gives an accurate approximation for the step size of each level.

In Table 2.3, we compare the average number of level-k nodes $|\mathcal{S}_k|$, with the continuum approximation $\rho W r_k$. Again, 100 random networks are simulated ($\tau = 0.4$, $\bar{P}_r = 1$, $P_s = 6$, $W = 2$, $L = 30$). Table 2.3 shows the ratio, $\frac{|\mathcal{S}_k|}{\rho W r_k}$, for $k = 1 \ldots 5$, and for $\rho = 5, 10, 50$. It is clearly seen that the ratio between the asymptotic value and the numerical average tend to 1 as the node density increases.

Fig. 2.7 shows one realization of a 500−node network. In particular, the

Table 2.3: The ratio $|\mathcal{S}_k|/\rho W r_k$ averaged over different realizations

k	1	2	3	4	5
$\rho = 5$	0.9351	0.9117	0.8913	0.8436	0.8466
$\rho = 10$	0.9232	0.8655	0.8435	0.8664	0.8615
$\rho = 50$	0.9931	0.9945	0.9801	0.9999	0.9883

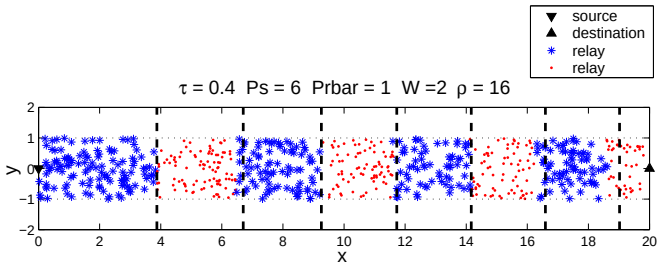

Figure 2.7: A realization of the random network

boundaries of the regions $\mathbb{S}_k$ (*i.e.,* the line $x = r_k$), $k = 1, \ldots 7$ are marked.

The step size in the continuum model is linear with the width of the strip W. Fig. 2.8 shows the expected $\tilde{r}_{10}$ as a function of W. Expectation is taken over 100 random networks for the 10^{th} level.

Fig 2.9 shows the probability of reaching the destination as a function of the threshold τ. The values are plotted for different network density. Here, $L = 15$, $W = 2$, $P_s = 5$, $\bar{P}_r = 1$. Clearly, the larger the τ, the smaller the probability of reaching to the destination. As ρ increases, the transition becomes sharper. When the network density is very high ($\rho = 50, 100$), we see an abrupt change around $\tau = 1.6$. The critical threshold obtained from the continuum model is $(\pi \ln 2)\bar{P}_r \approx 2.18$. We expect the threshold to shift towards 2.18 as ρ increases.

Next, we consider the random channel model. We simulate the random net-

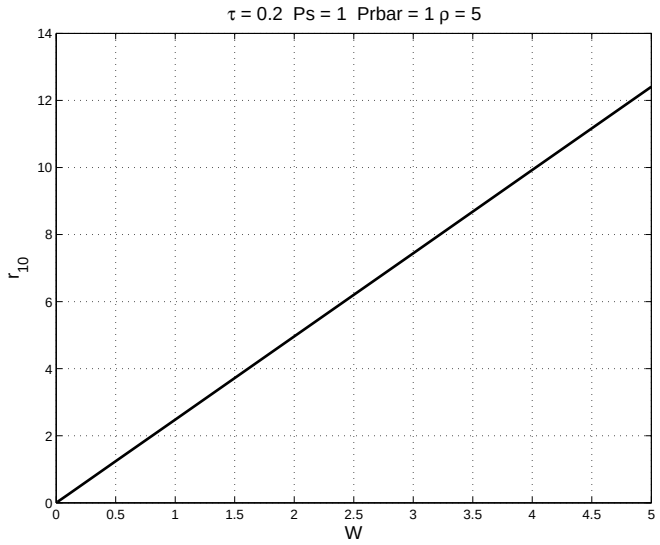

Figure 2.8: The expected $\tilde{r}_{10}$ vs. W

work, and obtain the empirical density of nodes at level-k with respect to the x coordinate. This together with the continuum result $P_k(x, 0)$ is shown for $\tau = 0.1$ and $\tau = 4$ in Figs. 2.10 and 2.11 respectively. The parameters are $W = 1$, $P_s = 5$, $\bar{P}_r = 1$, $\rho = 30$. In Fig. 2.10, the travelling wave behavior is observed as expected from the continuum model. On the other hand in Fig. 2.11, the transmissions die out. Notice that the continuum result $P_k(x, 0)$ is the smooth curve.

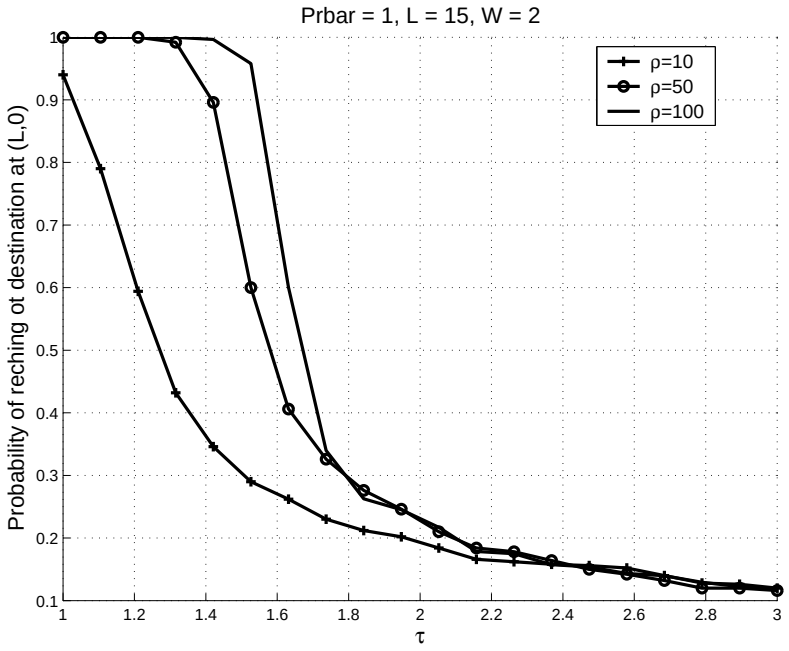

Figure 2.9: Probability of reaching the destination vs. τ

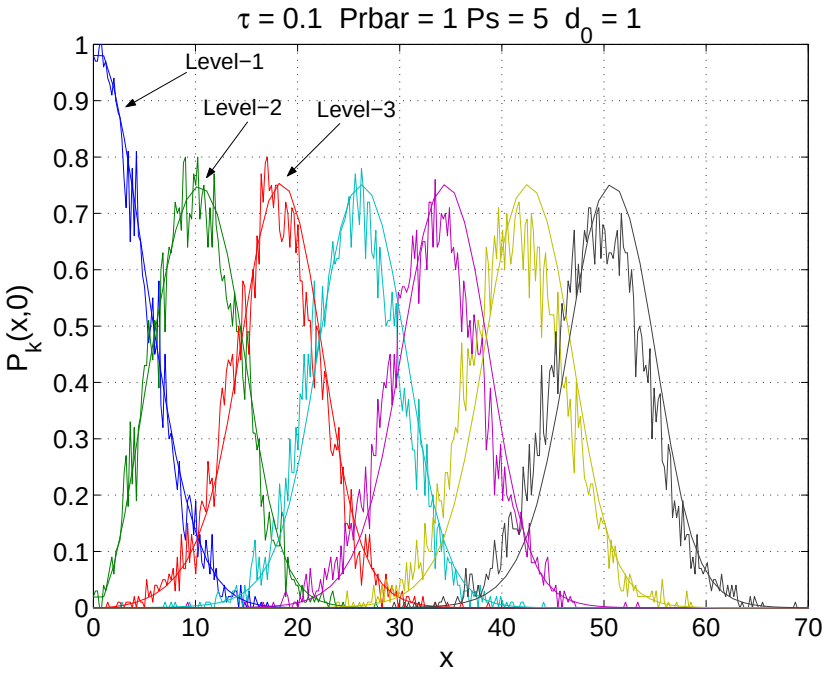

Figure 2.10: Travelling wave behavior

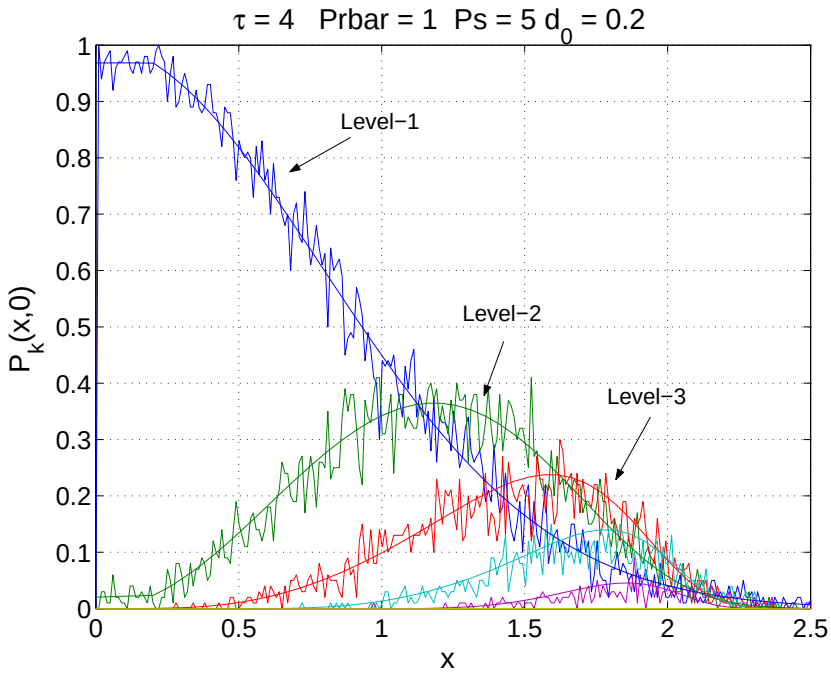

Figure 2.11: Transmissions die out

Appendix 2.A Proof of Lemma 1

i) First, let's prove that the function $f(y) := \int_y^{y+x} \frac{2}{u} \arctan(\frac{W}{2u})du$ is decreasing with respect to y. The derivative of $f(\cdot)$ is

$$f'(y) = \frac{2}{y+x} \arctan(\frac{W}{2(y+x)}) - \frac{2}{y} \arctan(\frac{W}{2y}).$$

By inspection it can be seen that $f'(y) < 0$. This proves that $f(\cdot)$ is decreasing. Notice that $f(0) = \infty$ and $f(\infty) = 0$. Thus, the equation $f(y) = \tau$ has a unique solution in terms of y.

ii) We know that $\int_{h(x)}^{h(x)+x} \frac{2}{u} \arctan(\frac{1}{2u})du = \frac{\tau}{P_r}$. By taking derivative of both sides with respect to x, we get

$$h'(x) = \frac{U(h(x)+x)}{U(h(x)) - U(h(x)+x)}, \tag{2.26}$$

where $U(x) := \frac{1}{x} \arctan(\frac{1}{2x})$. The derivative of $U(\cdot)$ is

$$U'(x) = \frac{-1}{x} \left(\frac{1}{x} \arctan(\frac{1}{2x}) + \frac{2}{4x^2+1} \right).$$

Since $U'(x) < 0$ for $x > 0$, $U(\cdot)$ is a decreasing function. This implies that $h'(x)$ is positive for $x > 0$. Thus, $h(\cdot)$ is increasing.

In order to simplify notation, we'll use h instead of $h(x)$. Next, we will prove that $h''(x) < 0$, which implies the concavity of $h(\cdot)$. Observe

$$h''(x) = \frac{(h'+1)U'(h+x)U(h) - U(h+x)U'(h)h'}{(U(h) - U(h+x))^2}.$$

In order to prove $h''(x) < 0$, we need to show that the numerator above is negative, *i.e.,*

$$(h'+1)U'(h+x)U(h) < U(h+x)U'(h)h'. \tag{2.27}$$

Since h' is positive, (2.27) is equivalent to

$$\frac{h'+1}{h'}U'(h+x)U(h) < U(h+x)U'(h). \tag{2.28}$$

Substitute (2.26), to get $\frac{h'+1}{h'} = \frac{U(h)}{U(h+x)}$. Hence, (2.28) is equivalent to

$$\frac{-U'(h+x)}{U^2(h+x)} > \frac{-U'(h)}{U^2(h)}.$$

It suffices to show that the function $l(x) := \frac{-U'(x)}{U^2(x)}$ is increasing. Substitute U to get

$$l(x) = \frac{\arctan(\frac{1}{2x}) + \frac{2x}{4x^2+1}}{\arctan^2(\frac{1}{2x})}.$$

It can be observed that this function is increasing. Therefore, $h(\cdot)$ is concave.

iii) We have

$$h'(0) = \lim_{x\to 0}\frac{h(x)-h(0)}{x} = \lim_{x\to 0}\frac{h(x)}{x}.$$

Apply the change of variables $v = u/x$ to the integral $\int_{h(x)}^{h(x)+x}\frac{2}{u}\arctan(\frac{1}{2u})du = \frac{\tau}{\bar{P}_r}$. Then

$$\int_{\frac{h(x)}{x}}^{\frac{h(x)}{x}+1}\frac{2}{v}\arctan(\frac{1}{2vx})dv = \frac{\tau}{\bar{P}_r}.$$

By taking the limit $x\to 0$,

$$\int_{h'(0)}^{h'(0)+1}\frac{2}{v}\lim_{x\to 0}\left\{\arctan(\frac{1}{2vx})\right\}dv = \frac{\tau}{\bar{P}_r}.$$

Since $\lim_{y\to\infty}\arctan(y) = \frac{\pi}{2}$,

$$\int_{h'(0)}^{h'(0)+1}\frac{\pi}{v}dv = \frac{\tau}{\bar{P}_r}.$$

Direct evaluation gives $h'(0) = 1/(e^{\frac{\tau}{\pi\bar{P}_r}}-1)$.

iv) From (2.26) observe that $h'(x)\to 0$ as $x\to\infty$. If $h'(0) > 1$, then $h(x) > x$ for $x > 0$ small enough. Since, $h(\cdot)$ is increasing and $h'(x)\to 0$, $h(x) < x$ for x

large enough. Since h is continuous, $h(x) = x$ for some $x > 0$. This fixed point is unique, since $h(\cdot)$ is increasing but not linear.

When $h'(0) < 1$, $h(x) < x$ for sufficient small $x > 0$. It follows from the concavity that $h(x) < x$ for all $x > 0$. Therefore, $h(x) = x$ can only happen at $x = 0$.

Chapter 3

Asymptotic Analysis of Multi-Stage Cooperative Broadcast

3.1 Organization

The organization of this chapter is as follows. In Section 3.2, the analysis of the network with the deterministic channel model is presented. In Section 3.3, the random channel model is derived and in Section 3.4 the continuum network behavior is characterized for the random channel models. In Section 3.5, simulation results are presented.

3.2 Network Behavior Under Deterministic Channel Model

In this section, we consider a simple *deterministic* model for modelling the received power of simultaneously transmitted signals. Suppose that every transmission with power P is received with power $P\ell(d)$ at distance d, where $\ell(.)$ is a *path-loss attenuation function*, which is assumed to be continuous and non-increasing (*e.g.,*

$\ell(d) = 1/d^2$). For convenience, we use the notation $\ell(x, y)$ to denote $\ell(\sqrt{x^2 + y^2})$.

In the deterministic channel model, it is assumed that if a set of relay nodes (say, level-n nodes = $\mathcal{L}_n$) transmits simultaneously, then node j receives with power

$$Pow(j) = P \sum_{i \in \mathcal{L}_n} \ell(d_{ij}) \tag{3.1}$$

where d_{ij} is the distance between the i'th and j'th nodes. In practice, this received power can be achieved via *maximal ratio combining* under the following scenarios: (i) the nodes in a given level transmit in orthogonal channels (as in TDMA or FDMA); (ii) the nodes use orthogonal or pseudo-orthogonal spreading codes with desirable correlation properties; (iii) simultaneously transmitting nodes employ a distributed orthogonal space-time code [10] designed for a large number of nodes.

3.2.1 Random Network

Suppose that N nodes are uniformly and randomly distributed in a disc with radius R and a single source is located at the center of a circular region. Let the source transmit with power P_s, and the relays transmit with power P_r. Let $\mathcal{S}$ denote the set of locations of relay nodes. The relay nodes decode and retransmit if and only if their SNR exceeds a certain threshold τ. Under the assumption that the channel noise is of unit power, the SNR threshold criterion is equivalent to a received power criterion, i.e.

$$Pow(j) \geq \tau.$$

At every broadcast step, the set of nodes with reception power exceeding τ, which has not transmitted so far, joins the next level. Therefore, the set of level-1 nodes

is given by

$$\mathcal{S}_1 = \{(x,y) \in \mathcal{S} : P_s \ell(x,y) \geq \tau\}. \tag{3.2}$$

Similarly, the set of level-k nodes for $k \geq 2$ is given by

$$\mathcal{S}_k = \{(x,y) \in \mathcal{S} \setminus \bigcup_{i=1}^{k-1} \mathcal{S}_i : \sum_{(x',y') \in \mathcal{S}_{k-1}} P_r \ell(x-x', y-y') \geq \tau\}. \tag{3.3}$$

When the node locations are random, a random number of nodes is reached by the source in every realization of the network. In order to study the effect of P_s, P_r and τ on the broadcast behavior, we will consider the continuum model, which is introduced next.

3.2.2 Continuum Network

Let $\mathbb{S} \triangleq \{(x,y) : x^2 + y^2 \leq R^2\}$ denote the disc containing the network. Let $\rho = N/\text{Area}(\mathbb{S})$ be the density [node/unit area] of relays within $\mathbb{S}$. In the continuum model, we are interested in the behavior of *high density* networks with *constant sum-power*. That is, the number of relays N goes to infinity, while $P_r N$ is fixed. This implies that the *relay power per unit area*

$$\bar{P}_r \triangleq \frac{P_r N}{\text{Area}(\mathbb{S})} = P_r \rho \tag{3.4}$$

is also fixed.

As the number of relays goes to infinity, the level-1 nodes become dense in the set

$$\mathbb{S}_1 \triangleq \{(x,y) \in \mathbb{S} : P_s \ell(x,y) \geq \tau\}.$$

Intuitively speaking, in this regime every infinitesimal area $dxdy$ in $\mathbb{S}_1$ contains $\rho dxdy$ nodes each with power P_r. Hence, the total transmission power from each

such infinitesimal area is $P_r\rho dxdy = \bar{P}_r dxdy$. Consequently, the level-2 nodes become dense in the set

$$\mathbb{S}_2 = \{(x,y) \in \mathbb{S} \setminus \mathbb{S}_1 : \iint_{\mathbb{S}_1} \bar{P}_r \ell(x-x', y-y')dx'dy' \geq \tau\}. \tag{3.5}$$

By recursion, it is seen that the level-k nodes, $k \geq 2$, become dense in

$$\mathbb{S}_k = \{(x,y) \in \mathbb{S} \setminus \bigcup_{i=1}^{k-1} \mathbb{S}_i : \iint_{\mathbb{S}_{k-1}} \bar{P}_r \ell(x-x', y-y')dx'dy' \geq \tau\}. \tag{3.6}$$

The sets $\mathbb{S}_1, \mathbb{S}_2, \cdots$ specify the continuum model.

The following theorem provides a rigorous relation between the random network and its continuum limit.

Theorem 5 *Let $\bar{P}_r$ and R be fixed, and*

$$P_r = \bar{P}_r/\rho, \qquad \rho = \frac{N}{\pi R^2} \tag{3.7}$$

be a function of N. For all $k \in \{1, 2, \cdots\}$ and open disc[1] $\mathbb{U} \subset \mathbb{R}^2$, the number of level$-k$ nodes in $\mathbb{U}$ scales as $\rho Area(\mathbb{U} \cap \mathbb{S}_k)$, i.e.,

$$\frac{|\mathbb{U} \cap \mathcal{S}_k|}{\rho Area(\mathbb{U} \cap \mathbb{S}_k)} \xrightarrow{\text{p}} 1 \quad as\ N \to \infty, \tag{3.8}$$

where $\xrightarrow{\text{p}}$ denotes convergence in probability.

Proof See Appendix 3.A.

[1] A set $\mathbb{U}$ is called an open disc if it is of the form $\{(x',y') : (x-x')^2+(y-y')^2 < z\}$ for some $(x,y) \in \mathbb{R}^2$ and $z > 0$. Although the proof in this thesis is only for disc shaped $\mathbb{U}$, the theorem actually holds for any *Jordan measurable* set $\mathbb{U}$ in $\mathbb{R}^2$. A set $\mathbb{U} \subset \mathbb{R}^2$ is called *Jordan measurable* if its area can be approximated by rectangles [53], *i.e.,* if $\sup \sum_i \text{Area}(U_i)$, where the supremum is over all disjoint rectangles (U_i's) inside $\mathbb{U}$, is equal to $\inf \sum_i \text{Area}(U_i)$, where the infimum is over all rectangles (U_i's) covering $\mathbb{U}$. The Jordan measure of a set, if exists, is the same as its Lebesgue measure.

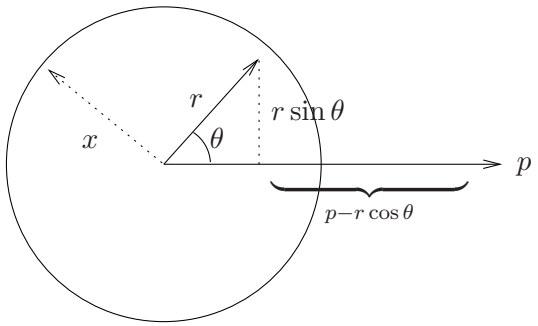

Figure 3.1: Illustration of $f(x,p)$.

Theorem 5 indicates that the locations of level-k nodes are approximately uniform in the set $\mathbb{S}_k$, when the network density is high. Choosing $\mathbb{U} = \mathbb{S}$ above suggests an approximation to the number of level-k nodes:

$$|\mathcal{S}_k| \approx \rho \text{Area}(\mathbb{S}_k), \quad \text{for large } N, \tag{3.9}$$

and an approximation to the total number of nodes reached by cooperative broadcast:

$$|\bigcup_{k=1}^{\infty} \mathcal{S}_k| \approx \rho \text{Area}(\bigcup_{k=1}^{\infty} \mathbb{S}_k), \quad \text{for large } N. \tag{3.10}$$

We will later demonstrate the validity of (3.9) and (3.10) also by simulation.

3.2.3 Explicit Characterization of Level Sets

In this section, we will give a more explicit characterization of the level sets $\mathbb{S}_1, \mathbb{S}_2, \cdots$ for general $\ell(\cdot)$ and for $\ell(d) = 1/d^2$. For ease of presentation, we will assume an unbounded network, *i.e.,* $R = \infty$. The results for $R < \infty$ follow trivially from the results in this section.

Lemma 2 *Define the function*

$$f(x,p) \triangleq \int_0^x \int_0^{2\pi} \ell(p - rcos\theta, rsin\theta) r d\theta dr. \tag{3.11}$$

Let $r_0, r_1, \cdots$ denote the solution of the recursive formula

$$f(r_{k-1}, r_k) - f(r_{k-2}, r_k) = \frac{\tau}{\bar{P}_r}, \qquad k = 2, 3, \cdots \tag{3.12}$$

with initial conditions $r_0 = 0,\ r_1 = \ell^{-1}(\frac{\tau}{P_s})$. If the solution of (3.12) exists, then each $\mathbb{S}_k$ is a disc shaped region *with inner and outer radii given by r_{k-1} and r_k, respectively.*

Proof The fact that each $\mathbb{S}_k$ is a disc follows from the assumption that the function $\ell(x, y)$ is circularly symmetric. If the solution of $P_s\ell(r_1) = \tau$ exists, then since $\ell(\cdot)$ is decreasing and continuous, $r_1 = \ell^{-1}(\frac{\tau}{P_s})$ forms the boundary of $\mathbb{S}_1$. Notice that the $\bar{P}_r f(x, p)$ is equal to the received power at a node with distance p from the source when a disc of radius x transmits (see Fig. 3.1). Hence, $\bar{P}_r[f(r_{k-1}, r_k) - f(r_{k-2}, r_k)]$ is the received power at a node with distance r_k from the source, when the *disc* between r_{k-2} and r_{k-1} transmits. If Eqn. (3.12) is satisfied, then the point r_k lies on the outer boundary of $\mathbb{S}_k$. The lemma follows.

Numerical solutions of $r_0,\ r_1, \cdots$ can be obtained from (3.12) for general path-loss models. In the following, we explicitly solve this recursive formula for the squared-distance path-loss model by simplifying it into an equivalent homogenous linear difference equation. The relation (3.12) does not seem to yield closed-form expressions for other path-loss models.

Theorem 6 *If $\ell(d) = \frac{1}{d^2}$, then $r_k = \sqrt{a_k}$, where the a_k depends on $\mu \triangleq \exp\left(\frac{\tau}{P_r \pi}\right)$ as follows.*

i) Case 1 ($\mu \leq 2$)*: The broadcast reaches to the whole network, i.e.,* $\lim_{k\to\infty} a_k = \infty$*, where*

$$a_k = \begin{cases} \frac{P_s(\mu-1)}{\tau(\mu-2)}\left(1 - \frac{1}{(\mu-1)^k}\right) & \text{if } \mu < 2 \\ \frac{P_s}{\tau}k & \text{if } \mu = 2. \end{cases} \tag{3.13}$$

ii) Case 2 ($\mu > 2$)*: The total area reached by the broadcast is bounded, i.e.,*

$$\lim_{k\to\infty} a_k = \frac{P_s(\mu-1)}{\tau(\mu-2)}, \tag{3.14}$$

where

$$a_k = \frac{P_s(\mu-1)}{\tau(\mu-2)}\left(1 - \frac{1}{(\mu-1)^k}\right). \tag{3.15}$$

Remark: Theorem 6 implies that the network behavior goes through a *phase transition* depending on the value of μ. If

$$\mu \leq 2 \quad \Leftrightarrow \quad \tau \leq (\pi \ln 2)\bar{P}_r, \tag{3.16}$$

i.e., the detection threshold is low enough with respect to the relay power per unit area, then the signal propagates to the whole network (see Fig. 3.2). On the other hand, if $\mu > 2$, then a finite portion of the network is reached, and from Theorem 5 the total number of nodes the message is delivered to is approximately equal to

$$|\bigcup_{k=1}^{\infty} \mathcal{S}_k| \approx \pi a_\infty \rho = \frac{\pi P_s \rho(\mu-1)}{\tau(\mu-2)}. \tag{3.17}$$

The right hand side of Eqn. (3.17) implies that the number of nodes reached by the broadcast is directly proportional to the source power.

Proof *(Theorem 6)* Under the squared distance path-loss model, $r_1 = \sqrt{\frac{P_s}{\tau}}$. Furthermore,

$$\begin{aligned} f(x,p) &= \int_0^x \int_0^{2\pi} \frac{r}{r^2 sin^2(\theta) + (p - r cos(\theta))^2} d\theta dr \\ &= \int_0^x \frac{2\pi r}{|p^2 - r^2|} dr \\ &= \pi \ln \frac{p^2}{|p^2 - x^2|}. \end{aligned} \tag{3.18}$$

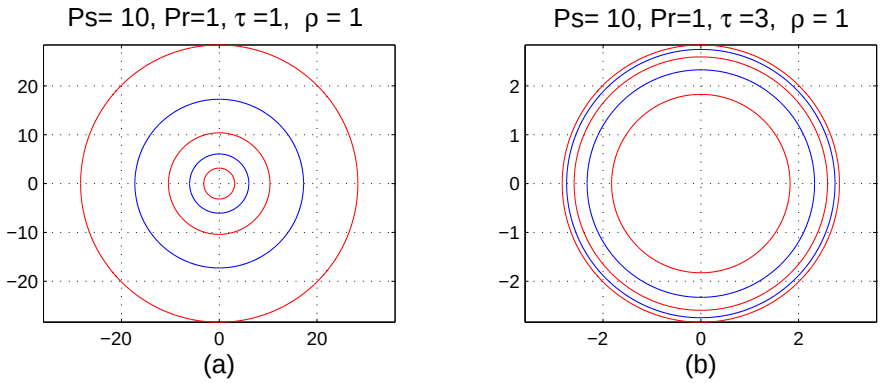

Figure 3.2: (a) Transmissions propagate. (b) Transmissions die off. Notice that the scale of (a) and (b) are vastly different.

Hence, (12) is equivalent to

$$f(r_{k-1}, r_k) - f(r_{k-2}, r_k) = \pi \ln \frac{|r_k^2 - r_{k-2}^2|}{|r_k^2 - r_{k-1}^2|} = \frac{\tau}{\bar{P}_r},$$

which yields

$$r_k^2 = \frac{r_{k-1}^2 \mu - r_{k-2}^2}{\mu - 1}, \quad k = 2, 3, \ldots.$$

Defining $a_k = r_k^2$, we get a linear difference equation:

$$a_{k+1} - \frac{\mu}{\mu - 1} a_k + \frac{1}{\mu - 1} a_{k-1} = 0 \tag{3.19}$$

with the initial conditions $a_0 = 0$ and $a_1 = \frac{P_s}{\tau}$.

Eqn. 3.19 can be solved as follows. Substituting $a_k = Aw^k$, we obtain

$$w^2 - \frac{\mu}{\mu - 1} w + \frac{1}{\mu - 1} = 0.$$

The roots are

$$w_1 = 1, \quad w_2 = \frac{1}{\mu - 1}.$$

If $\mu \neq 2$, the roots are different, and the solution is

$$a_k = A_1 + A_2 w_2^k, \tag{3.20}$$

where A_1 and A_2 have to be found from the initial conditions $a_0 = 0,\ a_1 = P_s/\tau$. The first condition implies $A_1 = -A_2 = A$, and the second one implies

$$A = \frac{P_s}{\tau}\left(\frac{\mu - 1}{\mu - 2}\right).$$

Thus, the solution is

$$a_k = \frac{P_s}{\tau}\frac{\mu - 1}{\mu - 2}(w_1^k - w_2^k).$$

If $\mu = 2$, then $w_1 = w_2 = 1$. In this case, (3.20) does not hold and the solution is of the form $a_k = A_1 + A_2 k$. Applying the boundary values, we get $A_1 = 0$ and

$$a_k = r_k^2 = \frac{P_s}{\tau}k. \tag{3.21}$$

The rest of the theorem follows by inspection of the solution.

3.2.4 Effect of Multihop Diversity

In this section, we analyze the phase transition behavior in the case of *multihop diversity*. In multihop diversity mode, each node stores the received signals from m previous levels and combines them via maximal ratio combining. The parameter m can be interpreted as the *memory* of the receiver. With multihop diversity, after the n-th level transmission, the reception power of node j is given by

$$Pow(j) = \sum_{i \in \bigcup_{l=(n-m+1)_+}^{n} \mathcal{L}_l} \frac{P_r}{d_{ij}^2}$$

where $(x)_+ \triangleq \max(0, x)$.

Theorem 7 *Consider the m-level multihop diversity network with the squared-distance path-loss model. The network exhibits two different behaviors depending on whether m is finite or infinite.*

i) If $m < \infty$, then the network goes through a phase transition at

$$\mu = m + 1 \quad \Leftrightarrow \quad \tau = (\pi \ln(m+1))\bar{P}_r \tag{3.22}$$

where $\mu = \exp\left(\frac{\tau}{\bar{P}_r \pi}\right)$ as before.

ii) If $m = \infty$, then there is no phase transition, and the message propagates to the whole network, i.e., $a_k \to \infty$, regardless of the value of τ.

Proof See Appendix 3.B.

Remark: Theorem 7 has a somewhat surprising implication: regardless of how low the $\bar{P}_r$ is, if the nodes accumulate and exploit all the transmissions before them, then the message will be delivered to the whole network. This result indicates that high-density cooperative networks with multihop diversity can indeed be very energy efficient as long as the network density is high enough.

Remark: In this section, we assume that the nodes retransmit if and only if the received SNR is above a threshold τ. We show that for the source message to propagate to the entire network, the condition $\tau \leq \tau_c$ (see Eqns. 3.16 and 3.22) should be satisfied. For a Gaussian channel, the threshold τ_c corresponds to information rate $\log(1 + \tau_c)$. Hence, we can interpret $\log(1 + \tau_c)$ as the maximum critical rate at which the information propagates to the entire network.

3.3 Derivation of Equivalent Channel Model for Fading Channels

A simplistic assumption we made in the previous section is that the power of simultaneously transmitted packets is equal to the sum of individual powers. This

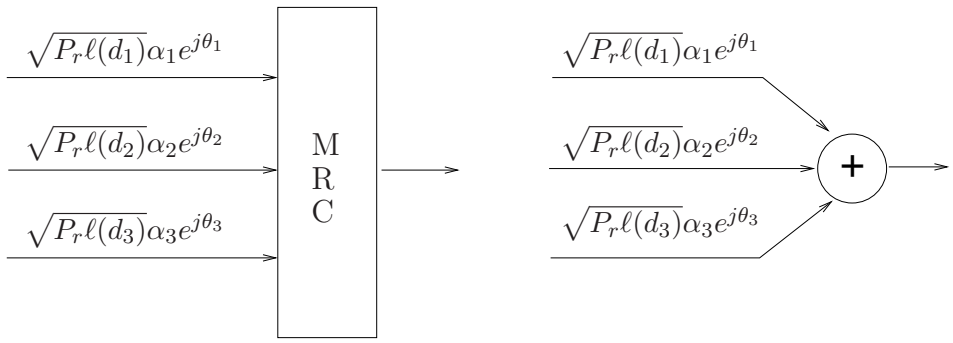

Figure 3.3: The reception models for random fading corresponding to orthogonal and non-orthogonal relay transmission.

assumption, however, does not hold if simultaneous transmissions are not in orthogonal dimensions. In this section, we first derive a *random channel model* in which the impulse response of simultaneously transmitted packets is modelled as a proper complex Gaussian random vector:

$$\mathbf{h} = \mathcal{N}_c(0, \tilde{\Sigma}), \tag{3.23}$$

where $\tilde{\Sigma}$ is a covariance matrix that depends on the network physical layer. The Gaussian channel assumption, *i.e., Rayleigh* distributed multi-path channel, is widely used in wireless communications [35]. In our setup, Gaussianity of $\mathbf{h}$ comes from the fact that there are many transmitters each with small power in the continuum asymptote. By choosing the $\tilde{\Sigma}$ appropriately, the model (3.23) can be used to take into account non-orthogonal narrowband transmissions, and in particular, the effects of channel fading, time differences between simultaneous transmissions and random phases. In sections 3.3.1 and 3.3.2, we provide a rigorous derivation of (3.23) and find the covariance matrix $\tilde{\Sigma}$ as a function of network physical layer parameters. The network behavior with the random channel model is analyzed in Section 3.4.

We also consider the case that the transmitted signals go through orthogonal *fading* channels, and the receiver does maximal ratio combining of channel outputs (Fig. 3.3). Interestingly, in the continuum limit the equivalent channel converges to a deterministic constant, despite the existence of fading. We discuss this convergence in Section 3.3.3. The behavior of the networks with orthogonal transmissions and non-orthogonal transmissions is compared in Section 3.4.

3.3.1 Transmitted and Received Signals for Non-orthogonal Transmissions

Consider a group of relay nodes $\mathcal{L}$ that transmit the same message simultaneously. Suppose that the message consists of M complex-valued samples $c[1], \cdots, c[M]$. Assume that all nodes in the network use an identical pulse-shaping filter $p(t)$. The base-band transmitted signal by the l'th node is modelled as

$$s^{(l)}(t) = \sqrt{P_r} \sum_{m=1}^{M} c[m] p(t - t_l - mT), \tag{3.24}$$

where T is the symbol period; t_l is the time the l'th node starts its transmission (*i.e.,* the relay time).

Consider a hypothetical node H at a given location (x, y). Let v_c denote the speed of light. The base-band received signal at node H is modelled as

$$r(t) = \sum_{l \in \mathcal{L}} \alpha_l e^{j\theta_l} \sqrt{\ell(d_l)} s^{(l)}(t - \frac{d_l}{v_c}) + w(t) \tag{3.25}$$

where α_l is the fading coefficient between nodes l and H; θ_l is the phase difference between modulator and demodulator clocks at nodes l and H; d_l is the distance between nodes l and H; d_l/v_c is the propagation delay; $w(t)$ is additive channel noise.

We assume that the broadcast signal is narrowband, *i.e.,* the coherence bandwidth of equivalent link provided to the relays is much larger than the transmission bandwidth. Hence in the following, we neglect the propagation delays d_l/v_c in (3.25).

After sampling at the symbol rate, the baseband received signal becomes

$$r[n] \triangleq r(nT) = \sum_{m=0}^{M-1} c[m] \sum_{l \in \mathcal{L}} \sqrt{P_r}\beta_l p_l[n-m] + w[n] \tag{3.26}$$

where

$$\beta_l \triangleq \sqrt{\ell(d_l)}\alpha_l e^{j\theta_l} \tag{3.27}$$

$$p_l[n-m] \triangleq p(nT - t_l - mT). \tag{3.28}$$

For consistency with the previous section, we will assume that $w[\cdot]$ is white with unit power. If we define the channel coefficients as

$$h[n] \triangleq \sqrt{P_r} \sum_{l \in \mathcal{L}} \beta_l p_l[n], \tag{3.29}$$

then the received signal can be compactly represented as

$$r[n] = h[n] * c[n] + w[n]. \tag{3.30}$$

In the following, $h[n], n = 0, \pm 1, \pm 2, \cdots$ will be referred to as the *equivalent channel impulse response* of the cooperative channel. We will also assume that the $h[n]$ is practically non-zero only for $2D+1$ terms, $h[-D], \cdots, h[D]$, and is zero elsewhere.

3.3.2 Asymptotic Channel Distribution

The set $\mathcal{L}$ is viewed as the set of nodes belonging to a certain level of broadcast. For tractability purposes, we make the following assumptions:

i) The locations of the nodes in $\mathcal{L}$ are independent and identically distributed (i.i.d.), and therefore, the distances d_l's are i.i.d. for different l.

ii) The starting times t_l's, $l \in \mathcal{L}$ are *zero-mean* i.i.d. distributed with a certain pdf $f(t)$. This models the situation that all the nodes in the same level transmit approximately around time zero, but there may be small variations due to differences between processing/relaying times at different nodes.

iii) The fading coefficients α_l's are i.i.d. with unit variance for different $l \in \mathcal{L}$. The phases θ_l are i.i.d. Uniform$[0, 2\pi]$ (*i.e.,* the modulator/demodulator clocks at different nodes are asynchronous).

iv) The $d_l,\ t_l,\ \alpha_l,\ \theta_l,\ l \in \mathcal{L}$ are independent.

The next theorem characterizes the asymptotic distribution of the channel.

Theorem 8 *Let L denote the number of nodes in $\mathcal{L}$. Suppose that the relay power P_r varies with L, and the total relay power converges to P_T as $L\to\infty$, i.e.,*

$$LP_r \to P_T, \quad \text{as } L\to\infty. \tag{3.31}$$

Let $\mathbf{h} \triangleq (h[-D], \cdots, h[D])$. Then, under assumptions i)-iv), the channel impulse response $\mathbf{h}$ satisfies

$$\mathbf{h} \xrightarrow{\mathrm{d}} \mathcal{N}_c(0, P_T\mathbb{E}\{\ell(d_l)\}\Sigma) \quad \text{as } L\to\infty, \tag{3.32}$$

where $\xrightarrow{\mathrm{d}}$ denotes convergence in distribution, and Σ is a matrix with entries

$$\Sigma[n, m] = \int_{-\infty}^{\infty} f(t)p(nT - t)p^*(mT - t)dt,$$

for $n,\ m \in \{-D, \cdots, D\}$.

Proof Rearrange $h[n]$ to get

$$h[n] = \sqrt{LP_r}\left[\frac{h[n]}{\sqrt{LP_r}}\right] = \sqrt{LP_r}\left[\frac{1}{\sqrt{L}}\sum_{l\in\mathcal{L}}\beta_l p_l[n]\right] \tag{3.33}$$

Here, the first quantity converges to $\sqrt{P_T}$ as $L\to\infty$, and the expression inside the parenthesis is the addition of L i.i.d. copies of the same signal divided by $\sqrt{L}$. We will use the Multivariate Central Limit Theorem (CLT) [53] to obtain (3.32). In order to apply CLT, observe that $\mathbb{E}\{\beta_l p_l[n]\} = 0$, since each β_l has zero mean. Furthermore, the autocovariance of $(\beta_l p_l[n] : -D \le n \le D)$ is given by

$$\begin{aligned} R[n,m] &= \mathbb{E}\{\beta_l\beta_l^* p_l[n]p_l^*[m]\} \\ &= \mathbb{E}\{|\beta_l|^2\}\mathbb{E}\{p_l[n]p_l^*[m]\} \\ &= \mathbb{E}\{\ell(d_l)\}\Sigma[n,m]. \end{aligned} \tag{3.34}$$

On the other hand, the pseudo autocovariance of $(\beta_l p_l[n] : -D \le n \le D)$ is

$$\bar{R}[n,m] = \mathbb{E}\{\beta_l^2\}\mathbb{E}\{p_l[n]p_l[m]\} = 0, \tag{3.35}$$

because each θ_l is Uniform$[0, 2\pi]$. Eqn. 3.35 implies that $(\beta_l p_l[n] : -D \le n \le D)$ is proper complex. From Multivariate CLT, we get that

$$\frac{\mathbf{h}}{\sqrt{LP_r}} \xrightarrow{\text{d}} \mathcal{N}_c(0, \mathbb{E}\{\ell(d_l)\}\Sigma).$$

The theorem follows.

3.3.3 Orthogonal Transmissions over Fading Channels

Another possibility is to consider the above model under the assumption that the transmissions are in orthogonal channels (*e.g.,* as in FDMA). In this scenario, for simplicity, we will assume that the receiver can perfectly recover the timing of each

transmitted signal and sample it at time zero. Hence, the sampled received signal from the l'th node is

$$r_l[n] = \sum_{m=0}^{M} c[m]\sqrt{P_r}\beta_l p[n-m] + w_l[n], \tag{3.36}$$

where $p[n-m] \triangleq p(nT - mT)$, and $w_l[n]$ is the noise in the l'th orthogonal channel. We assume that each $w_l[\cdot]$ is white with unit power, and is independent of one another.

If a Nyquist pulse $p(\cdot)$ is used, the signal $r_l[\cdot]$ has no intersymbol interference (*i.e.,* $p[n-m] = p(0)\delta[n-m]$). Consequently, maximal ratio combining of $r_l[\cdot],\ l \in \mathcal{L}$ gives the highest SNR:

$$\text{SNR} = P_r \sum_{l\in\mathcal{L}} |\beta_l|^2 |p(0)|^2. \tag{3.37}$$

Theorem 9 *Under assumptions i)-iv) and (3.31), the SNR of the maximal-ratio-combined received signal converges to a deterministic limit as $L\to\infty$, i.e.,*

$$SNR \to P_T \mathbb{E}\{\ell(d_l)\}|p(0)|^2, \qquad as\ L\to\infty, \tag{3.38}$$

almost surely.

Remark: Notice that the bandwidth requirement of the orthogonal system is proportional to L if FDMA or CDMA type signaling is used. Hence, taking the limit $L\to\infty$ without sacrificing from the transmission rate requires potentially infinite bandwidth, *i.e.,* the network operates in the wideband regime. On the other hand, by using distributed orthogonal space-time codes, it may be possible to get to the above performance without sacrificing bandwidth.

Proof Notice that

$$\text{SNR} = LP_r \left[\frac{1}{L}\sum_{l\in\mathcal{L}} |\beta_l|^2 |p(0)|^2\right].$$

Here, the first term converges to P_T and the second term converges almost surely to its mean due to the strong law of large numbers. The theorem follows.

The theorem indicates that the system with orthogonal channels, despite the existence of fading and randomness in the channel, has a deterministic SNR in the limit. As we will see in the next section, this property greatly simplifies the analysis in certain cases.

3.4 Network Behavior with Random Channels

In this section, we derive the continuum model for networks with random channels. Following the order of presentation in Section 3.2, we will first describe the network with random topology, and obtain its continuum model in the limit. This will be done both for orthogonal and non-orthogonal transmission models described in Section 3.3.1. The broadcast performance of these models will be compared in Section 3.4.5.

3.4.1 Random Network

Consider a network with N relay nodes located in the disc $\mathbb{S}$, where the source is located at the center. For a subset of relay nodes $\mathcal{L} \subset \{1, \cdots, N\}$, let

$$\mathbf{h}_{\mathcal{L}}(x,y) = \begin{cases} \sqrt{P_r} \sum_{l \in \mathcal{L}} \beta_l(x,y)\mathbf{p}_l, & \text{non-orthogonal} \\ \sqrt{P_r}\sqrt{\sum_{l \in \mathcal{L}} |\beta_l(x,y)|^2}\mathbf{p}, & \text{orthogonal} \end{cases} \tag{3.39}$$

be the channel impulse response vector from level set $\mathcal{L}$ to a hypothetical node at (x,y) in the non-orthogonal and orthogonal channel models. In (3.39), we made the dependence on the location of the receiving node (x,y) explicit wherever possible. Here, $\mathbf{p}_l = (p(nT - t_l) : -\infty < n < \infty)$ refers to the pulse shaping filter delayed by

t_l sampled at the Nyquist rate, and $\mathbf{p} = (p(0)\delta[n] : -\infty < n < \infty)$ is the sampled filter without delay. For the source transmission, the channel impulse response is

$$\mathbf{h}_0(x, y) = \sqrt{P_s}\beta_0(x, y)\mathbf{p} \tag{3.40}$$

for both the non-orthogonal and orthogonal transmissions.

The decision criterion of when to relay packets is a subtle issue in intersymbol interference channels. In practice, the packets are coded according to a certain channel code, and CRC (Cylic Redundancy Check) bits are placed into each packet. A packet reception is considered successful if the CRC test passes after decoding the channel code. A simple way to model this phenomena is via the notion of matched-filter upper bound $||\mathbf{h}_{\mathcal{L}}(x, y)||^2$ on received SNR, *i.e.,* to consider a reception successful if $||\mathbf{h}_{\mathcal{L}}(x, y)||^2$ exceeds a certain threshold τ. A more elaborate model for receptions can be derived based on the notion of outage capacity (*i.e.,* a reception is considered successful if the instantaneous mutual information of the equivalent channel exceeds a certain threshold). However, in this thesis we will focus on the simpler matched-filter upper bound approach.

Let $\mathcal{S} = \{(x_i, y_i) : i = 1, \cdots, N\}$ be the set of relay nodes that are randomly and uniformly distributed in $\mathbb{S}$. If the channel is random, then the set of level-1 nodes is given by

$$\mathcal{S}_1 = \{(x, y) \in \mathcal{S} : ||\mathbf{h}_0(x, y)||^2 \geq \tau\}.$$

The locations of the level-k nodes are given by

$$\mathcal{S}_k = \{(x, y) \in \mathcal{S} \setminus \bigcup_{i=1}^{k-1} \mathcal{S}_i : \ ||\mathbf{h}_{\mathcal{L}_{k-1}}(x, y)||^2 \geq \tau\}, \tag{3.41}$$

where $\mathcal{L}_{k-1} \subset \{1, \cdots, N\}$ is the index set of level $k-1$ nodes.

Throughout this section, we will assume that t_l's are i.i.d. for different l, $\alpha_l(x, y)$'s are i.i.d. for different l and (x, y); so are $\theta_l(x, y)$'s. Moreover, t_l's are

zero-mean with pdf $f(t)$, $\theta_l(x,y)$'s are Uniform$[0,2\pi]$, and $\alpha_l(x,y)$, t_l and $\theta_l(x,y)$'s are independent from one another. These assumptions extend ii)-iv) in Section 3.3.2 considering the spatial domain (x,y) as well as the node index l. We assume spatially independent fading for its simplicity. For correlated fading scenarios, refer to Section 3.4.7.

3.4.2 Continuum Network

In this section, we derive the continuum model for the network with random channels using the channel asymptotics derived in Section 3.3.

In the random network, a node at location (x,y) receives the source transmission successfully with probability

$$P_1(x,y) = \Pr\{||\mathbf{h}_0(x,y)||^2 \geq \tau\}.$$

This is also the probability that a node at (x,y) joins level-1. It follows from the law of large numbers that for each measurable set $\mathbb{U} \subset \mathbb{S}$, the number of level-1 nodes in $\mathbb{U}$ scales as $\iint_{\mathbb{U}} \rho P_1(x',y')dx'dy'$, *i.e.,*

$$\frac{|\mathbb{U} \cap \mathcal{S}_1|}{\iint_{\mathbb{U}} \rho P_1(x',y')dx'dy'} \to 1 \quad \text{as } \rho \to \infty \tag{3.42}$$

almost surely. When $P_r\rho$ is fixed to $\bar{P}_r$, the total transmit power of level-1 nodes $P_r|\mathbb{U} \cap \mathcal{S}_1|$ converges to

$$P_T \;=\; \iint_{\mathbb{S}} \bar{P}_r P_1(x',y')dx'dy' \tag{3.43}$$

almost surely. Furthermore, the locations of level-1 nodes are distributed according to the density $\tilde{\rho}(x',y') \triangleq \frac{P_1(x',y')}{\iint_{\mathbb{S}} P_1(x',y')dx'dy'}$. Hence,

$$\mathbb{E}\{\ell(d_l(x,y))\} = \iint_{\mathbb{S}} \tilde{\rho}(x',y')\ell(x-x',y-y')dx'dy', \tag{3.44}$$

for all $l \in \mathcal{L}_1$, and the total received power at location (x, y) due to level-1 transmissions is

$$\begin{aligned} \sigma_1^2(x,y) &\triangleq P_T \mathbb{E}\{\ell(d_l(x,y))\} \\ &= \iint_{\mathbb{S}} \bar{P}_r P_1(x',y') \ell(x-x', y-y') dx' dy'. \end{aligned} \tag{3.45}$$

If this $\sigma_1^2(x,y)$ is substituted into Theorems 8 and 9, we see that a node at (x,y) receives the level-1 transmission successfully with probability $\Pr\{||\mathbf{h}_1(x,y)||^2 \geq \tau\}$, where

$$\begin{aligned} \mathbf{h}_1(x,y) &\sim \mathcal{N}_c(0, \sigma_1^2(x,y)\Sigma), \quad \text{non-orthogonal} \\ ||\mathbf{h}_1(x,y)||^2 &= \sigma_1^2(x,y)|p(0)|^2, \quad \text{orthogonal} \end{aligned}$$

is the equivalent channel distribution in the limit that the number of level-1 nodes goes to infinity. The probability that a node at (x,y) joins level-2 is

$$\begin{aligned} P_2(x,y) &= \Pr\{\text{receives from level-1, does not receive from the source}\} \\ &= \Pr\{||\mathbf{h}_1(x,y)||^2 \geq \tau\} \; [1 - \Pr\{||\mathbf{h}_0(x,y)||^2 \geq \tau\}]. \end{aligned} \tag{3.46}$$

Now, we can generalize what is done so far.

Definition Let $P_k(x,y)$ denote the probability that a node at location (x,y) joins level-k, and $\sigma_k^2(x,y)$ be the sum of signal powers from level-k at location (x,y). For $k = 1, 2, 3, \cdots$, the equations

$$P_{k+1}(x,y) = \Pr\{||\mathbf{h}_k(x,y)||^2 \geq \tau\} \prod_{i=0}^{k-1} [1 - \Pr\{||\mathbf{h}_i(x,y)||^2 \geq \tau\}], \tag{3.47}$$

$$\sigma_k^2(x,y) = \iint_{\mathbb{S}} \bar{P}_r P_k(x',y') \ell(x-x', y-y') dx' dy', \tag{3.48}$$

where

$$\begin{aligned} \mathbf{h}_k(x,y) &\sim \mathcal{N}_c(0, \sigma_k^2(x,y)\Sigma), \quad \text{non-orthogonal} \\ ||\mathbf{h}_k(x,y)||^2 &= \sigma_k^2(x,y)|p(0)|^2, \quad \text{orthogonal} \end{aligned}$$

specify the *continuum model* for networks with random channels.

The functions P_k, σ_k^2 define a non-linear dynamical system which evolves with k. Although the analytical solution of this system is hard, it can be usually evaluated numerically. Another property of the continuum model is that the $P_k(x,y)$ and $\sigma_k^2(x,y)$ are only functions of $r = \sqrt{x^2+y^2}$. Therefore, the above dynamical system evolves only over 1-dimensional functions. For convenience, we will use the notations $P_k(x,y)$ and $P_k(r)$ interchangeably.

For our numerical evaluations in this section, we will use the following path-loss model

$$\ell(d) \triangleq \begin{cases} 1/d^2 & d_0 \leq d \\ 1/d_0^2 & 0 \leq d \leq d_0, \end{cases} \tag{3.49}$$

with a small $d_0 > 0$ to avoid the singularity in the integral (3.48). The squared-distance attenuation model $\ell(d) = 1/d^2$ comes from the free-space attenuation of electromagnetic waves, and it *does not* hold when d is very small [50]. This issue has been recognized by several researchers (*e.g.,* [42, 51]). We expect the results obtained from (3.49) to be more practically relevant.

3.4.3 Behavior of Continuum Network with Orthogonal Channels

The above equations for continuum network greatly simplify in case of orthogonal channels. There are two possibilities:

i) If there is no fading from the source to the relays, then $P_1(x,y)$ is binary (*i.e.,* $P_1(x,y) \in \{0,1\}$). Furthermore, each $\sigma_k^2(x,y)$ for $k = 2, 3, \cdots$ is deterministic. Therefore, $\Pr\{||\mathbf{h}_k(x,y)||^2 \geq \tau\}$ is binary as well. If we define

$$\mathbb{S}_k \triangleq \{(x,y) \in \mathbb{S} : P_k(x,y) = 1\},$$

then

$$\sigma_k^2(x,y) = \iint_{\mathbb{S}_k} \bar{P}_r \ell(x'-x, y'-y) dx' dy'.$$

Hence, for this scenario the continuum model reduces to the continuum model for deterministic channels.

ii) If the channels from the source to relays have fading, then $P_1(x,y)$ takes continuous values in $[0,1]$, but $\Pr\{||\mathbf{h}_k(x,y)||^2 \geq \tau\}$ is still binary. In our numerical evaluations we observed that the effect of $P_1(x,y)$ is transient, and the asymptotic behavior of the network is as in the deterministic model. In Fig. 3.4 and 3.5, we plot $P_k(r)$ in both low and high threshold regimes.

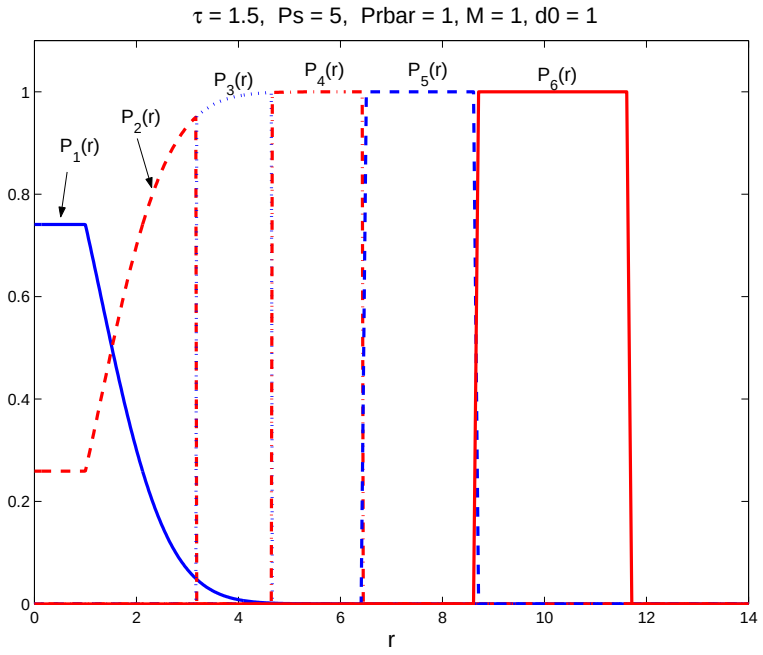

Figure 3.4: The parameters are $\tau = 1.5, P_s = 5, \bar{P}_r = 1, d_0 = 1, \Sigma = 1$. The transmissions continue.

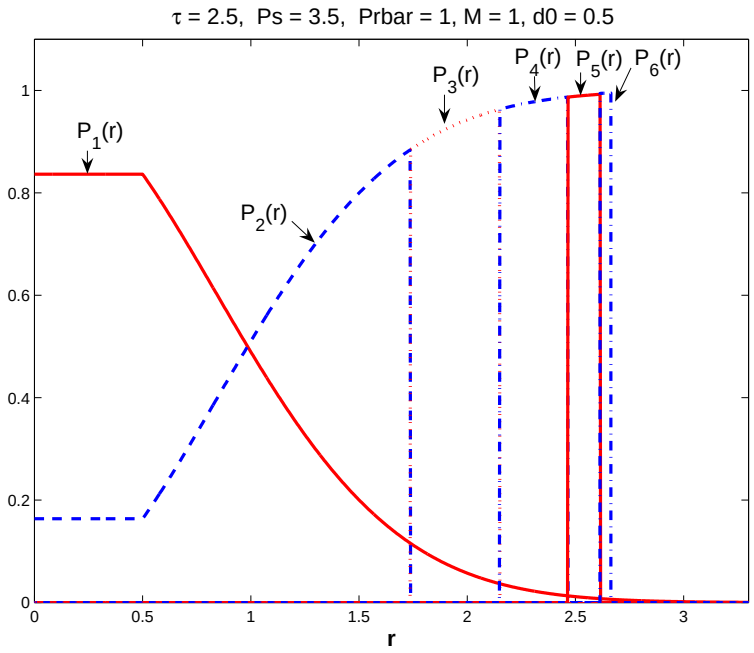

Figure 3.5: The parameters are $\tau = 2.5, P_s = 3.5, \bar{P}_r = 1, d_0 = 0.5, \Sigma = 1$. The transmissions die out.

3.4.4 Behavior of Continuum Network with Non-orthogonal Channels

The following lemma simplifies the task of computing $\Pr\{||\mathbf{h}_k(x,y)||^2 \geq \tau\}$ for non-orthogonal transmissions.

Lemma 3 *Let $\lambda_1, \cdots, \lambda_M$ denote the distinct eigenvalues of Σ with multiplicities $a_1, \cdots, a_M$, respectively. The characteristic function of $||\mathbf{h}_k(x,y)||^2$, where $\mathbf{h}_k(x,y) \sim \mathcal{N}(0, \sigma_k^2(x,y)\Sigma)$, is given by*

$$\Phi_k(jw) = \prod_{i=1}^{M} \frac{1}{(1 + jw\lambda_i\sigma_k^2(x,y))^{a_i}}. \tag{3.50}$$

Let $\Phi_k(jw)$ have the partial fraction expansion

$$\Phi_k(jw) = \sum_{i=1}^{M} \sum_{m=1}^{a_i} \frac{A_{im}}{(1 + jw\lambda_i\sigma_k^2(x,y))^{m}}. \tag{3.51}$$

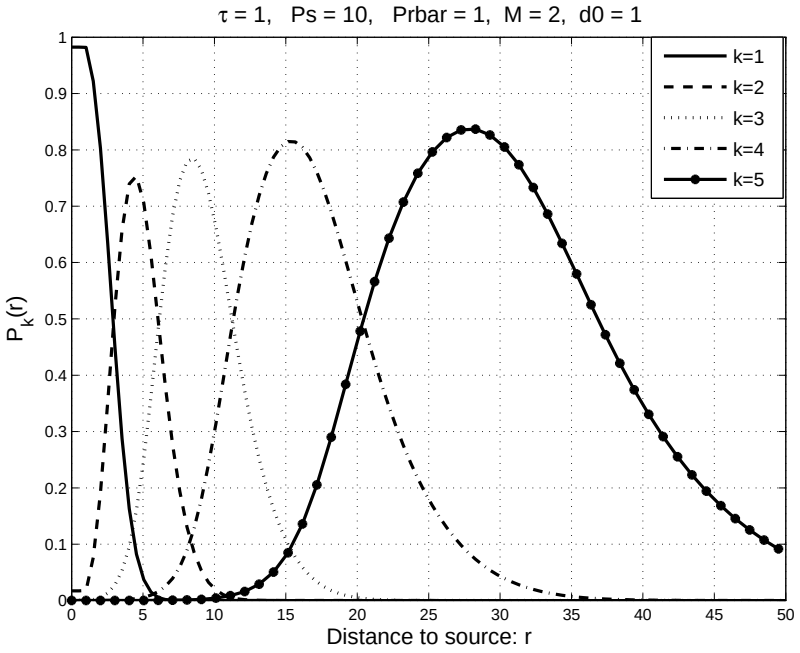

Figure 3.6: Transmissions continue. The parameters are $\tau = 1, P_s = 10, \bar{P}_r = 1, M = 2, d_0 = 1, \Sigma = \frac{1}{M}\mathbf{I}$, where $\mathbf{I}$ is the identity matrix.

Then,

$$\Pr\{||\mathbf{h}_k(x,y)||^2 \geq \tau\} = \sum_{i=1}^{M}\sum_{n=1}^{a_i} \frac{A_{in}}{(n-1)!}\Gamma(n, \frac{\tau}{\lambda_i \sigma_k^2(x,y)}), \tag{3.52}$$

where $\Gamma(a,x) = \int_x^\infty e^{-t}t^{a-1}dt$. *If the eigenvalues of* Σ *are distinct, then the above expression simplifies to*

$$\Pr\{||\mathbf{h}_k(x,y)||^2 \geq \tau\} = \sum_{i=1}^{M} A_{i1}e^{-\tau/\sigma_k^2(x,y)\lambda_i}. \tag{3.53}$$

Remark: Computation of the right hand side of (3.52)-(3.53) can be done in two steps. First, apply an eigenvalue decomposition to Σ to obtain $\lambda_1, \cdots, \lambda_M$. Then, apply partial fraction expansion to (3.50) to get A_{im}'s.

Proof The proof can be easily done utilizing well-known techniques [54].

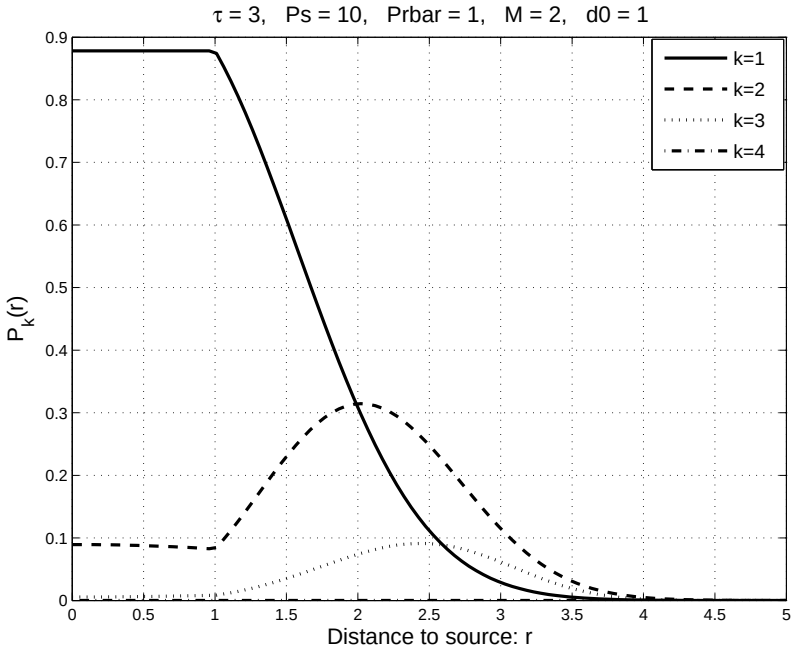

Figure 3.7: Transmissions die out. The parameters are $\tau = 3, P_s = 10, \bar{P}_r = 1, M = 2, d_0 = 1, \Sigma = \frac{1}{M}\mathbf{I}$, where $\mathbf{I}$ is the identity matrix.

The analytical solution of the continuum network in the case of non-orthogonal channels appears to be a non-trivial problem. In order to gain intuition, we evaluated (3.47) and (3.48) numerically for large R. Similar to the case of deterministic channels, it is observed that there exists a critical threshold τ_c. For $\tau > \tau_c$, the transmissions eventually die out, *i.e.,*

$$\sup_{(x,y)\in\mathbb{R}^2} P_k(x,y) \to 0 \quad \text{as} \quad k \to \infty.$$

Otherwise, the transmissions propagate to the whole network, while the level curves, $P_k(r), r \in \mathbb{R}$, become wider as k increases. See Figs. 3.6 and 3.7 for these two regimes.

In general, we do not have an explicit characterization of τ_c. However, the following Theorem gives a sufficient condition for the transmissions to die out.

Theorem 10 *Consider an infinite disc (i.e.,* $\mathbb{S} = \mathbb{R}^2$*). If the path-loss model satisfies*

$$\iint_{\mathbb{R}^2} l(x', y')dx'dy' < \infty, \tag{3.54}$$

then there exists $\tau_c < \infty$ *such that if* $\tau > \tau_c$*, then the transmissions eventually die out, i.e.,*

$$\sup_{(x,y)\in\mathbb{R}^2} P_k(x, y) \to 0, \quad as \quad k \to \infty. \tag{3.55}$$

Remark: Condition (3.54) does not hold for (3.49). However, it is satisfied for all $\ell(d) = \min\{1/d_0^u, 1/d^u\}, \quad u > 2, \ d_0 > 0$.

Proof See Appendix 3.C.

3.4.5 Comparison between non-orthogonal and orthogonal cooperative broadcast

In this section, we compare the message propagation behavior in random orthogonal and random nonorthogonal channels. Fig. 3.8 shows the $P_k(r)$ for both models. These plots are obtained for the parameters $\tau = 1, P_s = 5, \bar{P}_r = 1, M = 1, d_0 = 1$.

For both orthogonal and non-orthogonal models, $P_1(\cdot)$ is the same; however, the level curves $P_k(\cdot)$ differ significantly for large k. In particular, the level curves in the non-orthogonal case move faster. This is a rather counter-intuitive result, because the orthogonal system (with FDMA/CDMA) uses much more bandwidth than the non-orthogonal one, and the use of orthogonal channels is more reliable in the sense that the receiver eliminates/reduces the effects of fading via maximal ratio combining. Our result implies that the system *with fading* provides better broadcast behavior than the one without.

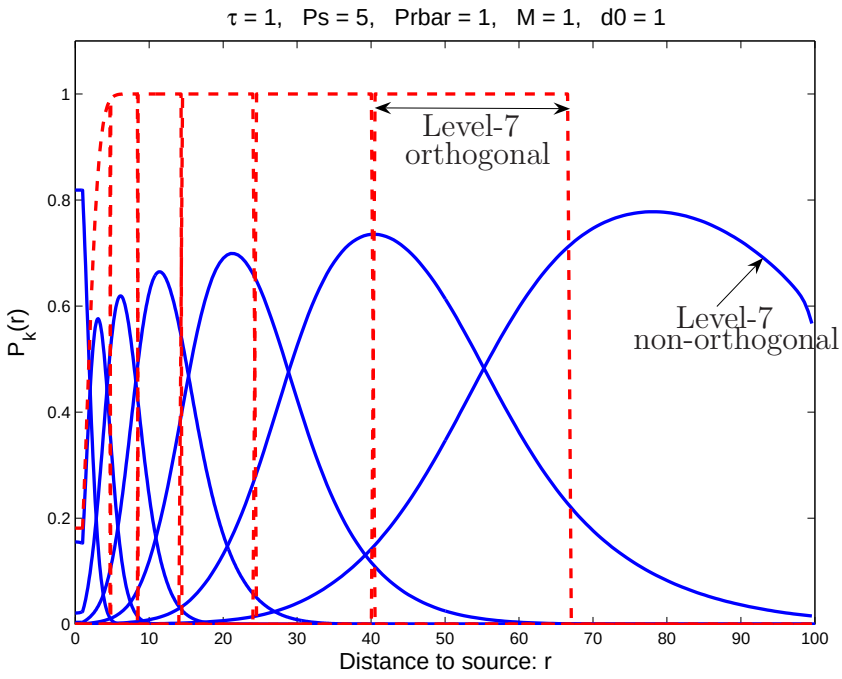

Figure 3.8: Wideband orthogonal vs. narrowband non-orthogonal: the upper, rectangular shaped levels are the orthogonal, the lower wave-like levels are non-orthogonal. The parameters are $\tau = 1, P_s = 5, \bar{P}_r = 1, M = 1, d_0 = 1, \Sigma = 1$.

We believe that this fact can be explained as follows. The maximal ratio combining method reduces the probability that the combined signal experiences a deep fade at the cost of reducing the probability that the signal experiences a favorable fade. In a dense network, favorable fading realizations are very valuable, because when the node density is high, although there is a small probability of having a good fading realization, there is always a fraction of nodes that experiences them. Once these lucky nodes receive and retransmit, the nodes neighboring them see a boost of signal power because of the properties of $\ell(d)$. In conclusion, we believe that the nodes that enable faster level movement are the ones at the forefront of each level.

In the narrowband system, favorable fading realizations occur, when the phases

of two or more simultaneously transmitting nodes happen to add coherently, or when one of the transmitting nodes experiences a very good channel with the receiver. Considering that non-orthogonal transmissions do not require infinite bandwidth, we conclude that the non-orthogonal scheme is more advantageous also in terms of end-to-end delay.

3.4.6 Multihop diversity under fading channels

If the nodes listen to m previous levels, the approach presented in the previous sections using the matched filter bound can be generalized by modifying (3.47) as

$$P_{k+1}(x,y) = \Pr\{\sum_{j=(k-m+1)_+}^{k} ||\mathbf{h}_j(x,y)||^2 \geq \tau\} \cdot \prod_{i=0}^{(k-1)} [1 - \Pr\{\sum_{j=(i-m+1)_+}^{i} ||\mathbf{h}_j(x,y)||^2 \geq \tau\}], \quad (3.56)$$

where $(x)_+ \triangleq \max(0,x)$. In conjunction with (3.48), Eqn. 3.56 determines the network behavior.

In case of narrowband non-orthogonal transmissions, the multihop diversity allows the signal to flow much faster (see Fig. 3.9). Furthermore, we expect to observe the threshold behavior. In case of wideband orthogonal transmissions, the behavior converges to the deterministic channel behavior in Section 3.2.4.

3.4.7 Extensions to correlated fading

In the previous sections, in order to derive our results, we assumed that the small-scale fading is spatially independent. The spatial independence is not actually needed in order to derive the results. The underlying assumption needed for the results in this chapter is that the channel coefficients between any pair of nodes

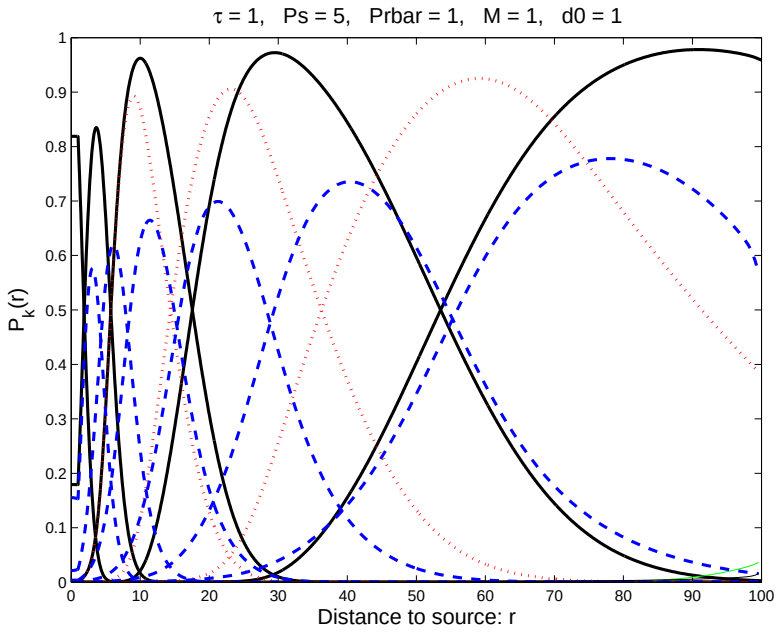

Figure 3.9: Narrowband non-orthogonal transmissions: $\tau = 1, P_s = 5, \bar{P}_r = 1, M = 1, d_0 = 1, \Sigma = 1$. Three different scenarios: (i) straight line $m = 3$, (ii) dotted line $m = 2$ (iii) dashed line $m = 1$. Note that first level curve $P_1(r)$ is the same for $m = 1, 2, 3$ and the second level curve $P_2(r)$ is the same for $m = 2, 3$.

are independent from one another. It is well-known in multiple-input multiple-out (MIMO) literature, it is reasonable to model that the channel gains at two receiving antennas separated by more than half the wavelength are independent. Hence, in a rich scattering environment (such as urban areas), the independent fading assumption is expected to be accurate.

The main difference of our problem from a MIMO transmitter is that we have different transmitters, hence the clocks at different transmitters are naturally assumed to be asynchronous. In addition to the rich scattering environments, considering an environment where *there is no small scale fading* ($\alpha(x, y) =$ constant $\forall(x, y)$) such that the channel gains depend only on the independent random

phases and pathloss gain, our analysis for the independent fading applies as it is.

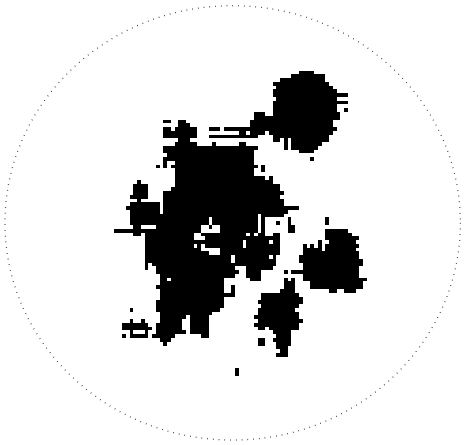

Figure 3.10: First level nodes for the correlated fading model (dark regions)

There are also scenarios where the independent fading assumption is not valid. In the case of spatially dependent fading, the analysis is intractable in general. For example, correlated fading implies that certain regions of the network can reliably receive the source message and the rest can not. Because of this reason, in general the set of level-1 nodes looks like "swiss cheese" (see Fig. 3.10), containing white regions that are in deep fade and can not receive source message. Hence the analysis becomes quite intractable for the higher levels.

Next, we provide two new methods to deal with the spatially correlated scenarios: (i) a conditional continuum model based on the instantaneous realization of the fading process α; (ii) a model for spatially dependent fading such that the CLT for dependent random variables holds.

In the following, we assume that the value of small scale fading is a function of the locations of the transmitter and the receiver. That is, assume the transmitter is located at (x', y') and the receiver is located at (x, y), then the small scale fading coefficient is denoted by $\alpha(x, y, x', y')$. Also, we assume that the phase shifts of

different transmitters are independent. Next we describe the network behavior.

i) Consider a specific realization of $\alpha(x, y, x', y')$, which is assumed to be continuous with respect to (x, y), (x', y'). Given $\alpha(x, y, x', y')$ and the locations (x, y), (x', y'), define $\beta(x, y, x', y') \triangleq \sqrt{l(x - x', y - y')}\alpha(x, y, x', y')e^{\theta(x', y')}$. Note that $\beta(x, y, x', y')$'s are conditionally independent for all (x', y') since $\theta(x', y')$'s are independent. The Eqns. 3.33-3.41 are still valid in this scenario. The equations in Section 3.4.2 can be updated as:

$$\begin{aligned} P_1(x, y|\alpha) &= \Pr\{||\mathbf{h}_0(x, y|\alpha)||^2 \geq \tau\} \\ \sigma_1^2(x, y|\alpha) &= \iint_{\mathbb{S}} \bar{P}_r|\alpha(x, y, x', y')|^2 \ell(x - x', y - y')P_1(x', y')dx'dy' \end{aligned}$$

where $\mathbf{h}_0(x, y|\alpha) = \sqrt{P_s}\beta_0(x, y, x_s, y_s)\mathbf{p}$ and the location of the source (x_s, y_s) is known and deterministic. Furthermore, for any level-k,

$$\begin{aligned} P_{k+1}(x, y|\alpha) &= \Pr\{||\mathbf{h}_k(x, y|\alpha)||^2 \geq \tau\} \prod_{i=0}^{k-1} [1 - \Pr\{||\mathbf{h}_i(x, y|\alpha)||^2 \geq \tau\}], \\ \sigma_k^2(x, y|\alpha) &= \iint_{\mathbb{S}} \bar{P}_r|\alpha(x, y, x', y')|^2 \ell(x - x', y - y')P_k(x', y')dx'dy' \end{aligned}$$

where

$$\begin{aligned} \mathbf{h}_k(x, y|\alpha) &\sim \mathcal{N}_c(0, \sigma_k^2(x, y|\alpha)\Sigma), \quad \text{non-orthogonal} \\ ||\mathbf{h}_k(x, y|\alpha)||^2 &= \sigma_k^2(x, y|\alpha)|p(0)|^2, \quad \text{orthogonal.} \end{aligned}$$

The above equations specify a conditional continuum model given the instantaneous realizations of α (*i.e.,* we treat α as a given deterministic function). One drawback of the conditional model (in general, correlated fading), is the network evolution is strictly a function of the instantaneous fading realization. Therefore, the continuum model exhibits different behavior for different realizations of the fading process, and it is hard to come up with conclusions.

ii) If there exists a fading model for $\alpha(x, y, x', y')$ such that the CLT for dependent random variables holds, then similar to the previous case, a continuum model can be derived. We know that certain generalizations of the cental limit theorem exist for dependent random variables [53]. Unfortunately, it is hard to directly apply these results in the literature to our problem. All we can claim at the moment is that such conditions are in general looser than the condition of independence.

For the fading models where the CLT for dependent random variables holds, the Eqns. 3.33-3.41 are still valid. The equations in Section 3.4.2 can be updated as:

$$P_1(x, y) = \Pr\{||\mathbf{h}_0(x, y)||^2 \geq \tau\}.$$

Given the location (x, y), the signal power received from level-1 at (x, y) is

$$\begin{aligned} \sigma_1^2(x, y) &= P_T \mathbb{E}_\ell\{|\beta_\ell(x, y, x_\ell, y_\ell)|^2\} \\ &= \iint_{\mathbb{S}} \mathbb{E}\{|\alpha(x, y, x', y')|^2\} \bar{P}_r P_1(x', y') \ell(x - x', y - y') dx' dy' \end{aligned}$$

Furthermore, for any level-k,

$$\begin{aligned} P_{k+1}(x, y) &= \Pr\{||\mathbf{h}_k(x, y)||^2 \geq \tau\} \prod_{i=0}^{k-1} [1 - \Pr\{||\mathbf{h}_i(x, y)||^2 \geq \tau\}] \\ \sigma_k^2(x, y) &= \iint_{\mathbb{S}} \mathbb{E}\{|\alpha(x, y, x', y')|^2\} \bar{P}_r P_k(x', y') \ell(x - x', y - y') dx' dy' \end{aligned}$$

where

$$\begin{aligned} \mathbf{h}_k(x, y) &\sim \mathcal{N}_c(0, \sigma_k^2(x, y)\Sigma), \quad \text{non-orthogonal} \\ ||\mathbf{h}_k(x, y)||^2 &= \sigma_k^2(x, y)|p(0)|^2, \quad \text{orthogonal.} \end{aligned}$$

3.5 Simulation Results

In this section, we check the accuracy of continuum approximations in predicting the behavior of the random network.

3.5.1 Deterministic Channel Model

First, in Table 3.1, we compare the approximate number of nodes that transmit in each level, calculated through continuum analysis, which is equal to $\pi\rho(a_k - a_{k-1})$ [see Eqn. 3.9], and the average number of nodes that belong to a certain level obtained from simulating 100 random networks. Specifically, for $\tau = 1$, $\bar{P}_r = 1$, $P_s = 1$, Table 3.1 shows the ratio, $\frac{|S_k|}{\pi\rho(a_k - a_{k-1})}$, for $k = 1, \ldots, 4$, and for $\rho = 1, 10, 100$. Similarly, in Table 3.2, we compare the approximate radii calculated through the continuum analysis, Eqn. 3.13, and the averaged radii obtained from simulating 100 random networks. Specifically, for $\tau = 1$, $\bar{P}_r = 1$, $P_s = 1$, Table 3.2 shows the ratio, $\frac{R_k}{\sqrt{a_k}}$, for $k = 1, \ldots, 4$, and for $\rho = 1, 10, 100$, where R_k is the maximum distance between the source and nodes in $\mathcal{S}_k$. It can be clearly seen that in both tables the ratios between the asymptotic value and the numerical average tend to 1 as the node density increases.

Figure 3.11 shows the histogram of the number of nodes reached by broadcast as a function of N, τ, and P_s. To obtain the histograms, we simulated random networks with 1000 nodes (500 trials, $\rho = 1$, $P_r = 1$). The values are plotted for different thresholds, τ, and source powers, P_s. The theoretical critical threshold is at $(\pi \ln 2)P_r\rho \approx 2.18$ [Eqn. (3.16)]. With the continuum model, for $\tau < 2.18$, the predicted number of nodes with SNR $\geq \tau$ corresponds to all nodes (1000 in this case) since the $a_k \to \infty$. Instead for $\tau > 2.18$, the number of nodes with SNR $\geq \tau$

Table 3.1: The ratio of expected number of nodes in each level to the approximate number of nodes, $\frac{|S_k|}{\pi\rho(a_k - a_{k-1})}$

k / ρ	1	10	100
1	0.7815	0.9651	0.9968
2	0.7428	0.9586	0.9926
3	0.6916	0.9534	0.9900
4	0.6615	0.9491	0.9895

Table 3.2: The ratio of expected radius of each level disc to approximate radius, $\frac{R_k}{\sqrt{a}_k}$

k / ρ	1	10	100
1	0.8992	0.9853	0.9968
2	0.9921	1.0307	1.0209
3	1.0214	1.0393	1.0221
4	1.0165	1.0327	1.0176

can be calculated from (3.17). For $P_s = 10, 50$ and $\tau = 1, 1.5, 3$, the continuum model correctly predicts the network behavior; all nodes in the network are reached for the values of the threshold $\tau = 1, 1.5$, and only a fraction is reached for $\tau = 3$. For $\tau = 2$, which is close to the critical threshold ≈ 2.18, and for $P_s = 50$ the signal reaches to the whole network; but this is no longer the case for $P_s = 1, 10$ in contrast to what the asymptotic analysis predicts.

Here, we see that the continuum approximation is not accurate in all cases

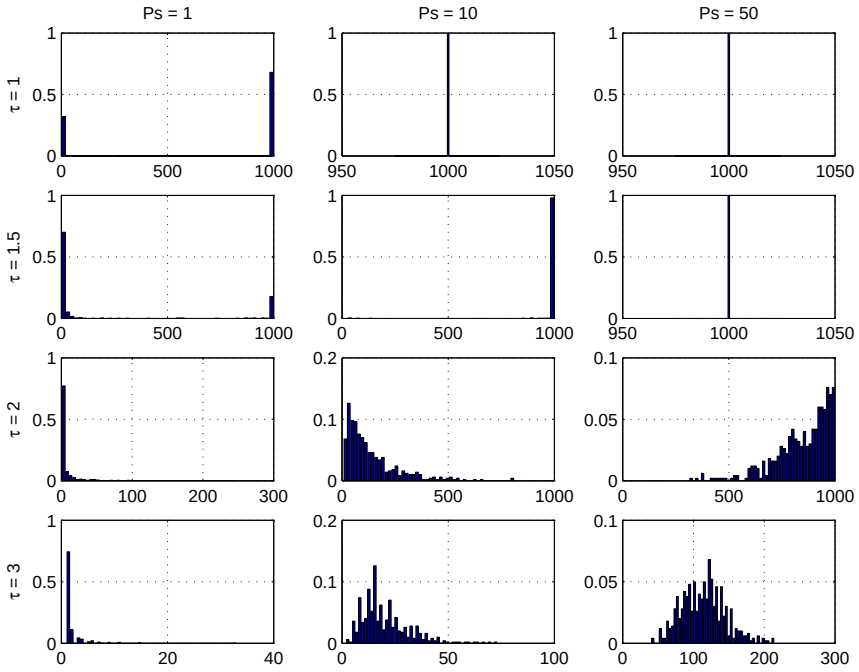

Figure 3.11: Probability of number of nodes that transmit in a 1000 node network, $\rho = 1$, $P_r = 1$. Note that the scales for both horizontal and vertical axis are different.

($\tau = 1$, $P_s = 1$) because we are testing the network exactly at the asymptotic threshold. This behavior is caused by the fact that the source power is too low, and for certain random network configurations, retransmission never starts. In random networks this possibility can only be avoided by boosting sufficiently the source power, P_s to initiate the broadcast with sufficient power.

Fig. 3.12 shows the expected number of nodes reached by the broadcast as a function of P_s and τ. Clearly, the smaller the τ, the smaller P_s is needed. Two regimes can be identified in the figure; for $\tau < 2.18$, the whole network is reached after some P_s. However, for $\tau > 2.18$, the expected number of nodes grows linearly with P_s. This is in accordance with (3.17). The slope s predicted by the continuum analysis is $s = \frac{\rho\pi(\mu-1)}{\tau(\mu-2)}$. Hence, for $\tau = 3$, $s = 2.7969$, and for $\tau = 4$, $s = 1.2849$.

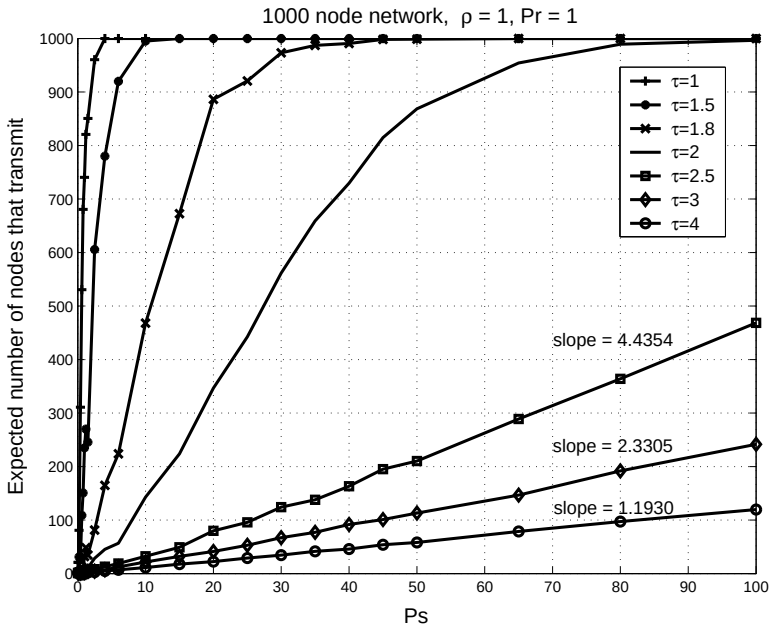

Figure 3.12: Expected number of nodes that transmits vs P_s

Note that these slopes are reasonably close to the predicted values. On the other hand, for $\tau = 2.5$, $s = 7.0702$, the expected slope is quite different than the simulated value, 4.4354. This is due to the fact that $\tau = 2.5$ is close to the critical threshold 2.18.

Fig. 3.13 gives a typical realization of a 1000-node network. Here, the dotted lines show the level radii estimated from the continuum approximation. Also, the nodes belonging to S_k, $k = 1, \ldots, 4$ are shown. The asymptotic analysis accurately predicts the locations of level sets.

3.5.2 Random Channel Model

Non-orthogonal transmission

We simulated the random network, and obtained the empirical density of nodes at level-k with respect to the distance to the source. This, together with the

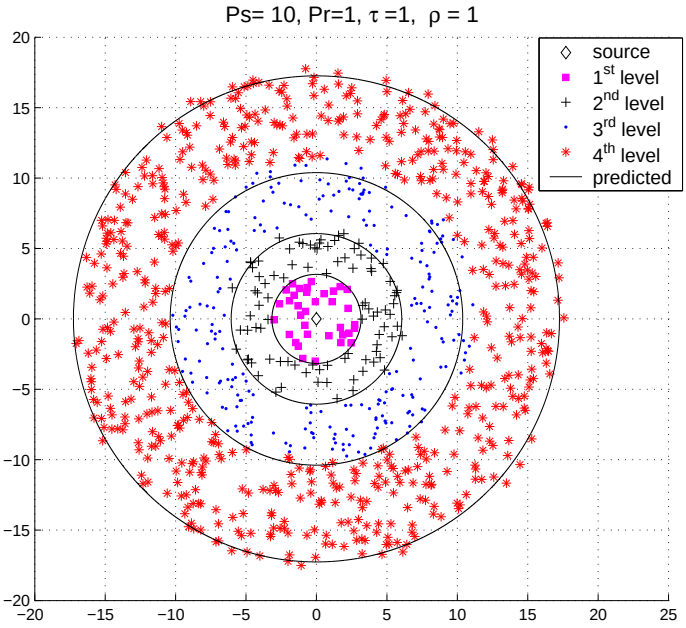

Figure 3.13: Random Network Realization vs Continuum Approx.

continuum result $P_k(r)$ is shown for $\tau = 1$ and $\tau = 3$ in Figs. 3.14 and 3.15 respectively. The parameters are $P_s = 5$, $\bar{P}_r = 1$, $\rho = 30$, $M = 3$, $\Sigma = \frac{\mathbf{I}}{M}$. The distribution of relay times, t_l's are assumed Uniform$\{-1, 0, 1\}$. The fading coefficients α_l's are $\mathcal{N}_c(0, 1)$. In Fig. 3.14, the moving wave behavior is observed, as expected from the continuum model. On the other hand in Fig. 3.15, the transmissions die out. Notice that the continuum result $P_k(r)$ is the smooth curve.

Orthogonal Transmission

Similar to the non-orthogonal scenario, we simulated the random network, and obtained the empirical density of nodes at level-k under wideband orthogonal channels. Figures 3.16 and 3.17 show the behavior respectively in low and high threshold regimes. The parameters are $P_s = 3.5$, $\bar{P}_r = 1$, $M = 1$, $\Sigma = \mathbf{I}$. The fading coefficients α_l are $\mathcal{N}_c(0, 1)$. The curves are obtained for a high node density,

$\rho = 100$. Fig. 3.16 shows the behavior for the low threshold regime. The effect of fading is transient, it *i.e.,* dies out after the first two levels, and the third level curve $P_3(r)$ almost takes binary values. In Fig. 3.17, the behavior for the high threshold region is shown. As expected, the effect of initial fading is transient and, the curves get narrower as the signal propagates. Notice that the continuum result $P_k(r)$ is the smooth curve.

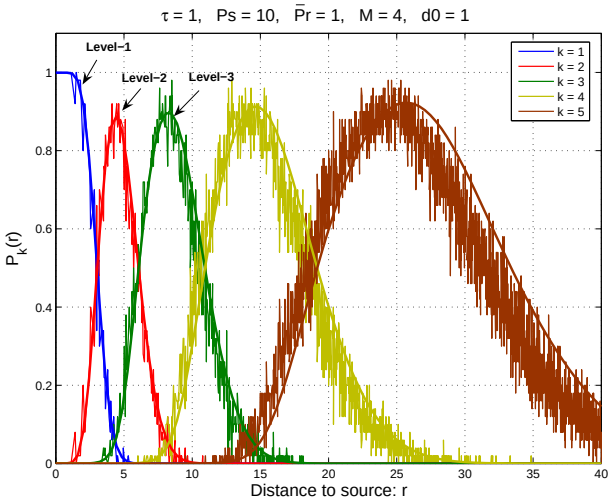

Figure 3.14: Transmissions continue

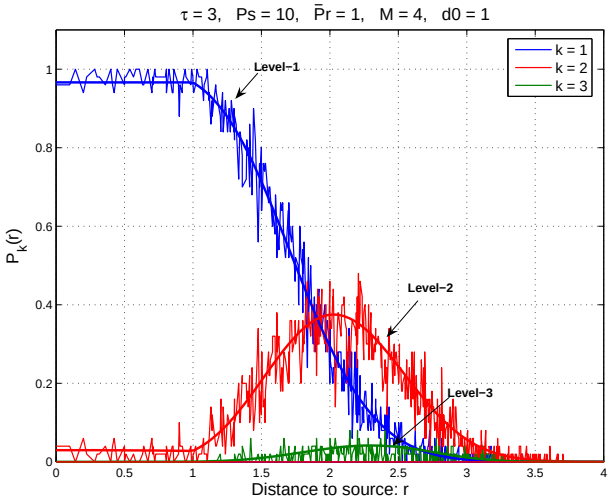

Figure 3.15: Transmissions die out

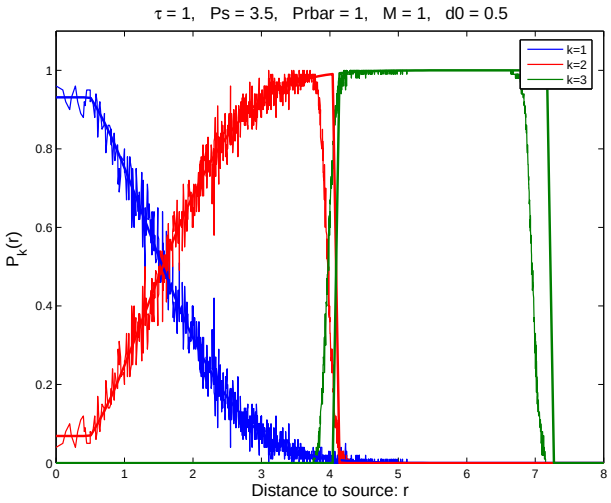

Figure 3.16: Transmissions continue

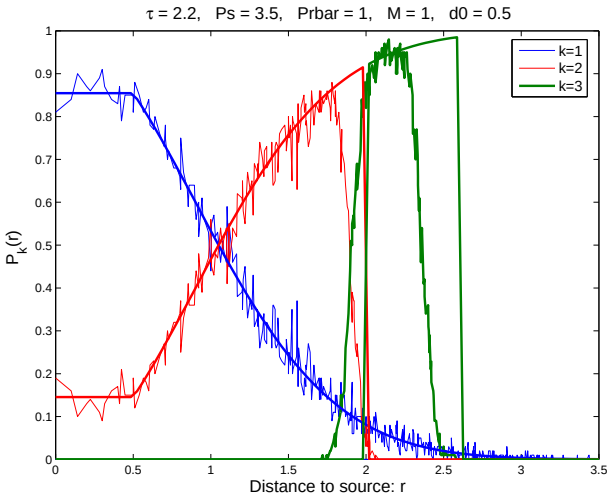

Figure 3.17: Transmissions die out

Appendix 3.A Convergence of Random Network to the Continuum- Proof of Theorem 5

Let

$$\mathbb{D}(r, r') = \{(x, y) : r \leq x^2 + y^2 \leq r'\}$$

denote the ring with inner and outer radii r and r', respectively. The following theorem, which is an instance of the so-called *uniform law of large numbers*, is a major step in the proof of Theorem 5.

Theorem 11 *Let $X_i \in \mathbb{R}^2,\ i = 1, 2, \cdots, N$ denote the location of nodes in the random network. Let $\mathcal{U}$ denote the set of all axis-aligned rectangles in $\mathbb{R}^2$.*[2] *There exists a real-valued sequence $\epsilon_N \to 0$ such that as $N \to \infty$,*

$$\Pr\left\{\sup_{U\in\mathcal{U}}\left|\frac{1}{N}\sum_{i=1}^{N} 1(X_i \in U) - \frac{Area(U \cap \mathbb{S})}{\pi R^2}\right| \leq \epsilon_N\right\} \to 1. \tag{3.57}$$

Proof It is a classic example in statistical learning theory that the VC dimension of the set $\mathcal{U}$ is finite (*e.g.,* see [55]). The result (3.57) directly follows from the Vapnik-Chervonenkis Theorem [56].

For convenience, we let

$$F_N(\epsilon_N) = \left\{\sup_{U\in\mathcal{U}}\left|\frac{1}{N}\sum_{i=1}^{N} 1(X_i \in U) - \frac{\text{Area}(U \cap \mathbb{S})}{\pi R^2}\right| \leq \epsilon_N\right\}$$

denote the event in (3.57). Let a_N be an integer-valued sequence such that

$$\begin{aligned} &\text{(i)} && a_N \text{ is monotone increasing.} \\ &\text{(ii)} && a_N \to \infty \text{ as } N \to \infty. \\ &\text{(iii)} && \epsilon_N / 2^{-a_N} \to 0 \text{ as } N \to \infty. \end{aligned} \tag{3.58}$$

[2] Each set in $\mathcal{U}$ is of the form $\{(x, y) : x_{\min} \leq x < x_{\max},\ y_{\min} \leq y < y_{\max}\}$ for some $x_{\min}, x_{\max}, y_{\min}, y_{\max} \in \mathbb{R}$.

Later, the motivation for such a sequence will be clearer. We would like to partition the Euclidian plane with squares of size $2^{-a_N} \times 2^{-a_N}$. In particular, we use the notation

$$\Delta_N(i,j) \triangleq \{(x,y) : i2^{-a_N} \leq x < (i+1)2^{-a_N},\ j2^{-a_N} \leq y < (j+1)2^{-a_N}\} \quad (3.59)$$

to denote these squares. The following lemma gives upper and lower bounds on the number of nodes in each $\Delta_N(i,j)$, given that $F_N(\epsilon_N)$ happened.

Lemma 4 *If the event $F_N(\epsilon_N)$ happened, then for every $\Delta_N(i,j) \subset \mathbb{S}$*

$$\rho 2^{-a_N+1}\left[1 - (\pi R^2)\frac{\epsilon_N}{2^{-a_N+1}}\right] \leq |\mathcal{S} \cap \Delta_N(i,j)| \leq \rho 2^{-a_N+1}\left[1 + (\pi R^2)\frac{\epsilon_N}{2^{-a_N+1}}\right]. \quad (3.60)$$

The upper bound is valid even for $\Delta_N(i,j)$ not in $\mathbb{S}$.

Proof Substituting $U = \Delta_N(i,j)$ into the definition of $F_N(\epsilon_N)$ gives

$$\left|\frac{1}{N}|\mathcal{S} \cap \Delta_N(i,j)| - \frac{\text{Area}(\Delta_N(i,j) \cap \mathbb{S})}{\pi R^2}\right| \leq \epsilon_N.$$

Eqn (3.60) is obtained easily after some algebraic manipulation.

Let $E_{k,N}(\delta)$ denote the event that first k level nodes are contained in the disk $\mathbb{D}(0, r_k + \delta)$ and the $\mathcal{S}_i,\ i = 1, \cdots, k$ contains all nodes in $\mathbb{D}(r_{i-1} + \delta, r_i - \delta)$, *i.e.,*

$$E_{k,N}(\delta) = \{\cup_{i=1}^{k}\mathcal{S}_i \subset \mathbb{D}(0, r_k + \delta),\ \ \mathcal{S} \cap \mathbb{D}(r_{i-1} + \delta, r_i - \delta) \subset \mathcal{S}_i,\ \ \forall i \in \{1, \cdots, k\}\}.$$

Theorem 12 *For all $k \in \{1, \cdots, k_{\max}\}$, there exists a non-increasing sequence $\delta_N \to 0$ such that $\Pr\{E_{k,N}(\delta_N)\} \to 1$ as $N \to \infty$.*

Proof We will prove the theorem by induction, *i.e.,* we will show that

i) There exists $\delta_N \to 0$ such that $\Pr\{E_{1,N}(\delta_N)\} \to 1$.

ii) If $\Pr\{E_{k,N}(\delta_N)\}\to 1$ for some non-increasing $\delta_N\to 0,\ k\in\{1,\cdots,k_{\max}-1\}$, then there exists non-increasing $\delta'_N\to 0$ such that $\Pr\{E_{k+1,N}(\delta'_N)\}\to 1$.

Part (i) immediately follows from the definitions of $\mathcal{S}_1,\ \mathbb{S}_1$ (choose $\delta_N=0,\ \forall N$). To prove (ii), assume that

$$\Pr\{E_{k,N}(\delta_N)\}\to 1 \tag{3.61}$$

for some non-increasing $\delta_N\to 0,\ k\in\{1,\cdots,k_{\max}-1\}$. For any sequence δ'_N, the inequality

$$\Pr\{E_{k+1,N}(\delta'_N)\}\geq \Pr\{E_{k,N}(\delta_N),\ F_N(\epsilon_N)\}\cdot\Pr\{E_{k+1,N}(\delta'_N)\mid E_{k,N}(\delta_N),\ F_N(\epsilon_N)\}$$

holds. Because of Theorem 11 and (3.61),

$$\Pr\{E_{k,N}(\delta_N),\ F_N(\epsilon_N)\}\to 1.$$

Thus, we are done if we can show the existence of $\delta'_N\to 0$ such that

$$\Pr\{E_{k+1,N}(\delta'_N)\mid E_{k,N}(\delta_N),\ F_N(\epsilon_N)\}\to 1. \tag{3.62}$$

In order to show (3.62) we will upper and lower bound the summation in (3.3) with relevant integrals. Our lower bound depends on a function $\underline{\ell}_N(x,y,x',y')$, which is constructed next. Consider the disc $\mathbb{D}(r_{k-1}+\delta_N, r_k-\delta_N)$ and a point (x',y') in $\mathbb{R}^2$.

- If a square $\Delta_N(i,j)$ is contained inside $\mathbb{D}(r_{k-1}+\delta_N, r_k-\delta_N)$, let the function $\underline{\ell}_N(x,y,x',y')$ take the value $\min_{(x'',y'')\in\Delta_N(i,j)}\ell(x''-x',y''-y')$ for all $(x,y)\in\Delta_N(i,j)$.
- If $(x,y)\in\Delta_N(i,j)$, but $\Delta_N(i,j)$ is not fully contained in $\mathbb{D}(r_{k-1}+\delta_N, r_k-\delta_N)$, let $\underline{\ell}_N(x,y,x',y')$ be zero.

More succinctly, the function $\underline{\ell}_N(x,y,x',y')$ is the *lower envelope* of $\ell(x-x',y-y')$ inside the region $\mathbb{D}(r_{k-1}+\delta_N, r_k-\delta_N)$, and is zero otherwise. The cross-sectional view of $\underline{\ell}_N(x,y,x',y')$ along the x-axis looks like Fig. 3.18.

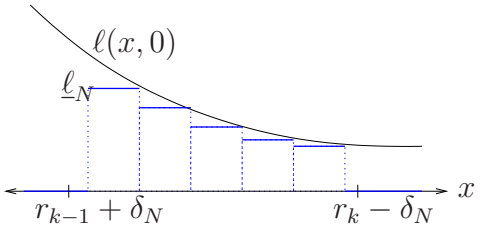

Figure 3.18: Illustration of $\ell_N(x,0,0,0)$ as a function of x.

An important property of this function is that $\underline{\ell}_N(x,y,x',y')$ is non-decreasing with N (for this, we need δ_N to be non-decreasing). Moreover, for all $(x,y),(x',y')$,

$$\underline{\ell}_N(x,y,x',y') \to \ell(x-x',y-y') \quad \text{as } N\to\infty, \tag{3.63}$$

since ℓ is continuous. Now, we want to examine why these properties are important. Under the assumption that the event $\{E_{k,N}(\delta_N),\ F_N(\epsilon_N)\}$ happened, for any $x,y\in\mathbb{R}$, we have

$$\begin{aligned}\sum_{(x',y')\in\mathcal{S}_{k-1}} P_r\ell(x-x',y-y') &\geq \sum_{(x',y')\in\mathcal{S}\cap\mathbb{D}(r_{k-1}+\delta_N,r_k-\delta_N)} P_r\ell(x-x',y-y') \\ &\geq \sum_{i,j=-\infty}^{\infty} P_r|\Delta_N(i,j)\cap\mathcal{S}\cap\mathbb{D}(r_{k-1}+\delta_N,r_k-\delta_N)|\cdot \\ &\qquad \min_{(x',y')\in\Delta_N(i,j)} \ell(x-x',y-y').\end{aligned}$$

Recall that $P_r=\bar{P}_r/\rho$, and observe that the final expression is lower bounded by

$$\geq \left[1-(\pi R^2)\frac{\epsilon_N}{2^{-a_N+1}}\right]\int_{\mathbb{D}(r_{k-1},r_k)} \bar{P}_r\underline{\ell}_N(x,y,x',y')dx'dy' \triangleq \underline{\mathrm{I}}_N(x,y).$$

The final lower bound has several important properties. First, due to Eqn. (3.58), the term $\left[1-(\pi R^2)\frac{\epsilon_N}{2^{-a_N+1}}\right]$ converges to 1. By the Monotone Convergence Theo-

rem, for all (x, y)

$$\int_{\mathbb{D}(r_{k-1},r_k)} \bar{P}_r \underline{\ell}_N(x, y, x', y')dx'dy' \to \int_{\mathbb{S}_k} \bar{P}_r \ell(x - x', y - y')dx'dy', \quad \text{as } N\to\infty. \tag{3.64}$$

Furthermore, by using the properties of the function ℓ, it can be shown that the convergence in (3.64) is *uniform* over $(x, y) \in \mathbb{D}(r_k + \gamma, r_{k+1})$ for all $\gamma > 0$. Also, since ℓ is non-increasing, the function $\underline{\mathrm{I}}_N(x, y)$ is non-increasing along the outward radial direction for all $(x, y) \in \mathbb{D}(r_k, \infty)$. All these properties lead to the fact that there exists non-increasing $\delta'_N \to 0$ such that

$$\underline{\mathrm{I}}_N(x, y) > \tau \quad \text{for all} \quad (x, y) \in \mathbb{D}(r_k, r_{k+1} - \delta'_N). \tag{3.65}$$

If the event $E_{k,N}(\delta_N)$ happened, then $\cup_{i=1}^{k} \mathcal{S}_i \subset \mathbb{D}(0, r_k + \delta_N)$, which means that the nodes in $\mathbb{D}(r_k + \delta_N, \infty)$ join level $k+1$ if their received power exceeds τ. Therefore,

$$\Pr\{\mathcal{S} \cap \mathbb{D}(r_k + \delta''_N, r_{k+1} - \delta''_N) \subset \mathcal{S}_{k+1} \ \mid \ E_{k,N}(\delta_N),\ F_N(\epsilon_N)\} \to 1, \tag{3.66}$$

as $N\to\infty$, where $\delta''_N \triangleq \max\{\delta_N, \delta'_N\}$.

We are done if we can show the existence of a sequence $\delta'''_N \to 0$ such that as $N\to\infty$,

$$\Pr\{\cup_{i=1}^{k+1} \mathcal{S}_i \subset \mathbb{D}(0, r_{k+1} + \delta'''_N)| \ \mid \ E_{k,N}(\delta_N),\ F_N(\epsilon_N)\} \to 1. \tag{3.67}$$

(notice that (3.66) and (3.67) imply (3.62)). Since the rest of the proof is quite similar, we will only give its outline. Under the condition that the event $\{E_{k,N}(\delta_N),$ $F_N(\epsilon_N)\}$ happened, if we can show that there exists $\delta'''_N \to 0$ such that

$$\underline{\mathrm{I}}_N(x, y) < \tau \quad \text{for all} \quad (x, y) \in \mathbb{D}(r_{k+1} + \delta'''_N, \infty), \tag{3.68}$$

we are done. First, notice that is if $E_{k,N}(\delta_N)$ happened, then

$$\mathcal{S}_k \subset [\cup_{i=1}^{k-1} \mathbb{D}(r_i - \delta_N, r_i + \delta_N) \ \cup \ \mathbb{D}(r_{k-1} + \delta_N, r_k + \delta_N)] \triangleq \tilde{\mathbb{S}}_{k,N}.$$

This is because all $\mathcal{S}_i,\ i = 1, \cdots, k$ are in $\mathbb{D}(0, r_k + \delta_N)$, yet the nodes in $\mathbb{D}(r_{i-1} + \delta_N, r_i - \delta_N)$ belong to level i, for $i = 1, \cdots, k-1$. Consequently, the following upper bound holds:

$$\sum_{(x',y')\in\mathcal{S}_{k-1}} P_r\ell(x-x', y-y') \leq \sum_{(x',y')\in\mathcal{S}\cap\tilde{\mathbb{S}}_{k,N}} P_r\ell(x-x', y-y').$$

$$\begin{aligned} &\leq \left[1 + (\pi R^2)\frac{\epsilon_N}{2^{-a_N+1}}\right] \int_{\mathbb{R}^2} \bar{P}_r\bar{\ell}_N(x,y,x',y')dx'dy' \\ &\triangleq \bar{I}_N(x,y), \end{aligned} \tag{3.69}$$

where the function $\bar{\ell}_N(x,y,x',y')$ is the *upper-envelope* of ℓ over the region $\tilde{\mathbb{S}}_{k,N}$, *i.e.,*

$$\bar{\ell}_N(x,y,x',y') = \begin{cases} \max_{(x'',y'')\in\Delta_N(i,j)} \ell(x''-x', y''-y'), \\ \qquad\qquad\qquad\qquad \text{if } (x,y)\in\Delta_N(i,j) \text{ and } \tilde{\mathbb{S}}_{k,N}\cap\Delta_N(i,j)\neq\phi, \\ 0, \qquad\qquad\qquad\qquad \text{otherwise.} \end{cases}$$

Monotone Convergence Theorem implies that $\bar{\ell}_N(x,y,x',y') \to \ell(x-x', y-y')$ for all $(x,y),\ (x',y')$. Using arguments similar to above, it is seen that (3.69) implies (3.68). The theorem follows. ■

Next, we will prove Theorem 5 using Theorem 11 and Theorem 12. In the following, we will give a proof of Theorem 5 under the assumption that $k_{\max} < \infty$. The same proof can be used for $k_{\max} = \infty$ after minor modifications.

Proof *(Theorem 5)* Let $\mathbb{V} \triangleq \mathbb{S}\cap\mathbb{U}$. Notice that

$$\frac{|\mathbb{U}\cap\mathcal{S}_k|}{\rho\text{Area}(\mathbb{U}\cap\mathbb{S}_k)} = \frac{|\mathbb{V}\cap\mathcal{S}_k|}{\rho\text{Area}(\mathbb{V}\cap\mathbb{S}_k)}.$$

In order to prove Theorem 5, we need to show that

$$\Pr\left\{\left|\frac{|\mathbb{V}\cap\mathcal{S}_k|}{\rho\text{Area}(\mathbb{V}\cap\mathbb{S}_k)} - 1\right| > s\right\} \to 0 \quad \text{as } N\to\infty, \quad \forall s > 0,$$

However, notice that this probability is upper bounded by

$$\begin{aligned} \leq \ & \Pr\{[F_N(\epsilon_N),\ E_{N,k_{\max}}(\delta_N)]^C\} \\ & + \Pr\left\{\left|\frac{|\mathbb{V}\cap\mathcal{S}_k|}{\rho\text{Area}(\mathbb{V}\cap\mathbb{S}_k)}-1\right| > s|F_N(\epsilon_N), E_{N,k_{\max}}(\delta_N)\right\} \quad (3.70) \end{aligned}$$

Because of Theorem 11 and Theorem 12, the term on the left hand side converges to zero. Therefore, to prove Theorem 5, it suffices to show that

$$\Pr\left\{\left|\frac{|\mathbb{V}\cap\mathcal{S}_k|}{\rho\text{Area}(\mathbb{V}\cap\mathbb{S}_k)}-1\right| > s \mid F_N(\epsilon_N), E_{N,k_{\max}}(\delta_N)\right\} \to 0 \quad \text{as } N\to\infty, \quad \forall s>0. \tag{3.71}$$

Under the assumption that $E_{N,k_{\max}}(\delta_N)$ happened, we have the relation

$$\mathcal{S}\cap\mathbb{D}(r_{k-1}+\delta_N, r_k-\delta_N) \subset \mathcal{S}_k \subset \tilde{\mathbb{S}}_{k_{\max},N}, \tag{3.72}$$

where

$$\tilde{\mathbb{S}}_{k,N} \triangleq [\cup_{i=1}^{k_{\max}}\mathbb{D}(r_i-\delta_N, r_i+\delta_N) \ \cup \ \mathbb{D}(r_{k-1}+\delta_N, r_k+\delta_N)],$$

as before. To see (3.71), we shall use the "partition into rectangles" trick, used above. Consider the partitioning $\Delta_N(i,j)$ introduced above. Define the sets

$$\begin{aligned} \bar{\mathbb{V}}_{k,N} &= \bigcup_{i,j}\{\Delta_N(i,j) : \Delta_N(i,j)\cap[\mathbb{V}\cap\tilde{\mathbb{S}}_{k,N}]\neq\phi\}, \\ \underline{\mathbb{V}}_{k,N} &= \bigcup_{i,j}\{\Delta_N(i,j) : \Delta_N(i,j)\subset\mathbb{V}\cap\mathbb{D}(r_{k-1}+\delta_N, r_k-\delta_N)\}, \end{aligned}$$

as outer and inner approximations of $\mathbb{V}$ with rectangles. Since $\mathbb{U}$ is a disc shaped region[3]

$$\lim_{N\to\infty}\text{Area}(\underline{\mathbb{V}}_{k,N}) = \lim_{N\to\infty}\text{Area}(\bar{\mathbb{V}}_{k,N}) = \text{Area}(\mathbb{V}\cap\mathbb{S}_k). \tag{3.73}$$

[3]The property (3.73), which is fairly obvious for disc shaped $\mathbb{U}$, is also true for all Jordan measurable $\mathbb{U}$. For conciseness, we will not prove it in this work, though.

Now, we examine why (3.73) is useful.

$$\begin{aligned}\frac{|\mathbb{V}\cap\mathcal{S}_k|}{\rho\text{Area}(\mathbb{V}\cap\mathbb{S}_k)} &\geq \frac{|\underline{\mathbb{V}}_{k,N}\cap\mathcal{S}|}{\rho\text{Area}(\mathbb{V}\cap\mathbb{S}_k)}\\ &\geq \left[\frac{1}{\rho\text{Area}(\mathbb{V}\cap\mathbb{S}_k)}\right]\frac{\text{Area}(\underline{\mathbb{V}}_{k,N})}{2^{-a_N+1}}(\rho 2^{-a_N+1})\left[1-(\pi R^2)\frac{\epsilon_N}{2^{-a_N+1}}\right].\end{aligned}$$

The lower bound converges to 1. Similarly,

$$\begin{aligned}\frac{|\mathbb{V}\cap\mathcal{S}_k|}{\rho\text{Area}(\mathbb{V}\cap\mathbb{S}_k)} &\leq \frac{|\bar{\mathbb{V}}_{k,N}\cap\mathcal{S}|}{\rho\text{Area}(\mathbb{V}\cap\mathbb{S}_k)}\\ &\leq \left[\frac{1}{\rho\text{Area}(\mathbb{V}\cap\mathbb{S}_k)}\right]\frac{\text{Area}(\bar{\mathbb{V}}_{k,N})}{2^{-a_N+1}}(\rho 2^{-a_N+1})\left[1+(\pi R^2)\frac{\epsilon_N}{2^{-a_N+1}}\right],\end{aligned}$$

which converges to 1 as well. The theorem follows.

Appendix 3.B Proof of Theorem 7

Similar to the case of $m = 1$, we can derive the difference equation for $k \geq m$ as

$$a_{k+1} - \frac{\mu}{\mu-1}a_k + \frac{1}{\mu-1}a_{k-m} = 0. \tag{3.74}$$

The initial conditions of this system are given by the following lemma.

Lemma 5 *The first initial condition is $a_1 = \frac{P_s}{\tau}$. Then k'th initial condition of the difference equation (3.74) is the unique solution of the equation*

$$g(p) \triangleq \frac{P_s}{p} + \pi\bar{P}_r \ln\frac{p}{|p-a_{k-1}|} = \tau, \quad 2 \leq k \leq m. \tag{3.75}$$

The initial conditions $a_2, \cdots, a_m$ can be obtained by solving (3.75) recursively.

Proof If we assume that the nodes have memory length of m, then for $k \leq m$, k'th level nodes consider the transmission from all levels transmitted previously including the source node. Then finding a_k simplifies to solving $g(p) = \tau$ for p. The claim is that the solution of the equation $g(p) = \tau$ exists and unique. This

can be seen as follows. By construction $a_k \geq a_{k-1}$. By inspecting the derivative of $g(p)$, it is seen that $g(p)$ is a decreasing continuous function for $p \geq a_{k-1}$. Note that $g(a_{k-1}) = \infty$ and $g(\infty) = 0$. Hence the equation $g(p) = \tau$ has a unique solution for $p \geq a_{k-1}$.

The characteristic function associated with the difference equation (3.74) is

$$f(r) = r^{m+1} - \frac{\mu}{\mu - 1} r^m + \frac{1}{\mu - 1} = 0. \tag{3.76}$$

The polynomial $f(r)$ is $(m+1)$-th order and has $(m+1)$ roots $r_i,\ i = 1 \ldots (m+1)$. The solution of the difference equation is determined by the roots of the polynomial $f(r)$ and the initial conditions (3.75). If there exists a root $|r_i| > 1$, then as $n \to \infty$, $a_n \to \infty$. On the other hand, if $|r_i| \leq 1, \forall i$ then as $n \to \infty$, $a_n \to a_\infty$, where a_∞ is a finite number. Hence, we would like to count the number of roots of $f(r)$ inside the unit circle and strictly outside the unit circle. The following lemma serves this purpose.

Lemma 6 *If $1 < \mu < m + 1$, then $f(r)$ has a root in the interval $(1, \infty)$. On the other hand, if $\mu > m + 1$, then $f(r)$ has m roots inside unit circle and a root on the unit circle.*

Proof The polynomial $f(r)$ is $(m+1)$-th order and has $(m+1)$ roots $r_1, \cdots, r_{m+1}$. We can easily rewrite

$$f(r) = \frac{(r-1)}{\mu - 1} \tilde{f}(r)$$

where

$$\tilde{f}(r) = (\mu - 1) r^m - r^{m-1} - r^{m-2} \ldots - r - 1.$$

Hence, $r_1 = 1$ is a root of $f(r)$ and the rest of the roots satisfy $\tilde{f}(r) = 0$. We will use this $\tilde{f}(r)$ and Rouché's Theorem [57] in the following.

- *Case 1:* For $1 < \mu < m+1$, $f(1) = \mu - 1 - m < 0$. Also we can easily see that $\lim_{r\to\infty} \tilde{f}(r) = \infty$. Since $\tilde{f}(r)$ is a polynomial, it is continuous. Hence, $\tilde{f}(r)$ has a root in $(1, \infty)$.

- *Case 2:* If $\mu > m+1$, then $\tilde{f}(r)$ have m roots inside unit circle. We can rewrite $\tilde{f}(r)$ as $\tilde{f}(r) = h(r) + g(r)$ where

$$\begin{aligned} h(r) &= (\mu - 1)r^m \\ g(r) &= -(r^{m-1} + r^{m-2} + \ldots + 1) \end{aligned}$$

We show that $|h(r)| > |g(r)|$ on the unit circle $\mathcal{C}$.

$$\begin{aligned} |h(r)| &=^a |(\mu-1)r^m| = |(\mu-1)| \\ &>^b m \\ &=^c |1| + |r| + |r^2| + \ldots + |r^m| \\ &>^d |1 + r + r^2 + \ldots + r^m| \\ &=^e |g(r)| \end{aligned} \tag{3.77}$$

where (a) is by definition and also $r \in \mathcal{C}$; (b) is assumed by the lemma; (c) follows from the fact that $r \in \mathcal{C}$; (d) is from the triangle inequality; (e) is by definition. Then, by using Rouché's theorem $h(r)$ and $\tilde{f}(r) = h(r) + g(r)$ have the same number of zeros inside the unit circle. The function $h(r)$ has m multiple zeros at $r = 0$, then $\tilde{f}(r)$ has m roots inside unit circle.

Proof of Theorem 7 i) follows from Lemmas 5 and 6. Part ii), can be seen as follows. If $m = \infty$, then a_k can be found by solving the following equation recursively

$$g(p) \triangleq \frac{P_s}{p} + \pi \bar{P}_r \ln \frac{p}{|p - a_{k-1}|} = \tau, \quad k \geq 1,$$

where $a_0 = 0$. The existence of unique solution to this equation is discussed previously in Lemma 5. We will use proof by contraction in the following. We assume that $a_k \to B$, such that $0 < B < \infty$. Note that as $k \to \infty$, $a_{k-1} \to B$. Then

$$\lim_{k\to\infty} g(a_k) = g(B) = \frac{P_s}{B} + \pi \bar{P}_r \ln \frac{B}{|B - B|} = \infty$$

which is a contraction since we know that $g(B) = \tau$ is finite.

Appendix 3.C Proof of Theorem 10

Assume that $\iint_{\mathbb{S}} l(x-u, y-v)dudv = C < \infty$. We will first upper bound the $\sigma_k^2(x, y)$. Using (3.48), we get

$$\begin{aligned} \sigma_k^2(x,y) &\leq \bar{P}_r \left(\sup_{(u,v)\in\mathbb{S}} P_k(u,v) \right) \iint_{\mathbb{S}} l(x-u, y-v)dudv \\ &\leq C\bar{P}_r \sup_{(u,v)\in\mathbb{S}} P_k(u,v) \end{aligned} \tag{3.78}$$

Also, by using (3.47) we can derive the following upper bound on $P_{k+1}(x, y)$ in terms of $\sigma_k^2(x, y)$. For simplicity, we assume that Σ has distinct eigenvalues (the following proof can be adapted easily for the other case). Apply (3.53) to obtain

$$\begin{aligned} P_{k+1}(x,y) &\leq \sum_{i=1}^{M} A_{i1} e^{-\tau/\sigma_k^2(x,y)\lambda_i} \\ &\leq \sum_{i=1}^{M} A_{i1} e^{-\tau/\lambda_i \sup_{(x,y)\in\mathbb{S}} \sigma_k^2(x,y)}, \\ &\leq \gamma e^{-\tau/\lambda_m \sup_{(x,y)\in\mathbb{S}} \sigma_k^2(x,y)} \end{aligned} \tag{3.79}$$

where the second inequality follows from the fact that $e^{-\tau/x}$ is an increasing function of x and in the third inequality $\gamma = M \max_i A_{i1}$ and $\lambda_m = \max_i \lambda_i$. Note that $\gamma > 0$, since it is a bound to a probability.

Let $M_k = \sup_{(x,y)\in\mathbb{S}} P_k(x, y)$. Combining (3.78) and (3.79), we have the relation

$$M_{k+1} \leq \gamma e^{-\beta/M_k}, \qquad k = 1, 2, \cdots, \tag{3.80}$$

where $\beta = \frac{\tau}{\lambda_m C \bar{P}_r}$. The initial condition is that

$$\begin{aligned} M_1 &= \sup_{(x,y)\in\mathbb{S}} P_1(x,y) \\ &= \sup_{(x,y)\in\mathbb{S}} \sum_{i=1}^{M} A_{i1} e^{-\tau/\sigma_0^2(x,y)\lambda_i} \\ &= \sum_{i=1}^{M} A_{i1} e^{-\tau/\sup_{(x,y)\in\mathbb{S}} \sigma_0^2(x,y)\lambda_i} \\ &= \sum_{i=1}^{M} A_{i1} e^{-\tau/P_s\lambda_i \sup_{(x,y)\in\mathbb{S}} \ell(x,y)}, \end{aligned}$$

where we only used the definitions of $P_1(x,y), \sigma_0^2(x,y)$.

Next, we will show that any sequence $M_1, M_2, \cdots$ satisfying (3.80) converges to zero. To this end, consider a sequence $L_1, L_2, \cdots$ satisfying $L_{k+1} = \gamma e^{-\beta/L_k}$ with the initial condition $L_1 = M_1$. We will first argue that $M_k \leq L_k, \ \forall k$. This can be easily proved by induction:

i) $M_1 \leq L_1$ by the definition of L_1.

ii) Assume that $M_k \leq L_k$ for some k. Then,

$$M_{k+1} \leq \gamma e^{-\beta/M_k} \leq \gamma e^{-\beta/L_k} = L_{k+1},$$

because the function $e^{-\beta/x}$ is increasing in x.

Second, we will observe that $L_k \to 0$ as $k \to \infty$ if

$$1 > \frac{\gamma}{\beta e} \quad \Leftrightarrow \quad \tau > \left(\gamma \lambda_m C e^{-1}\right) \bar{P}_r.$$

Observe that

$$\frac{L_{k+1}}{L_k} \leq \gamma \sup_{x\geq 0} \frac{e^{-\beta/x}}{x} = \frac{\gamma}{\beta e}; \tag{3.81}$$

by differentiation it can be seen that the function $\frac{e^{-\beta/x}}{x}$ is maximized at $x = \beta$. Eqn. (3.81) shows that $L_{k+1} \leq \frac{L_1}{(\beta e/\gamma)^k} \to 0$. Let $\tau_c = \gamma \lambda_m C e^{-1}$, then the theorem follows.

Chapter 4

Power Efficiency of Cooperative Broadcast in Dense Wireless Networks

4.1 Organization

The organization of the chapter is as follows. In Section 4.2, we describe the system model. In Section 4.3, we provide the general formulation of the optimal power allocation for the cooperative broadcasting and provide sufficient conditions under which the general formulation is simplified. In Section 4.4, we derive the optimal power density for dense networks. In Section 4.5, we propose practical schemes utilizing uniform power allocation. In Section 4.6, we compare the performance of the proposed schemes to the noncooperative multihop broadcasting. In Section 4.7, we provide simulations.

4.2 System Model

We consider a network formed by a single source and N relays, which are distributed randomly and uniformly in a given region. The source node initiates the transmission session. The relays which have received source message reliably at the kth time-slot are allowed to retransmit the message in the $(k+1)$th time slot. Nodes are half-duplex, i.e. can not receive and transmit at the same time. Note that relays do not transmit the same packet more than once.

Definition The relays that are allowed to retransmit at the kth time instant are called *level-k* nodes. We will denote the set of level-k nodes by $\mathcal{S}_k$.

In this thesis, we only consider a single-shot communication. We assume the nodes are stationary. We also assume that appropriate channel coding is used so that the decoding and retransmissions are correct as long as the received cumulative SNR is above a prescribed threshold. A training preamble in the message helps nodes to detect the packet's presence, estimate the received power and synchronize the retransmissions in a level. Next, we describe the reception model.

4.2.1 Reception Model

Let the ith node transmit with power P_i, let H_{ij} be the deterministic link power gain[1], and α_{ij} be the small scale-fading between the ith and jth nodes. Assume that $\mathbb{E}\{\alpha_{ij}\} = 0$, $\mathbb{E}\{|\alpha_{ij}|^2\} = 1$, and α_{ij}'s are independent and identically distributed. In the following, we consider two different models for the received power

[1]We do not consider the scenarios where the channel between any two nodes is frequency selective. However, we wish to point that it is possible to use OFDM transmission to tackle frequency selectivity.

of simultaneously transmitted signals. In the first one, if a set of relay nodes (say $\mathcal{L}$) transmit simultaneously, then node j receives with instantaneous power

$$Power_{inst} = \sum_{i \in \mathcal{L}} |\alpha_{ij}|^2 P_i H_{ij}. \tag{4.1}$$

This model is valid if the relays transmit in orthogonal channels, as in TDMA, FDMA or CDMA, or if the relays use orthogonal space-time codes as considered in [10] and the receiver is an optimum maximal-ratio-combiner (MRC) receiver [58]. In case of orthogonal channels, a large bandwidth is required, *i.e.,* the network should operate in the *wideband regime* [16]. Furthermore, in this case, a centralized scheduler, which assigns orthogonal channels to the nodes, is required. Note that when space-time codes are used, the scheduling problem can be resolved via randomization [59].

If the simultaneous transmissions are not in orthogonal dimensions, the cumulative power of transmitted packets depends on the relative delays and phases of individual overlapping signals. In literature, random addition of multiple signal paths is generally modelled as *Rayleigh fading* [35]. If the transmitted signal is narrowband, then the instantaneous received signal power is

$$Power_{inst} = \gamma \sum_{i \in \mathcal{L}} P_i H_{ij}, \tag{4.2}$$

where γ is a unit-mean exponential random variable (the square of a random Rayleigh fading envelope). Under this model, the scheduling is decentralized; however, the synchronization assumptions are stricter compared to the model (4.1).

If one needs to pick a deterministic quantity that best approximates the instantaneous received power, then the average is the best choice. Define

$$Power = \mathbb{E}\{Power_{inst}\} = \sum_{i \in \mathcal{L}} P_i H_{ij}. \tag{4.3}$$

The definition (4.3) has been also utilized in the related works [16, 19].

In our analysis, we assume that the channel coefficients are perfectly estimated (channel state information is available only at the receiver, *i.e.,* the transmitter does not know the channel state information) and each node can combine the packets that were received in different time intervals though MRC. We assume the pathloss attenuation is deterministic and time-invariant.

4.3 Power Allocation for OCB: Problem Formulation

In the optimal cooperative broadcast scheme, the source node initiates the transmission by sending a packet. Each node accumulates signal powers from all the nodes that transmitted previously (see Section 4.2.1). The nodes that have received sufficient signal power τ, *i.e.,* $Power \geq \tau$, are allowed to retransmit according to a given schedule. The $Power$ is defined in (4.3) and τ depends on the performance metric (e.g. outage capacity, bit error rate). We assume that the noise is of unit power; hence, τ will also be called the *SNR threshold*.

Let $\mathcal{I} = \{1, \ldots, N+1\}$ denote the set of node indices, where the source node is denoted by 1. The transmission schedule will be represented by a mapping S, *i.e.,* $S : \{1, \ldots, N+1\} \rightarrow \{1, \ldots, N+1\}$. Let P_i be the transmission power of the ith node. Let $\mathbf{H}$ be the channel matrix such that its (i, j)th entry denotes the channel gain from the jth node to the ith node H_{ij}. Our aim is to find the best *schedule* S and optimal power allocation $\{P_i, \forall i \in \mathcal{I}\}$ for a given network with channel matrix $\mathbf{H}$ and decoding threshold τ such that $\sum_i P_i$ is minimized under the described cooperative broadcast scheme. Note that the above mapping excludes the scenarios where nodes are allowed to transmit together, however, such scenarios can be easily mapped into the above formulation.

Let $\mathbf{e}_i$ denote the ith column of the identity matrix. We will associate a given schedule S with a permutation matrix $\mathbf{S} \triangleq [\mathbf{e}_{S(1)}\mathbf{e}_{S(2)} \dots \mathbf{e}_{S(N+1)}]$. The optimal $\mathbf{S}$ and power allocation vector $\mathbf{p} \triangleq [P_1, P_2, \dots, P_{N+1}]$ are the solutions of the following linear optimization problem (see also [16, 19, 20]):

$$\min_{\mathbf{S},\mathbf{p}} \mathbf{1}^T\mathbf{p} \;\text{ subject to }\; \mathcal{L}(\mathbf{S}\mathbf{H}\mathbf{S}^T)\mathbf{S}\mathbf{p} \geq \tau\mathbf{b},\; \mathbf{p} \geq \mathbf{0}, \tag{4.4}$$

where $\mathbf{b} = [\mathbf{1}; 0]$, $\mathbf{1}$ denotes a vector of all 1's, $\mathbf{0}$ denotes a vector of all 0's and $[\mathbf{x}; \mathbf{y}]$ denotes column concentration of vectors $\mathbf{x}$ and $\mathbf{y}$. The operator $\mathcal{L}$ models the causality in the system and it is defined as follows: Let $a_{i,j}$ be the (i,j)th element of $(N+1) \times (N+1)$ matrix $\mathbf{A}$ and $l_{i,j}$ be the (i,j)th element of $\mathcal{L}(\mathbf{A})$, then for $1 \leq i, j \leq N+1$,

$$l_{i,j} = \begin{cases} a_{i+1,j} & \text{if } i \geq j,\; i < N+1, \\ 1 & \text{if } i = N+1,\; j = N+1, \\ 0 & \text{otherwise.} \end{cases}$$

The last scheduled node does not need to transmit, *i.e.,* the optimal $P_{S(N+1)} = 0$. This is enforced in the above formulation via the definitions of $\mathbf{b}$ and $\mathcal{L}$. In the following, we will denote the set of all possible permutation matrices with $\boldsymbol{\mathcal{P}_S}$, where $|\boldsymbol{\mathcal{P}_S}| = N!$ (the transmission is initiated by the source node, hence out of $(N+1)!$ possibilities $N!$ of them represent valid schedules).

For a given permutation matrix $\mathbf{S}$, the constrained optimization problem (4.4) can be solved in polynomial time as a function of the number of relays N by utilizing efficient linear programming algorithms. However, finding the optimal scheduling, i.e. finding the best permutation matrix $\mathbf{S}$ out of $N!$ possibilities was shown to be an NP-complete problem [16, 19, 20]. Hence, the problem is intractable in general. In the next section, we provide conditions under which the

best scheduling is easily determined and problem (4.4) can be solved in polynomial time.

4.3.1 Further Results on the Best Scheduling for Cooperative Broadcast

In Fig. 4.1, we present a linear network where the source node is located at the edge. For this network, under the effect of pathloss attenuation, for example $\ell(r) = 1/r^2$, the optimal schedule is such that the nodes transmit in the order of their distances from the source node [19, 20]. In the following, this will be referred as the *trivial scheduling*. We ask the question if there exist other networks where trivial scheduling is optimal. In Lemma 7, we provide sufficient conditions on the channel matrix $\mathbf{H}$ so that the overall complexity of the problem (4.4) is decreased considerably.

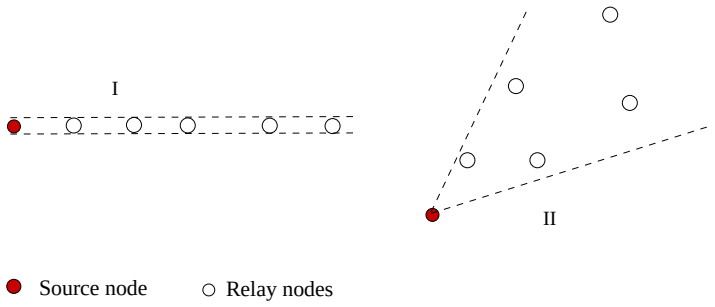

Figure 4.1: Network topologies for which the optimal scheduling is trivial

Lemma 7 *Consider the optimal power allocation and scheduling problem in (4.4). Assume that* $\mathbf{H}$ *has non-negative values. Let* $\boldsymbol{\mathcal{P}_S}$ *denote the set of all possible permutation matrices.*

a) If there exits a permutation matrix $\hat{\mathbf{S}} \in \boldsymbol{\mathcal{P}_S}$ *such that* $\mathcal{L}(\hat{\mathbf{S}}\mathbf{H}\hat{\mathbf{S}}^T)$ *is column-ordered*[2]*, then* $\hat{\mathbf{S}}$ *corresponds to the optimal schedule.*

b) If there exits a permutation matrix $\hat{\mathbf{S}} \in \boldsymbol{\mathcal{P}_S}$ *such that* $\mathcal{L}(\hat{\mathbf{S}}\mathbf{H}\hat{\mathbf{S}}^T)$ *is both column- and row-ordered*[3]*, then the optimal power allocation can be obtained by solving*

$$\mathcal{L}(\hat{\mathbf{S}}\mathbf{H}\hat{\mathbf{S}}^T)\hat{\mathbf{S}}\mathbf{p} = \tau\mathbf{b}. \tag{4.5}$$

Proof See Appendix 4.A.

Lemma 7a) provides a sufficient condition on the channel matrix $\mathbf{H}$ to determine the optimal schedule. The validity of the sufficient condition can be determined by ordering the first column of $\mathbf{H}$ and by checking if the rest of the columns are ordered. This sorting and comparing algorithm has complexity $O(N^2)$. Using Lemma 7a), we can determine that the trivial scheduling is the best schedule for both the network topologies in Fig. 4.1 under a pathloss attenuation model. Lemma 7b) provides a sufficient condition so that the optimal power allocation problem has the same complexity as inverting a lower triangular matrix, which is $O(N^2)$.

For the linear networks and linear-like configurations (among the two dimensional networks, see Fig. 4.1), the trivial scheduling is optimal under an appropriate pathloss attenuation model. These observations provide us the intuition and back-

[2]Let $\mathbf{L}$ be an $N \times N$ lower triangular matrix. Let $\mathbf{c}_i = [c_{i,1}c_{i,2}\ldots c_{i,N}]^t$ be the ith column of $\mathbf{L}$. We say $\mathbf{L}$ is *column-ordered* if the columns of $\mathbf{L}$ are decreasing from top to down (ignoring the zeros), *i.e.,* $c_{i,i} \geq c_{i,i+1} \geq \ldots \geq c_{i,N},\ \forall i$.

[3]Let $\mathbf{L}$ be an $N \times N$ lower triangular matrix. Let $\mathbf{r}_i = [r_{i,1}r_{i,2}\ldots r_{i,N}]$ be the ith row of $\mathbf{L}$. We say $\mathbf{L}$ is *row-ordered* if the rows of $\mathbf{L}$ are increasing from left to right (ignoring the zeros), *i.e.,* $r_{i,1} \leq r_{i,2} \leq \ldots \leq r_{i,i},\ \forall i$.

ground that will be utilized for dense large-scale networks in the next section. The interesting fact is that trivial scheduling tends to be optimal in dense networks.

4.4 Optimum Cooperative Broadcast in Dense Networks

In this section, we consider the problem of optimal power allocation for dense networks under cooperative broadcasting. Suppose that N nodes are uniformly and randomly distributed within $\mathbb{S} = \{(x, y) : x^2 + y^2 \leq R^2\}$ and the source node is located at the origin (see Fig. 4.2). In our analysis, we consider only the effect of pathloss attenuation on the channel gain. Let $\ell(\cdot)$ denote the pathloss attenuation function. For a transmitter that is located at (x, y) and a receiver that is located at (x', y'), we assume that $\ell(\cdot)$ is a1) a function of the distance $d := \sqrt{(x - x')^2 + (y - y')^2}$ between the transmitter and the receiver; a2) continuous, non-negative and decreasing in d; a3) circularly symmetric. We will use the notations $\ell(x - x', y - y')$ and $\ell(d)$, interchangeably.

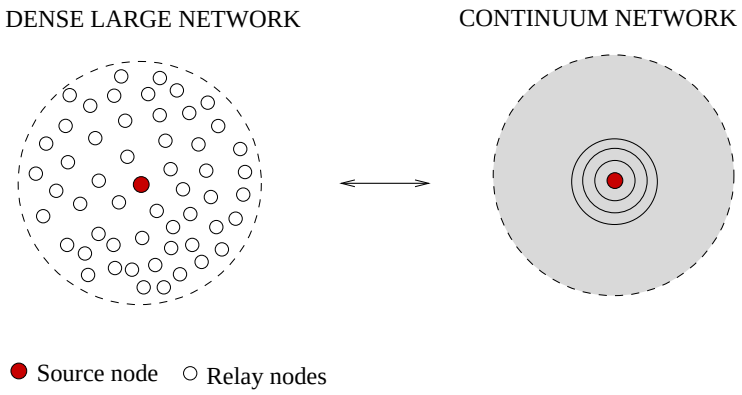

Figure 4.2: Continuum approximation of dense networks

Consider the network topologies in Fig. 4.3. Under the pathloss attenuation that satisfies assumptions a1)-a3), the trivial scheduling is optimal in these sce-

narios and the best schedule assigns the relays that are positioned at the same distance from the source node to the same level. Furthermore, the optimal power allocation assigns equal powers to the nodes that belong to the same level. Intuitively, this is obvious due to the symmetry in the network topology and the properties of the pathloss attenuation function. The optimal power allocation can be simplified further for such networks, thanks to the next lemma.

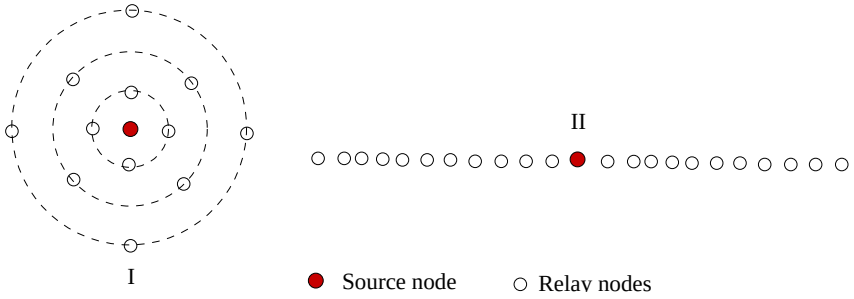

Figure 4.3: Network topologies for which the optimal power allocation scheme assigns equal powers to nodes belonging to the same level.

Lemma 8 *Consider a network with channel matrix* $\mathbf{H}$*. Let* S_k *be the set of level-k nodes. If the optimal power allocation policy assigns equal powers* P_k *to nodes in the same level* S_k*, then the power allocation problem simplifies to*

$$\min_{\mathbf{S},\bar{\mathbf{p}}} \mathbf{1}^T \bar{\mathbf{p}} \quad \textit{subject to} \quad \mathcal{L}(\mathbf{S}\bar{\mathbf{H}}\mathbf{S}^T)\bar{\mathbf{p}} \geq \mathbf{b},\ \bar{\mathbf{p}} \geq 0, \tag{4.6}$$

where $\bar{\mathbf{p}} = [\bar{P}_1 \bar{P}_2 \dots \bar{P}_M]$*,* $\bar{P}_k = |S_k| P_k$*. The* (i,k)*th element of* $\bar{\mathbf{H}}$ *is* $[\bar{\mathbf{H}}]_{ik} = \sum_{m \in S_k} [\mathbf{H}]_{im} / |S_k|$*.*

Proof See Appendix 4.B.

We approximate dense networks with a continuum of nodes where the relay density goes to infinity. In the continuum, after the source transmission, a certain

region of the network will receive sufficient signal power. This region will be called first level and it will be denoted by $\mathcal{A}_1$, which is a disc for broadcasting (Fig. 4.2). We conjecture that under the optimal broadcast scheme for the continuum network the nodes in the same level transmit with equal power. This follows due to the following reasons: (i) the pathloss attenuation function $\ell(r)$ is continuous, non-negative, decreasing and circularly symmetric; (ii) the network topology is symmetric w.r.t. source location and, hence, the nodes at the same distance from the source should behave identically. Under these conditions, each level $\mathcal{A}_k$ becomes a thin disc. In the continuum, the transmission power will be replaced by the power density $p(r)$, which is power per unit area. Define the function

$$H(r,u) \triangleq \frac{1}{2\pi}\int_0^{2\pi} \ell(\sqrt{r^2+u^2-2ur\cos(\theta)})d\theta. \tag{4.7}$$

Note that $H(r,u)$ represents the effective channel gain at a distance r due to transmission of nodes located at a distance u from the source in the continuum network.

Theorem 13 *Consider the continuum network* $\mathbb{S} \triangleq \{(x,y) : x^2+y^2 \leq R^2\}$ *with the source located at the center. Let* $\ell(r)$ *denote the pathloss attenuation function that satisfies the assumptions a1)-a3). Assume that* $\ell(r)$ *is such that*

a4) the function $H(r,u)$ *(see Eqn. 4.7) is decreasing in* r *and increasing in* u *for* $0 \leq u \leq r \leq R$.

Then, the optimal power density $p(r)$ *can be found as the unique continuous solution of*

$$\underbrace{\frac{\tau\ell(r)}{\ell(0)}}_{source\ contribution} + \underbrace{\int_0^r K(r,u)p(u)du}_{relay\ contribution} = \tau, \quad \forall r \leq R \tag{4.8}$$

where

$$K(r,u) = H(r,u)2\pi u = \int_0^{2\pi} \ell(\sqrt{r^2+u^2-2ur\cos(\theta)})ud\theta. \tag{4.9}$$

Proof See Appendix 4.C.

The linear integral equation in (4.8) is known as the first-order Volterra's equation [60, 61]. Next, we provide a framework to solve Eqn. 4.8.

Lemma 9 *Assume that (i)* $K(r,u)$ *and* $\frac{\partial K(r,u)}{\partial r}$ *are continuous in* $0 \le u \le r \le R$, *(ii)* $K(r,r)$ *does not vanish anywhere on* $0 \le r \le R$, *(iii)* $\ell(r)$ *and* $\ell'(r)$ *are continuous on* $0 \le r \le R$. *Then, the optimal power density* $p(r)$ *can be found by evaluating the following equation recursively, i.e.,* $p(r) = \lim_{n\to\infty} p_n(r)$, *and*

$$p_n(r) = \int_0^r p_{n-1}(u)V(r,u)du + \tau Z(r), \tag{4.10}$$

$$\textit{where,} \quad V(r,u) = -\frac{1}{K(r,r)}\frac{\partial K(r,u)}{\partial r}, \quad Z(r) = -\frac{l'(r)}{\ell(0)K(r,r)} \tag{4.11}$$

Proof Under the given conditions, the Volterra equation of first kind (4.8) can be converted into a Volterra equation of second kind via differentiation [61, Theorem 5.1, page 67]. The proof follows by using the method of successive approximation [60, page 15].

Given that the pathloss function $\ell(r)$ satisfies the assumptions a1)-a3), using the definition of $K(r,u)$ in (4.9), the functions $V(r,u)$ and $Z(r)$ take non-negative values. This guarantees that $p_n(r)$ converges to a non-negative function given that the initial choice is appropriate, *i.e.,* $p_0(r) \ge 0$. The next lemma characterizes the limiting optimal power density.

Lemma 10 *Consider the continuum network* $\mathbb{S} \triangleq \{(x,y) : x^2+y^2 \le R^2\}$ *where the source is located in the center. Assume that the pathloss attenuation function*

$\ell(r)$ satisfies assumptions a1)-a4). Let $p(r)$ be the optimal power allocation for this network. Assume that $p(r)$ is non-increasing and the function $G(r) \triangleq \int_0^r K(r,u)du$ is increasing for large r values. Then,

$$\lim_{r\to\infty} \frac{p(r)}{\frac{\tau}{\gamma G(r)}} = 1. \tag{4.12}$$

where $1 \leq \gamma < \infty$ and defined as $\gamma = \lim_{r\to\infty} \int_0^r \frac{K(r,u)}{G(u)}du$.

Proof The result follows by taking the limit in Eqn. 4.8 under the given assumptions.

Remark 1 *Theorem 13 and Lemma 9 also apply to linear networks (see Fig. 4.4) where $K_1(r,u) = \ell(r-u)$ and $K_2(r,u) = \ell(r-u)+\ell(r+u)$ for these configurations.*

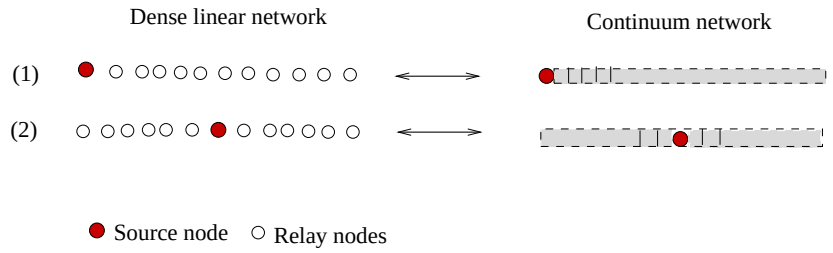

Figure 4.4: Continuum approximation of dense networks-linear configurations

Example 1 *In this example, we consider the pathloss model $\ell(r) = 1/(1+r^2)$ which is the free-space model for large r, $\ell(r) \approx 1/r^2$, and for small r, the model limits the received power at a distance r, $P_t\ell(r)$ to the transmit power P_t. Under the given pathloss model,*

$$K(r,u) = \frac{2\pi u}{\sqrt{(r^2+u^2+1)^2 - 4r^2u^2}}, \quad \frac{\partial K(r,u)}{\partial r} = \frac{-4\pi ur(r^2-u^2+1)}{((r^2+u^2+1)^2-4r^2u^2)^{3/2}}.$$

[4]Pathloss model $\ell(r) = 1/(1+r^2)$ violates the assumption a4 when $u \leq r \leq \sqrt{u^2+1}$. We think that this does not effect the asymptotic behavihor of $p(r)$. Furthermore, analysis can be extended to pathloss models $\ell(r) = 1/(a+r^2)$, $a > 0$ easily under which the asymtotic behavihor is the same and the region where a4 violated is smaller for small values of a.

In Fig. 4.5, we plot the optimal power density which we evaluated by utilizing the recursive formulation (4.10-4.11). Using Lemma 10, we derive $G(r) = \pi \ln((1 + \sqrt{1+4r^2})/2)$ *and* $\gamma = 1$*, then the asymptotic behavior of optimal power density for the pathloss model* $\ell(r) = 1/(1+r^2)$ *as* $r \to \infty$ *is given by*

$$p(r) \approx \frac{\tau}{\pi \ln(r)}. \tag{4.13}$$

In Fig. 4.5, we also plot the limiting power density (4.13). Furthermore, the total power transmitted by the entire network is approximately equal to

$$P_T \approx \int_2^R \frac{\tau}{\pi \ln(r)} 2\pi r dr \approx \frac{\tau R^2}{\ln(R)}, \tag{4.14}$$

for large networks, i.e., as $R \to \infty$.

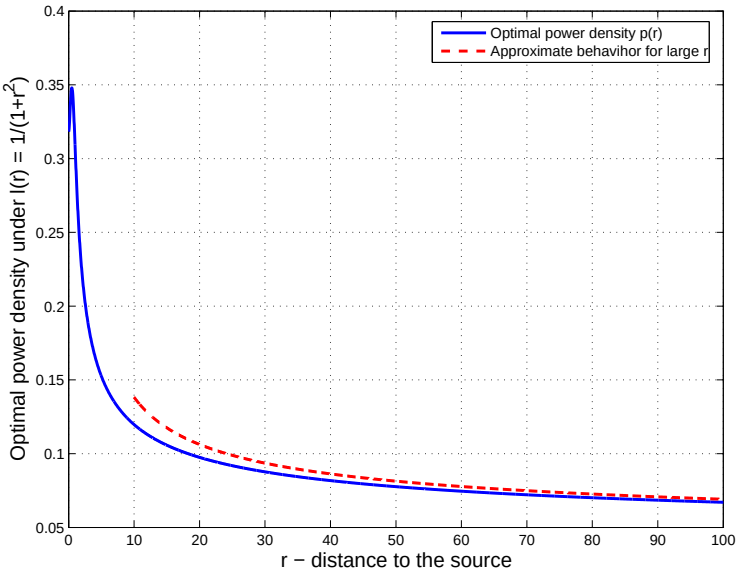

Figure 4.5: Optimal power density - circular network

Remark 2 *The analysis provided though continuum approximation allows us to draw conclusions for networks with finite number of nodes. Consider a finite network with node density* ρ*. Let* D_r *denote the infinitesimal disc at a distance* r *from*

the source. The optimal power for a relay located at the distance r from the source can be approximated as

$$P_{opt}(r) = \frac{total\ relay\ power\ in\ D_r}{total\ number\ of\ nodes\ in\ D_r} = \frac{p(r)2\pi r dr}{\rho 2\pi r dr} = \frac{p(r)}{\rho}. \tag{4.15}$$

We argue that in the high density asymptote, the most power efficient scheme allows the nodes to transmit in the order of their distances from the source with power $p(r)/\rho$.

Remark 3 *Note that the optimal power control policy can be implemented in a distributed fashion if the nodes know their own locations. In general, OCB needs a central control unit, which requires the knowledge of all the link gains in order to schedule the transmissions. It is interesting that this is not necessary in dense networks.*

Remark 4 *The OCB allows nodes to transmit in smaller groups (most scenarios one-by-one) in order to increase the number of receptions at any node; hence, in this way the total power consumption is decreased. The main drawback of OCB is its low spectral efficiency. In general, the latency of OCB is in the order of the number of nodes,* $O(N)$ *(see formulation (4.4) - each level is a single node); for dense networks, it is* $O(\sqrt{N})$ *(levels are thin discs). This is actually consistent with the fundamental result by Verdu [62] who showed that the maximum energy efficiency is achieved when the spectral efficiency is close to zero.*

In the next section, we propose practical and distributed cooperative broadcasting schemes and analyze their performance. Although these schemes are suboptimal, their power consumption is considerably better than noncooperative schemes.

4.5 Cooperative Broadcast with Uniform Power Allocation

In this section, we design a low complexity cooperative broadcasting scheme which is distributed. The proposed scheme is based on our previous work [24]. We consider a simple uniform power allocation policy. The main motivation behind the uniform power allocation scheme is based on our analysis of OCB in Section 4.4. In (4.14), we observed that the total power consumption of OCB is $O(R^2/\ln(R))$ for a circular network with radius R. For large R, the effect of $\ln(R)$ is negligible when compared with R^2. Let $\bar{P}$ denote the relay power density. If the source node reaches the entire network through relaying with uniform power, then the total relay power consumption is

$$P_{total} = \bar{P}\pi R^2 = O(R^2). \tag{4.16}$$

The equations (4.14) and (4.16) scale similarly for large R. This motivates us to design and analyze cooperative broadcasting schemes with uniform power allocation.

In the following, we describe the scheme and the results obtained in [24], and compare it to OCB. In Section 4.5.2, we provide an extension of the scheme, which is more power efficient.

4.5.1 Previous work and its comparison to OCB

In [24], we studied the connectivity of cooperative networks employing a multi-stage transmission scheme with uniform power control policy. Similar to OCB, the scheme in [24] utilizes multiple replicas of the same message from different transmitters.

Suppose that N nodes are uniformly and randomly distributed within $\mathbb{S} =$

$\{(x,y) : x^2+y^2 \leq R^2\}$ and the source node is located at the origin. The scheme is as follows. The source node initiates the transmission by sending a message with power P_s. After source transmission, the group of nodes that receives the message with sufficient SNR τ will be called level-1 nodes. We will denote the location of level-1 nodes by the set $\mathcal{S}_1 = \{(x,y) \in \mathbb{S} : P_s\ell(x,y) \geq \tau\}$. We assume that the message is channel coded so that the nodes with received SNR greater than or equal to τ can decode the message correctly. Let P denote the transmission power of each relay. After the transmission of the nodes in $\mathcal{S}_1$, the nodes that receive the message with SNR (see Section 4.2.1) greater and equal to τ will be called level-2 nodes. It is assumed that each relay accumulates signals from m previous levels. The set of locations of level-k nodes $\mathcal{S}_k$ is given as

$$\mathcal{S}_k = \{(x,y) \in \mathbb{S} \setminus \bigcup_{i=1}^{k-1} \mathcal{S}_i : \sum_{(x',y')\in\mathcal{U}_k} P\ell(x-x', y-y') \geq \tau\}, \quad k \geq 2, \tag{4.17}$$

where $\mathcal{U}_k = \bigcup_{i=(k-m)_+}^{k-1} \mathcal{S}_i$.

In order to obtain the results in [24], we first considered a random network in which the node locations are randomly and uniformly distributed, and we obtained a continuum model from the random network by letting the number of nodes go to infinity while fixing the total relay power. Let $\rho = N/\text{Area}(\mathbb{S})$ be the density (node/unit area) of relays within the region $\mathbb{S}$. Define the *relay power per unit area* as $\bar{P} \triangleq PN/\text{Area}(\mathbb{S}) = P\rho$.

Under the continuum model, each level becomes a disc with inner radius r_{k-1} and outer radius r_k, *i.e.,* the level-k set $\mathcal{S}_k$ can be approximated by the region $\mathcal{A}_k = \{(x,y) : r_{k-1}^2 < x^2+y^2 \leq r_k^2\}$ [24, Theorem 1, Lemma 1]. We explicitly determined level discs, *i.e.,* $\{r_k\}$ and analyzed network dynamics as a function of decoding threshold τ, relay power P_r, and source power P_s. Furthermore, we showed that there exists a *phase transition* in the network behavior: if the SNR threshold is

below a *critical value*, the message is delivered to the whole network. Otherwise, only a fraction of the nodes is reached proportional to the source transmit power. That is,

$$\lim_{k\to\infty} r_k \to \begin{cases} \infty & \text{if } \tau \leq \pi \ln(m+1)\bar{P} \\ \mathrm{C} & \text{if } \tau > \pi \ln(m+1)\bar{P} \end{cases} \tag{4.18}$$

where $C < \infty$ depends on $P_s, \tau/\bar{P}$. The result (4.18) is obtained under the pathloss attenuation model $\ell(r) = 1/r^2$.

There are two main differences between the scheme in [24] and OCB. In [24], (1) each relay uses a fixed predetermined power level P; (2) each relay considers the receptions from only m previous levels in order to decide whether or not to retransmit. On the other hand, under OCB, relays utilize the optimal power control policy and consider the reception from all previous nodes, *i.e.,* $m = \infty$.

In the considered scheme [24], a large number of nodes transmit at each level. Note that the nodes in a given level can utilize space-time codes (or transmit narrowband signals) in order to increase the spectral efficiency. Hence, the scheme in [24] has improved spectral efficiency when compared with OCB. In addition, it is obvious that the scheme has much lower complexity than OCB. The question that we consider next is how do their performance compare in terms of power efficiency.

Let $\bar{P}_{min}$ be the minimum relay power density such that source message reaches entire network. We can interpret the critical threshold phenomena in [24] from the viewpoint of critical power density. Using (4.18) we obtain

$$\bar{P}_{min} = \tau/(\pi \ln(m+1)). \tag{4.19}$$

The minimum power consumption of the broadcasting scheme in [24] is $P_T^{(coop)} = \bar{P}_{min}\pi R^2$.

In Section 4.6, we compare the power efficiency of the simple scheme in [24] with noncooperative multihop transmission. Further power gains can be achieved by modifying the scheme such that part of the nodes are shut off. In the next section, we propose an extension of the scheme. In Section 4.7, we discuss how close these schemes to OCB in terms of power efficiency.

4.5.2 Double-Threshold Cooperative Broadcast (DTCB)

In this section, we extend the scheme in [24] so as to come close to the OCB bound. The key idea is to silence nodes whose contributions are strongly attenuated at the next level. Consider the scheme described in the previous subsection. Among level-1 nodes, the ones that have received source transmission with high SNR ($Power \geq K\tau$, where $K > 1$) are the ones that are closer to the source due to the properties of the pathloss attenuation function $\ell(\cdot)$. However, these nodes are further away from the level-2 nodes, and have a lesser contribution to the received signal at the level-2 nodes. This observation motivates us to propose a double threshold scheme, which is described next.

The source node initiates the transmission. Similar to the previous section, we define the level-1 nodes as the set of nodes that receives source transmission with SNR at least τ. Among the level-1 nodes, the nodes that receive the source transmission with SNR within the range $[\tau, K\tau)$ are allowed to retransmit with uniform power P. We will also call this set *active* level-1 nodes. In [24], K is assumed to be ∞.

For brevity, we avoid the theoretical analysis of the network behavior under DTCB; however, the extension follows easily from [24]. Intuitively, we can see that the level sets become discs as in [24] (see Fig. 4.6) and the phase transition

behavior occurs at a critical power density that depends also on K.

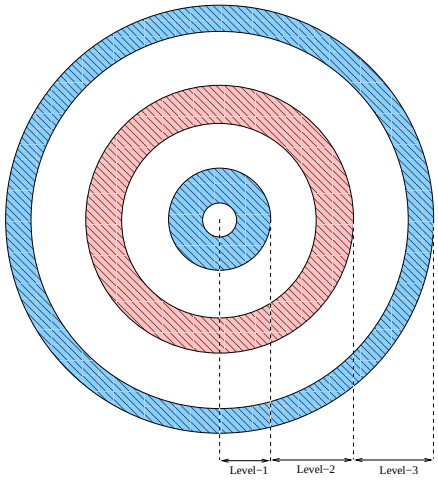

Figure 4.6: Double-Threshold Uniform Power Allocation: the shaded regions correspond to the active portions of the levels

Remark 5 *The parameters K and m effect not only the power efficiency but also the speed of transmission. The larger these values are, the faster the message reaches the entire network. There is a trade-off between the complexity (large m) and the performance. By choosing K close to 1 and setting $m = \infty$, the DTCB power consumption approaches the OCB bound. This is also supported by simulations in Section 4.7.*

4.6 Cooperative versus noncooperative Broadcast

In this section, we compare the power efficiency of cooperative broadcasting with that of noncooperative multihop broadcasting. The results are based on the continuum model.

4.6.1 Noncooperative multihop broadcast

In the noncooperative transmission, each node receives the message from its neighbor and the message propagates through multihop transmissions. We assume that each relay hop covers a circular area with radius r. In order to calculate the minimum power spent under this scheme, we need to calculate the minimum number of circles with radius r, which will be denoted by N_r, required to cover the entire network, such that the circles have their centers on the circumference of the neighboring circles (see Fig. 4.7). We provide a lower bound on N_r using a hexagonal tessellation such that the nodes located at the vertices and the centers of the hexagons transmit.

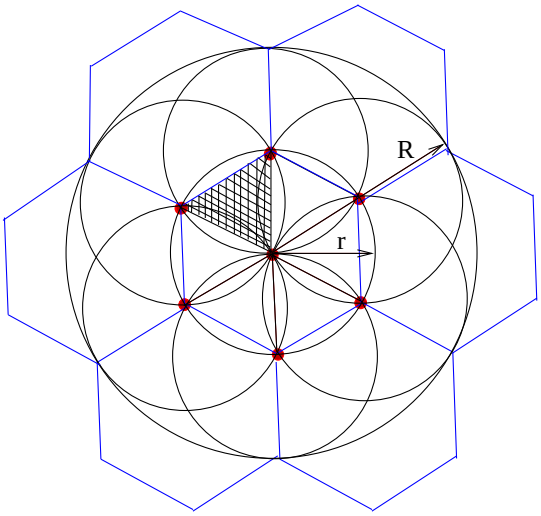

Figure 4.7: Noncooperative multihop broadcast: shaded area = $\frac{r^2\sqrt{3}}{4}$

Assume that the nodes lie on a region with area A. The total number of transmissions N_r can be lower bounded as follows. Consider the shaded triangular region in Fig. 4.7. By dividing the total area A with the area of this triangle, we obtain the number of triangles required to cover the area A. Each triangle corresponds to 3 nodes (vertices of the triangle), and each vertex is common to 6

triangles. Hence, N_r can be lower bounded as

$$N_r \geq \frac{3}{6}\frac{A}{\text{Triangular Area}} = \frac{2A}{\sqrt{3}r^2}, \tag{4.20}$$

where the shaded triangular region is shown in Fig. 4.7. Let P_r denote the minimum power required by a transmitter so that the nodes within a radius r around the transmitting node, receive the message with at least SNR τ. For the pathloss attenuation function $\ell(r)$, $P_r = \tau/\ell(r)$. Note that by fixing r, we fix the total number of hops required to cover the area A. The best multihop scheme minimizes the total power consumption by optimizing over the number of hops, which is a function of r. Hence, the minimum total power spent by the multihop transmission is

$$P_T^{(noncoop)} = \min_r N_r P_r \geq \min_r \frac{2A\tau}{\sqrt{3}\ell(r)r^2}. \tag{4.21}$$

Note that the derivation above is for the multihop transmission and does not include the direct transmission because of the way we calculate N_r (see Fig. 4.7).

4.6.2 Direct transmission

In direct transmission, the source node transmits with power such that the entire network is reached. In general, per node power constraints may not allow this. Under the assumption that the source has unconstrained power, the power spent by direct transmission to cover an area A is

$$P_T^{(direct)} = \tau/\ell(\sqrt{A/\pi}). \tag{4.22}$$

4.6.3 Power efficiency of DTCB for $\ell(r) = 1/r^2$

In this subsection, we show the power efficiency of DTCB under the worst-case scenario, *i.e.,* with parameters $K = \infty, m = 1$. Note that the gain increases if we

increase m or decrease K.

Under the pathloss attenuation model $\ell(r) = 1/r^2$, the total power spent by the multihop transmission is independent of the number of hops, and (4.21) simplifies further to

$$P_T^{(noncoop)} \geq 2A\tau/\sqrt{3}. \tag{4.23}$$

Next, we calculate the total power expenditure under the cooperative scheme with parameters $K = \infty$ and m (Section 4.5.1) so that the nodes within an area A receive the message reliably. Under the pathloss model $\ell(r) = 1/r^2$, we derived the critical power density to reach the entire network (4.19). Using this result,

$$P_T^{(coop)} \quad = \quad A\bar{P}_{min} = A\tau/(\pi \ln(m+1)). \tag{4.24}$$

Using (4.23) and (4.24) for $m = 1$, the gain of cooperative transmission is lower bounded as,

$$Gain = \frac{P_T^{(noncoop)} - P_T^{(coop)}}{P_T^{(noncoop)}} \times 100 \geq 60\%. \tag{4.25}$$

This shows that the percentage gain attained with cooperation in dense networks is close to 60% under the pathloss model $\ell(r) = 1/r^2$.

Note that under pathloss model $\ell(r) = 1/r^2$, the power consumption of direct transmission is $P_T^{(direct)} = A\tau/\pi$, which is more power efficient than the multihop noncooperative broadcast and also cooperative broadcast with $m = 1$. However, cooperative broadcast becomes more efficient for $m > 1$. Note that, for pathloss attenuation with exponents $\alpha > 2$, the performance of direct transmission gets worse substantially (see (4.22)).

4.7 Simulations

In this section, we look at the performance of the cooperative broadcast in networks with finite number of nodes. The results are averaged over 100 random networks. The nodes are uniformly distributed in a disc with radius R. The source node is located at the center.

In Figs. 4.8 and 4.9, we display the performance of the policy that allows the nodes to transmit with power $p(r)/\rho$, where $p(r)$ is the optimal power density obtained from continuum analysis, and ρ is the node density (see Example 1 and Remark 2). The nodes transmit in the order of their distance from the source r. In Fig. 4.8, we plot the percentage of the nodes that receive the source message, and in Fig. 4.9, we plot the total power consumption as a function of ρ. The pathloss model is $\ell(r) = 1/(1+r^2)$ and the network radius is $R = 5.64$. Note that the OCB bound is equal to $P_{OCB} \triangleq \int_0^R p(r) 2\pi r dr = 18.16 \approx R^2/\ln(R)$. As node density increases, the total power consumption approaches P_{OCB} while almost all of the nodes receive the message.

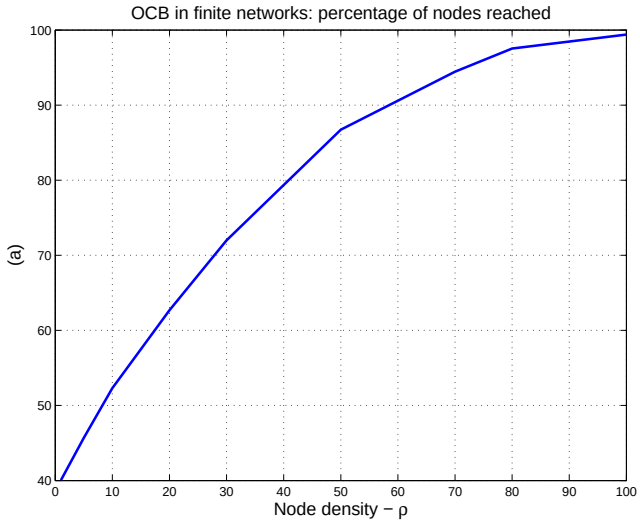

Figure 4.8: Percentage of the nodes reached by the source

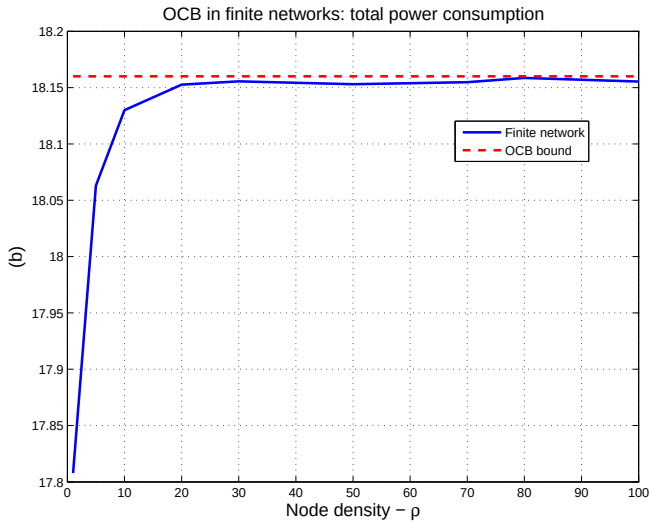

Figure 4.9: Total power consumption

Next, we check the accuracy of the continuum analysis in approximating the critical relay power (see Section 4.5). In Fig. 4.10, we plot P_{min}, which is calculated via an exhaustive search, as a function of the node density ρ. We also display the analytical result $P^a_{min} \triangleq \bar{P}_{min}/\rho$, where $\bar{P}_{min}$ is given by (4.19). As expected, we observe that P^a_{min} becomes a good approximation of the critical per node power as the node density increases.

In Fig. 4.11, we plot the total power consumption of DTCB as a function of the network area A. In addition, we plot the power consumption of OCB obtained from continuum analysis, P_{OCB}. We consider the pathloss attenuation function $\ell(r) = 1/(1 + r^2)$. The critical relay power for DTCB is obtained via exhaustive search. As K decreases and m increases, the performance of DTCB approaches the OCB bound. Note that the performances of DTCB with parameters $\{K = \infty, m = 10\}$ and $\{K = 1.5, m = 3\}$ are similar.

In Fig. 4.12, we plot the total power consumption of different cooperative schemes and noncooperative scheme as a function of the network area A for pathloss

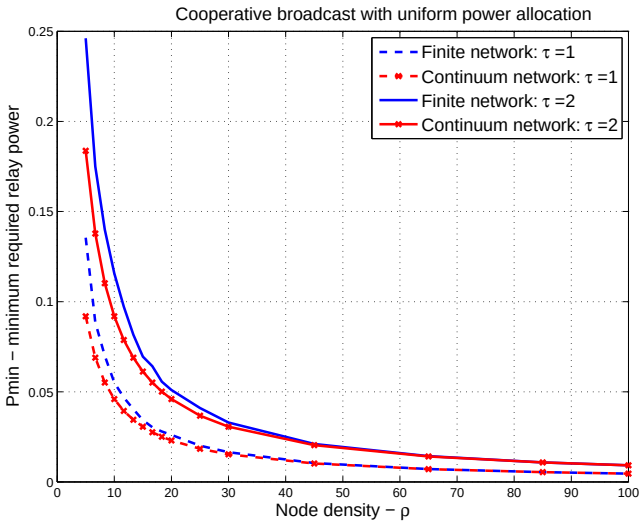

Figure 4.10: The critical power per node required to cover an area $A = 20m^2$, where $P_s = \tau$, $m = 1$.

models $\ell(r) = 1/(1 + r^\alpha), \alpha \in \{2, 4\}$. For cooperative broadcast, the critical relay power is obtained via exhaustive search. For noncooperative multihop broadcast, we use (4.21) and for direct transmission we use (4.22). In Fig. 4.13, we compare the cooperative scheme and the noncooperative scheme under the condition that the number of hops required to cover A for both schemes are the same. Note that suboptimal cooperative broadcasting schemes have considerable power gains.

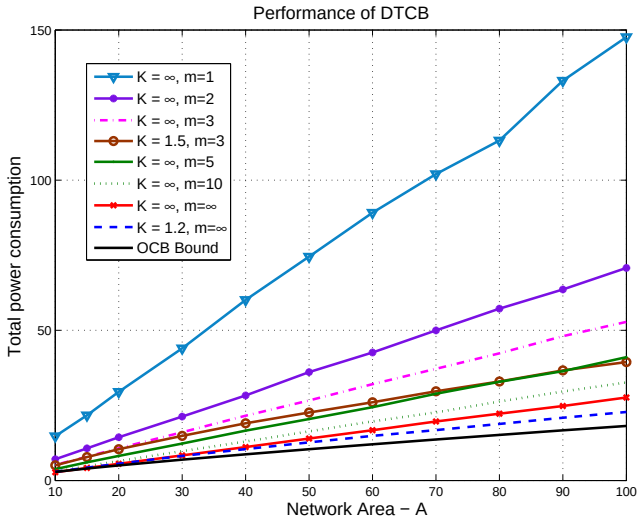

Figure 4.11: Total power spent to cover an area A by both optimal and suboptimal cooperative broadcasting schemes. The node density is $\rho = 20$.

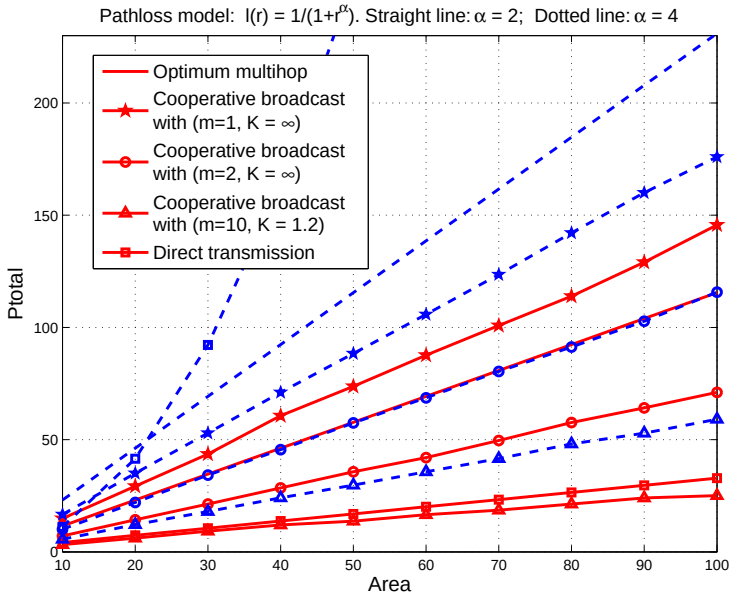

Figure 4.12: Total power spent to cover an area A. The node density is $\rho = 20$ and decoding threshold is $\tau = 1$. For cooperative broadcast, $P_s = 1.5$.

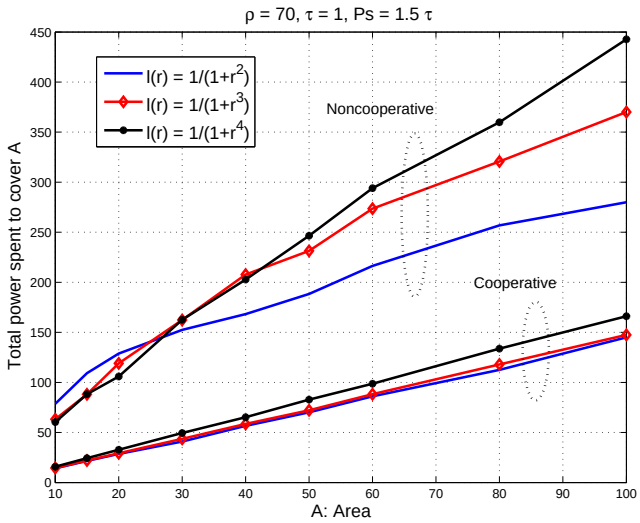

Figure 4.13: Cooperative versus noncooperative under fixed number of hops. Cooperative scheme with $K = \infty$ and $m = 1$.

Appendix 4.A Proof of Lemma 7

The problem in (4.4) can be reexpressed as

$$\min_{\mathbf{S},\mathbf{p}} \mathbf{1}^T\mathbf{p} \;\text{ subject to }\; \mathcal{L}(\mathbf{S}\mathbf{H}\mathbf{S}^T)\mathbf{p} \geq \mathbf{b}_\tau,\; \mathbf{p} \geq 0, \tag{4.26}$$

where $\mathbf{b}_\tau = \tau[\mathbf{1}; 0]$. It can be easily shown that $\{\tilde{\mathbf{p}}, \tilde{\mathbf{S}}\}$ is the optimal solution for (4.26) if and only if $\{\tilde{\mathbf{S}}^t\tilde{\mathbf{p}}, \tilde{\mathbf{S}}\}$ is the optimal solution for (4.4).

Proof of a):

We will assume that $\mathcal{L}(\mathbf{H})$ is column-ordered and $N = 2$. Next, we will show that for any given permutation matrix $\mathbf{S}$ and $\tilde{\mathbf{p}} \geq \mathbf{0}$,

$$\mathcal{L}(\mathbf{S}\mathbf{H}\mathbf{S}^T)\tilde{\mathbf{p}} \geq \mathbf{b}_\tau \Rightarrow \mathcal{L}(\mathbf{H})\tilde{\mathbf{p}} \geq \mathbf{b}_\tau. \tag{4.27}$$

The statement (4.27) means that for a given $\mathbf{S}$, if $\tilde{\mathbf{p}}$ is in the feasible set of $\mathbf{p}$'s of the optimization problem

$$\min_{\mathbf{p}} \mathbf{1}^T\mathbf{p} \;\text{ subject to }\; \mathcal{L}(\mathbf{S}\mathbf{H}\mathbf{S}^T)\mathbf{p} \geq \mathbf{b}_\tau,\; \mathbf{p} \geq 0, \tag{4.28}$$

then, $\tilde{\mathbf{p}}$ is also in the feasible set of the optimization problem

$$\min_{\mathbf{p}} \mathbf{1}^T\mathbf{p} \;\text{ subject to }\; \mathcal{L}(\mathbf{H})\mathbf{p} \geq \mathbf{b}_\tau,\; \mathbf{p} \geq 0. \tag{4.29}$$

This implies that the feasible set for the linear program (4.28) is a subset of the feasible set for the linear program (4.29); hence, the optimal solution of the problem (4.26) is obtained by setting $\mathbf{S} = \mathbf{I}$ (this is under the assumption $\mathcal{L}(\mathbf{H})$ is column-ordered). The theorem follows easily. The proof for general N can be found in [63].

Proof of b):

Since $\mathcal{L}(\hat{\mathbf{S}}\mathbf{H}\hat{\mathbf{S}}^T)$ is column-ordered, $\hat{\mathbf{S}}$ corresponds to the optimal schedule and the optimal power allocation can be found as the solution of

$$\min_{\mathbf{p}} \mathbf{1}^T\mathbf{p} \;\text{ subject to }\; \mathcal{L}(\hat{\mathbf{S}}\mathbf{H}\hat{\mathbf{S}}^T)\mathbf{p} \geq \mathbf{b}_\tau,\; \mathbf{p} \geq 0. \tag{4.30}$$

Next, we will use proof by contradiction. We assume that $\mathcal{L}(\hat{\mathbf{S}}\mathbf{H})$ is row-ordered and the optimal power vector $\mathbf{p}^* = [P_1^* \dots P_{N+1}^*]$ is such that

$$\mathcal{L}(\hat{\mathbf{S}}\mathbf{H}\hat{\mathbf{S}}^T)\mathbf{p}^* > \mathbf{b}_\tau. \tag{4.31}$$

For simplicity, assume that the first row satisfies (4.31) with strict inequality, *i.e.,* $[\mathcal{L}(\hat{\mathbf{S}}\mathbf{H}\hat{\mathbf{S}}^T)\mathbf{p}^*]_1 > \tau$. Define

$$\beta := \max_{i\geq 3} \frac{\alpha_{i1}}{\alpha_{i2}},$$

where α_{ij} is the (i,j)'th element of $\mathcal{L}(\hat{\mathbf{S}}\mathbf{H}\hat{\mathbf{S}}^T)$. Since $\mathcal{L}(\hat{\mathbf{S}}\mathbf{H}\hat{\mathbf{S}}^T)$ is row-ordered, $\beta < 1$ (assuming $\exists i$ such that $\alpha_{i1} \neq \alpha_{i2}$). Define

$$\mathbf{p}^{**} := [P_1^* - \epsilon \, , P_2^* + \beta\epsilon \, , P_3^*, \dots, P_{N+1}^*]$$

for some $\epsilon > 0$. Since

$$\mathbf{1}^T\mathbf{p}^{**} < \mathbf{1}^T\mathbf{p}^*, \ \mathcal{L}(\hat{\mathbf{S}}\mathbf{H}\hat{\mathbf{S}}^T)\mathbf{p}^{**} \geq \mathbf{b}_\tau, \ \mathbf{p}^{**} \geq \mathbf{0},$$

$\mathbf{p}^*$ can not be optimal solution. Hence, the proof follows by contradiction. The proof can be easily generalized if the k'th row, $k \neq 1$ satisfies (4.31) with strict inequality, *i.e.,* $[\mathcal{L}(\hat{\mathbf{S}}\mathbf{H}\hat{\mathbf{S}}^T)\mathbf{p}^*]_k > \tau$.

Appendix 4.B Proof of Lemma 8

Assume that the optimal scheduling is such that there exist at least a level that has more than one node. We assume that nodes do not transmit and receive at the same time. In this case, each node in a given level receives the transmission of previously scheduled nodes with the same power. That is, $\forall i, j \in S_m$,

$$\sum_{k=0}^{m-1} \sum_{n\in S_k} H_{in}P_n = \sum_{k=0}^{m-1} \sum_{n\in S_k} H_{jn}P_n. \tag{4.32}$$

This can be proved by contradiction. Assume that there exists $i, j \in S_m$, such that (4.32) is untrue; assume that node j receives the previous transmissions with higher power. In this case, by assigning node j to transmit before node i, we can decrease the total power expenditure. The proof of the lemma follows from (4.32) and the assumption that the nodes in a given level transmit with the same power by using simple matrix manipulations.

Appendix 4.C Proof of Theorem 13

Let P_1 denote the optimal transmission power of the source. In the continuum, under the pathloss function $\ell(r)$ that satisfies the assumptions a1-a3, each level is a thin disc shaped region. We conjecture that the optimal power allocation allocates equal powers to the nodes in the same level. Consider the i'th (located at a distance r) and k'th (located at a distance u) levels. By using Lemma 8, we obtain the simplified formulation (4.6). Furthermore, in the continuum,

$$[\bar{\mathbf{H}}]_{ik} \rightarrow H(r,u) \triangleq \int_0^{2\pi} \frac{1}{2\pi} \ell(\sqrt{r^2+u^2-2ur\cos(\theta)}) d\theta.$$

See Fig. 4.14 for the derivation of $H(r,u)$. Furthermore, in the continuum,

$$\bar{P}_k = |S_k| P_k \rightarrow P(u) \triangleq 2\pi u p(u) du.$$

Since $H(r,u)$ is decreasing in r and increasing u for $0 \leq u \leq r \leq R$, utilizing Lemma 7-b and replacing summations with integrals, we obtain

$$P_1 \ell(r) + \int_0^r p(u) K(r,u) du = \tau, \forall r.$$

By taking the limit $r \rightarrow 0$, we find that optimal source transmission power $P_1 = \tau / l(0)$. Hence, the theorem follows.

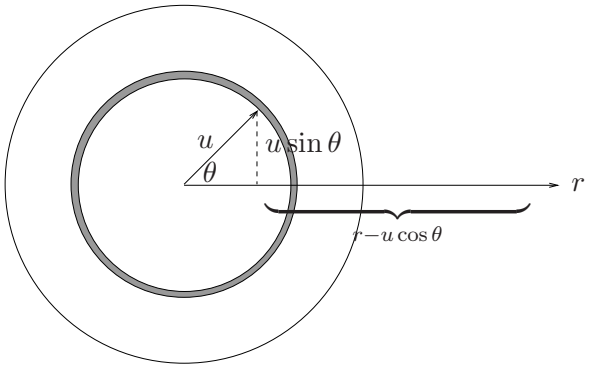

Figure 4.14: Derivation of $H(r, u)$.

Chapter 5

Randomized Space-Time Coding for Distributed Cooperative Communication

5.1 Organization

The chapter is organized as follows: In Section 5.2, we describe the system model and the proposed scheme. In Section 5.3, we characterize the diversity order of the randomized space-time codes and provide design criteria that leads to full diversity order. In Sections 5.4, we present specific examples for the randomization matrix $\boldsymbol{\mathcal{R}}$. In Section 5.5, we provide the extended version of antenna selection scheme [36]. In Section 5.6, we present the simulations.

5.2 System Model and the Proposed Protocol

We consider a system where a random number of nodes N collaborate in order to transmit a common message to a destination distributively. This problem arises in decode-and-forward communication schemes, where a source node transmits to a group relays (Phase I); N of the relays successfully decode the source message, and transmit the same message simultaneously after re-encoding (Phase II). Fig. 5.1 describes an analogous scenario, where the end receiver is remotely located relative to the network.

In this chapter, we will assume that: 1) the Phase I of the communication has taken place; 2) each relay node can determine whether or not it has reliably decoded the message, 3) only the nodes that has decoded reliably transmit the message, 4) the end receiver uses only the data received from Phase II to decode the message. We will deal exclusively with the Phase II of the communication, and assume that the number of transmitting nodes N (*i.e.,* the *active nodes*) is random due to the error-free decoding constraint.

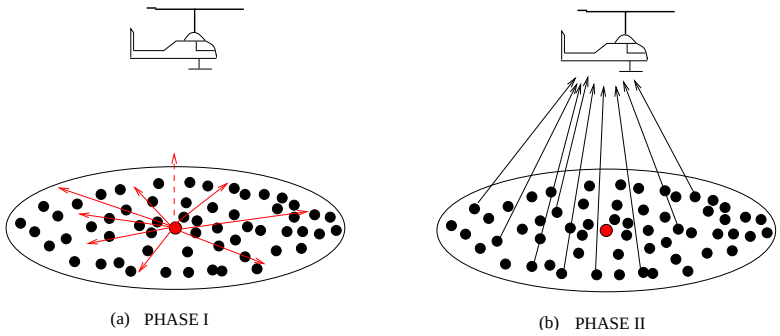

Figure 5.1: Two phase cooperative communication.

The output signal for a block space-time coded transmission over a point-to-point $N \times 1$ MISO (multiple-input-single-output) link is generally expressed as

follows [25]:

$$\mathbf{y} = \mathbf{X}\mathbf{h} + \mathbf{w}, \tag{5.1}$$

where $\mathbf{X} = [X_{ij}] \in \mathbb{C}^{P \times N}$ denotes the transmitted signal (i is the time index, j is the transmitter antenna index), $\mathbf{h} = [h_j] \in \mathbb{C}^{N \times 1}$ denotes the channel gains from different antennas, and $\mathbf{w}$ is the channel noise.

In a block space-time coded cooperative network, the same system model (5.1) can be used under certain assumptions. For the cooperative system, the j in X_{ij} denotes the user index and h_j is the channel gain from user j to the destination. Furthermore, we assume that the following are satisfied:

a1) The relative receiver and transmitter motion is negligible so that the channels do not change during the course of the transmission of several blocks of data.

a2) Frequency drifts among transmissions from different nodes are negligible. Frequency errors at different nodes are time-invariant over the transmission of several space time codes and the slow phase fluctuations can be incorporated into the channel coefficients $\mathbf{h}$.

a3) There is negligible time-offset among transmissions compared to the symbol interval, *i.e.,* there is no inter-symbol interference (ISI).

We assume a1), a2), a3) to be able to describe the system concisely using equation (5.1), and also for the analysis of the proposed protocol. Nevertheless, it should be emphasized that for the application of the proposed protocol assumption a3) can be relaxed. The proposed protocol is also applicable to time-asynchronous relays, as discussed in [64].

Before proceeding any further, we would like to note that ISI, which is traditionally viewed as an impairment, can actually improve the system performance

by providing frequency diversity. Wei et al. [44] actually proposed introducing random delays to relay transmissions to increase diversity, and showed significant improvements in system performance.

The path-loss and shadowing effects are modelled as a block Rayleigh fading with $\mathbf{h} \sim \mathcal{N}_c(\mathbf{0}, \mathbf{\Sigma}_h)$, where $\mathbf{\Sigma}_h$ is a positive definite matrix. The receiver noise is modelled by $\mathbf{w} \sim \mathcal{N}_c(0, N_0\mathbf{I})$, where $\mathbf{w}$ is independent of $\mathbf{h}$.

Notation: In the following, $\det(\mathbf{A})$, $\text{rank}(\mathbf{A})$, $\text{Tr}(\mathbf{A})$ denote the determinant, rank and trace of a matrix $\mathbf{A}$ respectively. In addition, $\text{diag}(a_1, a_2, \ldots, a_n)$ denotes $n \times n$ diagonal matrix such that (i, i)'th element is equal to a_i. The identity matrix is denoted by $\mathbf{I}$. All the matrices and vectors will be denoted by bold symbols. A $L \times N$ matrix $\mathbf{A}$ is said to be *full-rank* if $\text{rank}(\mathbf{A}) = \min\{L, N\}$.

5.2.1 Proposed Diversity Scheme

Let $\mathbf{s} = [s_0 \ s_1 \ldots s_{n-1}]$ be the block of source symbols to be transmitted to the destination. We assume that the message is known perfectly at the active nodes in Phase II. We will consider the transmission of one block of data for simplicity, although the source message can consist of several blocks, although the source message will, in general, consist of several blocks. In the following, we describe the processing at each node and analyze the decoding performance at the destination.

At each node, the $\mathbf{s}$ is mapped onto a matrix $\boldsymbol{\mathcal{G}}(\mathbf{s})$ as is done in standard space-time coding:

$$\mathbf{s} \rightarrow \boldsymbol{\mathcal{G}}(\mathbf{s}),$$

where $\boldsymbol{\mathcal{G}}$ is a $P \times L$ space-time code matrix. Here, L denotes the number of antennas in the underlying space-time code. In our scheme each node transmits a block of P symbols, which is a random linear combination of columns of $\boldsymbol{\mathcal{G}}(s)$. Let $\mathbf{r}_i$ be

the $L \times 1$ random vector that contains the linear combination coefficients for the i'th node. Define $\mathbf{X} = [\mathbf{x}_1\ \mathbf{x}_2 \dots \mathbf{x}_N]$ as the $P \times N$ random code matrix whose rows represent the time and columns represent the space, where $\mathbf{x}_i = \boldsymbol{\mathcal{G}}(\mathbf{s})\mathbf{r}_i$ is the code transmitted by the i'th node. The randomized space time coding can be expressed as the double mapping:

$$\mathbf{s} \rightarrow \boldsymbol{\mathcal{G}}(\mathbf{s}) \rightarrow \boldsymbol{\mathcal{G}}(\mathbf{s})\boldsymbol{\mathcal{R}}, \tag{5.2}$$

where $\boldsymbol{\mathcal{R}} = [\mathbf{r}_1\ \mathbf{r}_2 \dots \mathbf{r}_N]$. In the following, the $L \times N$ matrix $\boldsymbol{\mathcal{R}}$ will be referred to as the *randomization matrix*. Since each node's processing is intended to be local, $\mathbf{r}_i$'s should be independent for each $i = 1 \dots N$, and we will also assume that they are identically distributed. This property allows the randomized space-time coding to be implemented in a decentralized fashion. In other words, each node chooses a random set of linear combination coefficients from a given distribution, which does not depend on the node index.

Let $\mathbf{y}$ be the received signal at the destination. Using (5.1), we can rewrite the received signal as

$$\mathbf{y} = \boldsymbol{\mathcal{G}}(\mathbf{s})\boldsymbol{\mathcal{R}}\mathbf{h} + \mathbf{w}, \tag{5.3}$$

where $\mathbf{w} \sim \mathcal{N}_c(\mathbf{0}, N_0\mathbf{I})$ and $\mathbf{h} \sim \mathcal{N}_c(\mathbf{0}, \boldsymbol{\Sigma}_\mathbf{h})$.

Definition Define $\mathbf{X} \triangleq \boldsymbol{\mathcal{G}}(\mathbf{s})\boldsymbol{\mathcal{R}}$ as the *randomized space-time code* and $\tilde{\mathbf{h}} \triangleq \boldsymbol{\mathcal{R}}\mathbf{h}$ as the *effective channel*.

These two definitions express two critical interpretations of the proposed scheme. If $\boldsymbol{\mathcal{G}}(\mathbf{s})\boldsymbol{\mathcal{R}}$ is considered as a whole, then the scheme can be viewed as a randomized space-time code $\mathbf{X}$ transmitted over channel $\mathbf{h}$. On the other hand, if $\boldsymbol{\mathcal{R}}\mathbf{h}$ is considered as a whole, then the scheme can be viewed as a deterministic space-time code $\boldsymbol{\mathcal{G}}(\mathbf{s})$ transmitted over a randomized channel $\tilde{\mathbf{h}}$.

The second interpretation is especially important for decoding purposes at the receiver. In order to perform coherent decoding, the receiver needs to estimate the channel coefficients. Instead of estimating the channel vector $\mathbf{h}$ and the randomization matrix $\boldsymbol{\mathcal{R}}$ separately, the receiver can estimate the effective channel coefficients $\tilde{\mathbf{h}}$. For this, the training data at the transmitters should use the same randomization procedure. Estimating the effective channel provides two main advantages: i) decoders already designed for multiple-antenna space-time codes can be directly used for randomized space-time coding; ii) the number of coefficients that are estimated is less when $L \leq N$, since in this case the effective channel vector $\tilde{\mathbf{h}}$ is shorter that the actual channel vector $\mathbf{h}$.

Yiu et al. [46] proposed a deterministic version of the randomized space-time code scheme (5.3), where each column of matrix $\boldsymbol{\mathcal{R}}$ is a pre-determined deterministic code allocated to a specific user. The main advantage of this scheme is that it provides robustness to the uncertainty as to which group of relays will transmit in Phase II. That is, the diversity order N is achieved as long as $N \leq L$ irrespective of which N relay nodes transmit. This is different from the orthogonal space-time code approach in [10], because there, if two nodes happen to be allocated the same transmit antenna, then the diversity order is no longer N. Both in [46] and [10], the nodes have to be allocated antennas or codes. The main advantage of randomized space-time coding is that it achieves the full diversity order N for $N < L$ without code or antenna allocation.

Symbols: N denotes the number of active relays in Phase II; L and P denote the number of columns and rows of the underlying space time code matrix $\boldsymbol{\mathcal{G}}(\mathbf{s})$ respectively (L is also the maximum diversity order of the underlying space-time code while P is its time duration, in terms of number of symbol intervals). The

signal-to-noise ratio (SNR) is denoted by SNR; $P_e(\text{SNR})$ is the average error probability; d^* is the diversity order of the randomized space-time code. Often, the notation $\boldsymbol{\mathcal{G}}(\mathbf{s})$ will be replaced simply by $\boldsymbol{\mathcal{G}}$.

5.2.2 Performance Metrics

Traditional space-time codes are designed using the probability error as a performance criterion [25]. We will adopt a similar approach for the design of randomized space-time codes. Our main focus is the maximum diversity that can be achieved by the scheme.

Let $\mathcal{M} = \{\mathbf{s}_1, \mathbf{s}_2, \ldots \mathbf{s}_{|\mathcal{M}|}\}$ be the message set, where each message is chosen equally likely. Define $\text{SNR} = 1/N_0$ (Eqn. 5.3). Assume that the effective channel $\tilde{\mathbf{h}}$ is known at the destination (*i.e.,* the receiver has channel side information). Let $P_e(\text{SNR})$ denote the symbol error probability at the destination under the maximum likelihood detection rule, *i.e.,* the probability that a message $\mathbf{s}_i$ is transmitted, but the decoder produces another message $\mathbf{s}_j,\ j \neq i$ (averaged over i and $\tilde{\mathbf{h}}$).

Definition The diversity order d^* of a scheme with probability of error $P_e(\text{SNR})$ is defined as

$$d^* = \lim_{\text{SNR}\to\infty} \frac{-\log P_e(\text{SNR})}{\log \text{SNR}}. \tag{5.4}$$

We say that the randomized space-time code achieves *diversity order* d if $d \leq d^*$. The randomized space-time code is said to achieve a *coding gain* G if $P_e(\text{SNR}) \leq G\ \text{SNR}^{-d^*}$.

In this chapter, we will consider two different types of performance metrics: i) symbol error rate $P_e(\text{SNR})$ (by an upper bound and simulations); ii) diversity

order d^* (analytically and by simulations). These metrics do not take channel coding into account. Instead of P_e and d^*, we could analyze outage probability that also takes into account the effect of channel coding. We do not treat this case, however we wish to remark that, in the case of orthogonal space-time codes the outage probability analysis can be easily derived from the error probability analysis carried out here.

5.3 Design and Analysis of Randomized Space-time Codes

In this section, we analyze the performance of randomized space-time codes and come up with some principles that facilitate the design of the randomization matrix $\boldsymbol{\mathcal{R}}$. Without loss of generality, we assume that $P \geq L$ for the $P \times L$ deterministic space-time code matrix $\boldsymbol{\mathcal{G}}$. Define $\boldsymbol{\mathcal{G}}_i \triangleq \boldsymbol{\mathcal{G}}(\mathbf{s}_i)$.

There is a vast literature on the design of deterministic space-time codes $\{\boldsymbol{\mathcal{G}}_i\}$, and the design of $\{\boldsymbol{\mathcal{G}}_i\}$ problem has been thoroughly investigated by many authors. Our objective in this section is the design of the randomization matrix $\boldsymbol{\mathcal{R}}$ and the analysis of its effect on the diversity order. We will assume that the underlying space-time code satisfies the rank criterion [25], which is expected to be satisfied by any optimal design.

C1) *The Rank Criterion for $\boldsymbol{\mathcal{G}}$:* For any pair of space-time code matrices $\{\boldsymbol{\mathcal{G}}_k, \boldsymbol{\mathcal{G}}_i\}$, the matrix $(\boldsymbol{\mathcal{G}}_k - \boldsymbol{\mathcal{G}}_i)$ is full-rank, *i.e.,* of rank L.

5.3.1 Exact Characterization of the Diversity Order

The performance degradation in fading channels results from the *deep fade event* as discussed in [35, Ch. 3]. In this section, we first define what the deep fade

event means for our communication system and characterize its diversity order. The following lemma asserts that we can equivalently consider the deep fade event instead of P_e for diversity calculations.

Lemma 11 *Let* $\{||\boldsymbol{\mathcal{R}}\mathbf{h}||^2 \leq \mathrm{SNR}^{-1}\}$ *be the deep fade event, and*

$$P_{deep}(\mathrm{SNR}) \triangleq \Pr\{||\boldsymbol{\mathcal{R}}\mathbf{h}||^2 \leq \mathrm{SNR}^{-1}\} \tag{5.5}$$

its probability. If the assumption C1) is satisfied, then the diversity order of P_e *is the same as that of the deep fade event, i.e.,*

$$d^* = \lim_{\mathrm{SNR}\to\infty} \frac{-\log P_{deep}(\mathrm{SNR})}{\mathrm{SNR}}.$$

Remark 6 *An interesting corollary from the lemma is that the diversity order* d^* *is completely independent of the underlying code* $\{\boldsymbol{\mathcal{G}}_i\}$ *as long as the underlying code is full rank. The main utility of Lemma 11 is that the diversity order of* P_{deep} *is much easier to analyze than that of* P_e*.*

Proof The proof is given in Appendix 5.A.

In the following, we will equivalently consider $||\boldsymbol{\mathcal{R}}\boldsymbol{\Sigma}_h^{1/2}\hat{\mathbf{h}}||^2,\ \hat{\mathbf{h}} = [\hat{h}_1, \ldots, \hat{h}_N] \sim \mathcal{N}_c(\mathbf{0}, \mathbf{I})$ instead $||\boldsymbol{\mathcal{R}}\mathbf{h}||^2,\ \mathbf{h} \sim \mathcal{N}_c(\mathbf{0}, \boldsymbol{\Sigma}_h)$. Let $\mathbf{U}^H\mathbf{S}\mathbf{U}$ be the eigenvalue decomposition of $\boldsymbol{\Sigma}_h^{1/2}\boldsymbol{\mathcal{R}}^H\boldsymbol{\mathcal{R}}\boldsymbol{\Sigma}_h^{1/2}$, where $\mathbf{U}$ is a random Hermitian matrix and $\mathbf{S} = \mathrm{diag}(\sigma_1^2, \cdots, \sigma_\eta^2)$ are the ordered eigenvalues (squared singular values of $\boldsymbol{\mathcal{R}}\boldsymbol{\Sigma}_h^{1/2}$). Using the properties of the circularly symmetric Gaussian distribution, we obtain

$$P_{deep} = \Pr\left\{\sum_{i=1}^{\eta} \sigma_i^2 |\hat{h}_i|^2 \leq \mathrm{SNR}^{-1}\right\}. \tag{5.6}$$

The following theorem provides a very general and clean characterization of the diversity order in terms of the distribution of the singular values of $\boldsymbol{\mathcal{R}}\boldsymbol{\Sigma}_h^{1/2}$. Let

notation 0^- denote a negative real number that is close to zero and $\Gamma(\alpha_1, \cdots, \alpha_\eta)$ represent the following function:

$$\Gamma(\alpha_1, \ldots, \alpha_\eta) = \lim_{\mathrm{SNR}\to\infty} \frac{-\log \Pr(\sigma_1^2 \leq \mathrm{SNR}^{-\alpha_1}, \cdots, \sigma_\eta^2 \leq \mathrm{SNR}^{-\alpha_\eta})}{\log \mathrm{SNR}}. \tag{5.7}$$

We call the parameters $\alpha_1, \cdots, \alpha_\eta$ *the deep fade exponents of the singular values.*

Theorem 14 *If the assumption C1) is satisfied, then the diversity order of the randomized space-time code is*

$$d^* = \inf_{(\alpha_1,\cdots,\alpha_\eta)} \left(\Gamma(\alpha_1, \ldots, \alpha_\eta) + \sum_{i=1}^{\eta} (1 - \alpha_i) \right), \tag{5.8}$$

where the infimum is over $\alpha_i \in [0^-, 1],\ i = 1, \cdots, \eta$.

Intuition and proof: Consider the following events:

i) The singular values are such that $\sigma_i^2 \leq 1/\mathrm{SNR}^{\alpha_i},\ i = 1, \cdots, \eta$ (i.e. σ_i^2 is in deep fade with exponent α_i).

ii) The channel coefficients are such that $|\hat{h}_i|^2 \leq 1/(\eta \mathrm{SNR}^{1-\alpha_i}),\ i = 1, \cdots, \eta$ (i.e. $\hat{h}_i$ is in deep fade with exponent $1 - \alpha_i$).

To calculate the diversity we note that any sufficient condition for the deep fade event provides an upper bound on d^*. If events i) and ii) occur simultaneously, we have a deep fade event $\sum_{i=1}^{\eta} \sigma_i^2 |\hat{h}_i|^2 \leq \mathrm{SNR}^{-1}$, as defined in (5.6). Because the events i) and ii) are independent, the probability is going to be a product of probabilities and diversity orders are, therefore, additive. With this in mind, the second term ($\sum_{i=1}^{\eta}(1-\alpha_i)$) in equation (5.8) follows from the Rayleigh distribution; in fact, the diversity order of each event ii) is $(1 - \alpha_i)$. The first term follows from the definition in (5.7). Therefore, $d^* \leq \Gamma(\alpha_1, \ldots, \alpha_\eta) + \sum_{i=1}^{\eta}(1-\alpha_i)$, which implies that

$$d^* \leq \inf_{(\alpha_1,\cdots,\alpha_\eta)} \left(\Gamma(\alpha_1, \ldots, \alpha_\eta) + \sum_{i=1}^{\eta} (1 - \alpha_i) \right). \tag{5.9}$$

For the opposite inequality see Appendix 5.B for a rigorous proof. ■

The theorem is easiest to understand when $\mathbf{\Sigma}_h = \mathbf{I}$. In this case, σ_i's are the singular values of the randomization matrix $\boldsymbol{\mathcal{R}}$. In simpler terms, the theorem states that the deep fade event happens because of the simultaneous fades of the randomization matrix and the channel coefficients with exponents α_i's and $1-\alpha_i$'s, respectively. Hence, in our scheme, the randomization of the space-time code matrix may be ill-conditioned.

In order to distinguish between "good" and "bad" design choices for $\boldsymbol{\mathcal{R}}$, we need to understand the conditions under which the σ_i^2's are more likely to be small. Since the singular values $\sigma_\eta^2 \leq \cdots \leq \sigma_1^2$ are ordered, it is easiest for the σ_η^2 to fade. The σ_η^2 fades if and only if the columns of the matrix turn out to be completely or partially confined into a $\eta - 1$ dimensional subspace. This may happen, for example, if two column vectors turn out to be almost parallel to each other, or a column vector approximately lies within the plane spanned by two other column vectors, etc.

In Section 5.4, for $\mathbf{\Sigma}_h = \mathbf{I}$, we analyze a number of specific designs for $\boldsymbol{\mathcal{R}}$ and conclude that the best designs have random column vectors in $\boldsymbol{\mathcal{R}}$ which have the least probability of being aligned. In fact, the design that performs best among the ones we examine in Section 5.4 has $\boldsymbol{\mathcal{R}}$ with i.i.d. columns uniformly distributed in the complex unit sphere.

A few remarks follow from Theorem 14:

Remark 7 *i) In general, finding the distribution of the singular values for a given random matrix distribution is not an easy task. Fortunately, Theorem 14 only requires knowledge of the distribution of the singular values of* $\boldsymbol{\mathcal{R}}\mathbf{\Sigma}_h^{1/2}$ *around zero. We will utilize this observation in Section 5.4.*

ii) Theorem 14 completely characterizes the diversity order of a randomized space-time code for a given $\boldsymbol{\mathcal{R}}$; however, it is non obvious how to use Theorem 14 constructively. In fact, it is unclear how one can choose the singular vector and singular value distributions such that, the singular value distribution has the local properties that are required to maximize d^* in (5.8) and, at the same time, the columns of $\boldsymbol{\mathcal{R}}$ are statistically independent.

iii) Theorem 14 gives the upper bound

$$d^* \leq \eta = \min(L, N) \tag{5.10}$$

(choose $\alpha_i = 0^-,\ \forall i$), which says that the diversity order is always bounded by the minimum of the number of relays and the underlying code dimension.

iv) A necessary condition for the randomized code to have maximum diversity order η is that the exponent of the smallest singular value σ_η^2 should be at least 1, i.e.,

$$\lim_{\mathrm{SNR}\to\infty} \frac{-\log \Pr(\sigma_\eta^2 \leq \mathrm{SNR}^{-1})}{\log \mathrm{SNR}} \geq 1. \tag{5.11}$$

This can be seen by substituting $\alpha_i = 0^-,\ i = 1, \cdots, \eta - 1$ in (5.8) except $\alpha_\eta = 1$. The distribution of the smallest singular value is generally easier to obtain than the joint distribution of all singular values. Consequently, (5.11) is a simpler condition to check than the condition in Theorem 14.

v) Theorem 14 presents an interesting result. The diversity orders can be fractional *depending on $\Gamma(\cdot)$. We will see concrete examples of this in Section 5.4.*

5.3.2 Upper Bound to the Probability of Error

A brief word about our notation. Let $\mathbf{A}$ be a $n \times n$ Hermitian matrix with eigenvalues $\lambda_1 \geq \lambda_2 \geq \ldots \lambda_m > 0 \geq \lambda_{m+1} \ldots \geq \lambda_n$. We use the notation $|\mathbf{A}|_{k+}$ to denote the product of k smallest positive eigenvalues of the matrix $\mathbf{A}$, *i.e.,* $|\mathbf{A}|_{k+} = \prod_{i=1}^{k} \lambda_{m-i+1}$. In case all eigenvalues are positive, then $|\mathbf{A}|_{n+} = \det(\mathbf{A})$.

We know that the diversity order of the randomized space-time code is always upper bounded by the minimum of the number of relay nodes and the size of the underlying space-time code, *i.e.,* $d^* \leq \min\{N, L\} \triangleq \eta$.

The following theorem provides an upper bound to the average error probability and a sufficient condition for the randomized code to have diversity order η.

Theorem 15 *Suppose that* $\{\boldsymbol{\mathcal{G}}_i\}$ *satisfies C1), and the randomization matrix* $\boldsymbol{\mathcal{R}}$ *satisfies*

C2) Rank criterion for $\boldsymbol{\mathcal{R}}$: *The matrix* $\boldsymbol{\mathcal{R}}$ *is full-rank with probability 1.*

C3) Finiteness of $\mathbb{E}\{|\boldsymbol{\mathcal{R}}\boldsymbol{\mathcal{R}}^H|_{\eta+}^{-1}\}$: *The expectation* $\mathbb{E}\{|\boldsymbol{\mathcal{R}}\boldsymbol{\mathcal{R}}^H|_{\eta+}^{-1}\}$ *is finite.*

Then, the P_e *is bounded as*

$$P_e \leq \frac{4^{-\eta}(|\mathcal{M}|-1)\mathrm{SNR}^{-\eta}}{\min_{(i,j)}\{\ |(\boldsymbol{\mathcal{G}}_i - \boldsymbol{\mathcal{G}}_j)^H(\boldsymbol{\mathcal{G}}_i - \boldsymbol{\mathcal{G}}_j)|_{\eta+}\}\ |\boldsymbol{\Sigma}_h|_{\eta+}} \mathbb{E}\left\{\frac{1}{|\boldsymbol{\mathcal{R}}\boldsymbol{\mathcal{R}}^H|_{\eta+}}\right\}. \tag{5.12}$$

Proof See Appendix 5.C.

Remark 8 *Note that here, it is assumed that the channel* $\mathbf{h}$ *and the randomization matrix* $\boldsymbol{\mathcal{R}}$ *changes over the transmission so that the packet experiences multiple realizations.*

Remark 9 *Notice that the diversity order of the upper bound in (5.12) is η. Since the diversity order d^* cannot exceed η, we observe from Theorem 15 that the randomized space-time code has maximum diversity order η, as long as C1)-C3) are satisfied.*

What kind of random matrices satisfy the rank criterion for $\boldsymbol{\mathcal{R}}$? We know that almost all square matrices over the field of real or complex numbers are invertible, *i.e.,* the set of singular square matrices have Lebesgue measure zero. In general, any random matrix with independent columns drawn from a continuous distribution satisfies the rank criterion. However, this alone does not guarantee the diversity order η. The upper bound in (5.12) is useful only if $\mathbb{E}\left\{|\boldsymbol{\mathcal{R}}\boldsymbol{\mathcal{R}}^H|_{\eta+}^{-1}\right\} < \infty$. This is a rather stringent condition, and not all almost-surely full rank matrices satisfy it. In the next section, we will present some sufficient conditions for this to be true.

The bound in Eqn. 5.12 can be tightened by improving the coding gain. The following conditions are needed: i) $\min_{(i,j)} |(\boldsymbol{\mathcal{G}}_i - \boldsymbol{\mathcal{G}}_j)^H(\boldsymbol{\mathcal{G}}_i - \boldsymbol{\mathcal{G}}_j)|_{\eta+}$ should be maximized with respect to $\{\boldsymbol{\mathcal{G}}_i\}$; ii) $\mathbb{E}\left\{|\boldsymbol{\mathcal{R}}\boldsymbol{\mathcal{R}}^H|_{\eta+}^{-1}\right\}$ should be minimized with respect the distribution of $\boldsymbol{\mathcal{R}}$. Note that condition i) is a slightly modified version of the determinant criterion in [25].

5.3.3 Diversity Order for Randomized Space-time Codes with Power Constraint

In this section we will employ a transmit power constraint on the relay nodes to facilitate the analysis of randomized space-time codes. Let $P_T < \infty$ be the total

relay power available to the network such that[1]

$$\mathrm{Tr}(\boldsymbol{\mathcal{R}}\boldsymbol{\mathcal{R}}^H) \leq P_T \quad \text{with probability 1.} \tag{5.13}$$

Under the conditions of the following theorem, we show that C3) holds, and therefore the diversity order of the randomized scheme is η.

Theorem 16 *Let $\boldsymbol{\mathcal{R}}$ be an $L \times N$ random* complex *matrix and $p(\boldsymbol{\mathcal{R}})$ its probability density function. Assume that the function $p(\boldsymbol{\mathcal{R}})$ is bounded and it satisfies the total power constraint (5.13). For $N \neq L$, if C1) and C2) are satisfied, then $\mathbb{E}\{|\boldsymbol{\mathcal{R}}\boldsymbol{\mathcal{R}}^H|_{\eta+}^{-1}\} < \infty$. Therefore, the diversity order of the randomized space-time code is given by*

$$d^* = \begin{cases} N & \text{if } \ N \leq L-1 \\ \\ L & \text{if } \ N \geq L+1 \end{cases} \tag{5.14}$$

For $N = L$, the diversity order is such that $N - 1 \leq d^* \leq N$.

Proof See Appendix 5.D.

Remark 10 *The above result shows that the randomized space-time codes achieve the maximum diversity order N achievable by any scheme if $N < L$. It also indicates the diversity order saturates at L if the number of relay nodes is greater than or equal to $L+1$. This problem can be solved by using space-time codes with large enough dimensions. However, N may be random and may take large values in practical networks. In such cases, using smaller L may be preferred for decoding simplicity. For fixed L, randomized space-time codes still give the highest order L for $N \geq L+1$.*

[1]Notice that there is no expectation in the power condition. We want it to be satisfied almost surely. Condition (5.13) implies that the pdf of $\boldsymbol{\mathcal{R}}$ has bounded support.

Corollary 1 *Let $\boldsymbol{\mathcal{R}}$ be an $L \times N$ random* real *matrix and $p(\boldsymbol{\mathcal{R}})$ its probability density function, which is assumed to be bounded. Suppose that C1) and C2) are satisfied, and the total power constraint (5.13) holds. Then, the diversity order of the randomized space-time code is given by*

$$d^* = \begin{cases} N & \text{if } N \leq L-2 \\ \\ L & \text{if } N \geq L+2 \end{cases} \tag{5.15}$$

For $N \in \{L-1, L, L+1\}$, the diversity order is such that $N-2 \leq d^* \leq \min(N, L)$.

Proof The proof follows from modifying the proof of Theorem 16 for the real valued $\boldsymbol{\mathcal{R}}$. We avoid it for brevity.

Remark 11 *The diversity order of a randomized space-time code is closely related to how ill-conditioned the matrix $\boldsymbol{\mathcal{R}}$ is. This relates to the behavior of the joint distribution of the singular values around origin (Theorem 14). Theorem 16 indicates that, for $N \neq L$ it is quite hard for a complex valued matrix $\boldsymbol{\mathcal{R}}$ to be ill-conditioned. On the other hand, for real valued matrices, ill-conditioned matrices are more likely and, hence, we need at least $|N-L| \geq 2$.*

5.4 Specific Designs and Their Performance

In this section, we propose different randomized space-time codes and derive the diversity order of these designs using Theorem 14 and Theorem 16. Furthermore, in Section 5.6, the average error probabilities of these designs are obtained via Monte-Carlo simulations. In the following, we assume that $\mathbf{h} \sim \mathcal{N}(0, \mathbf{I})$.

5.4.1 Complex Gaussian distribution

Let us assume elements of the $L \times N$ dimensional randomization matrix $\boldsymbol{\mathcal{R}}$ are zero-mean independent and complex Gaussian. In the random matrix literature, the Gaussian random matrix is one of the most studied [65, 66]. The joint probability density function of the non-zero eigenvalues $\lambda_1 \geq \lambda_2 \geq \ldots \lambda_\eta$ of the matrix $\boldsymbol{\mathcal{R}}\boldsymbol{\mathcal{R}}^H$ (known as Wishart) is given as

$$f(\lambda_1, \ldots, \lambda_N) = C_{N,L} \exp(-\sum_{i=1}^{\eta} \lambda_i) \prod_{i=1}^{\eta} \lambda_i^{|N-L|} \prod_{i<j} (\lambda_i - \lambda_j)^2, \tag{5.16}$$

where $C_{N,L}$ is a constant. In the following, we provide the diversity order of this scheme.

Case $N \neq L$

Using the results in [65], we obtain

$$\mathbb{E}\{|\boldsymbol{\mathcal{R}}\boldsymbol{\mathcal{R}}|_{\eta+}^{-1}\} = \begin{cases} \frac{(N-L-1)!}{(N-1)!} & \text{if } N \geq L+1 \\ \frac{(L-N-1)!}{(L-1)!} & \text{if } L \geq N+1, \end{cases}$$

where $\eta = \min(L, N)$. Since $\mathbb{E}\{|\boldsymbol{\mathcal{R}}\boldsymbol{\mathcal{R}}|_{\eta+}^{-1}\} < \infty$ when $N \neq L$, the upper bound on the average error probability is given as follows (using Theorem 15):

$$P_e \leq \frac{4^{-\eta}(|\mathcal{M}|-1)\mathrm{SNR}^{-\eta}}{\min_{(i,j)}\{|(\boldsymbol{\mathcal{G}}_i - \boldsymbol{\mathcal{G}}_j)^H(\boldsymbol{\mathcal{G}}_i - \boldsymbol{\mathcal{G}}_j)|_{\eta+}\}\ |\boldsymbol{\Sigma}_h|_{\eta+}} \frac{(|N-L|-1)!}{(\max(N,L)-1)!}. \tag{5.17}$$

Eqn. 5.17 shows that (5.14) also holds for $\boldsymbol{\mathcal{R}}$ with i.i.d. complex Gaussian elements. Note that the total power constraint (5.13) is not satisfied in this scenario. However, we arrive at the same conclusion on the diversity order d^* which we derived previously through Theorem 16.

Case $N = L$

We can approximate the probability density of non-zero eigenvalues of the Wishart matrix $\boldsymbol{\mathcal{R}}\boldsymbol{\mathcal{R}}^H$ (Eqn. 5.16) around zero as

$$f(\lambda_1, \ldots, \lambda_N) \approx c\lambda_1^{2(N-1)}\lambda_2^{2(N-2)} \ldots \lambda_{(N-1)}^2. \tag{5.18}$$

Using Theorem 14 and (5.18), the diversity order is

$$d^* = \inf_{\alpha_1,\ldots,\alpha_N} \underbrace{(2N-1)\alpha_1 + (2N-3)\alpha_2 + \ldots + \alpha_1}_{\Gamma(\alpha_1,\ldots,\alpha_N)} + \sum_{i=1}^{N}(1-\alpha_i) = N,$$

where the infimum is obtained when $\alpha_i = 0, \forall i$. Hence, if the elements of the randomization matrix $\boldsymbol{\mathcal{R}}$ are drawn independently and identically from a zero mean complex Gaussian distribution, the full diversity is also achieved for the $N = L$ case.

5.4.2 Real Gaussian distribution

Let us assume that the elements of the randomization matrix $\boldsymbol{\mathcal{R}}$ are zero-mean independent and real Gaussian. The joint probability density function of the non-zero eigenvalues $\lambda_1 \geq \lambda_2 \geq \ldots \lambda_\eta$ of the Wishart matrix $\boldsymbol{\mathcal{R}}\boldsymbol{\mathcal{R}}^T$ is given as

$$f(\lambda_1, \ldots, \lambda_N) = \tilde{C}_{N,L} \exp(-\sum_{i=1}^{\eta}\lambda_i) \prod_{i=1}^{\eta} \lambda_i^{\frac{(|N-L|-1)}{2}} \prod_{i<j}(\lambda_i - \lambda_j), \tag{5.19}$$

where $\tilde{C}_{N,L}$ is a constant. We can approximate the probability density of the eigenvalues (5.19) around zero as

$$f(\lambda_1, \ldots, \lambda_\eta) \approx c \prod_{i=1}^{\eta} \lambda_i^{\frac{|N-L|-1}{2}+\eta-i}. \tag{5.20}$$

We then find $\Gamma(\cdot)$ as $\Gamma(\alpha_1, \ldots, \alpha_\eta) = \sum_{i=1}^{\eta}\left(\frac{|N-L|-1}{2} + \eta\right)\alpha_i$. Using Theorem 14 and (5.20), the diversity order is obtained as follows:

Case $N \neq L$

For this case, $d^* = \eta$ where the infimum is obtained when $\alpha_i = 0, \forall i$.

Case $N = L$

For this case, $d^* = \inf_{\alpha_1,\ldots,\alpha_\eta}(\sum_{i=1}^{\eta}(\eta - i/2) + \sum_{i=1}^{\eta}(1-\alpha_i)) = \eta - 0.5$. The infimum is obtained when $\{\alpha_i = 0, i = 1 \ldots \eta, \alpha_\eta = 1\}$.

Therefore, in this case the diversity order d^* is given by

$$d^* = \begin{cases} \eta & \text{if } N \neq L, \\ \eta - 0.5 & \text{if } N = L, \end{cases}$$

where $\eta = \min(N, L)$. Note that the scheme provides a fractional diversity order when $N = L$.

5.4.3 Uniform phase distribution

Let us assume that the k'th column of the $L \times N$ randomization matrix is $\mathbf{r}_k = a_k[e^{j\theta_i[0]}, \ldots, e^{j\theta_i[L]}]^t$ where each $\theta_i[N] \sim U(0, 2\pi)$ and $a_k \sim U(1-\epsilon, 1+\epsilon)$ for some small $\epsilon > 0$, where $U(a, b)$ denotes the uniform distribution in the interval (a, b) and all $\theta_i[N], a_k$ are independent of each other. The main advantage of this scheme lies in its ability to control the transmission power at each node. The total power is bounded as

$$\mathrm{Tr}(\boldsymbol{\mathcal{R}}\boldsymbol{\mathcal{R}}^H) = L\sum_{i=1}^{N}|a_i|^2 \leq NL(1+\epsilon)^2.$$

Case $N \neq L$

Using Theorem 16, we conclude that the diversity order d^* satisfies (5.14).

For $\epsilon = 0$, that is $\mathbf{r}_k = [e^{j\theta_i[0]}, \ldots, e^{j\theta_i[L]}]^t$, the randomization matrix $\boldsymbol{\mathcal{R}}$ can be interpreted as a random phase matrix. In this case, unfortunately the probability

density function of $\boldsymbol{\mathcal{R}}$ does not exist[2], hence we can not directly use Theorem 16. However, we believe the result (5.14) is also valid in this scenario and we will see that this is true by numerical examples.

Case $N = L = 2$

Consider the random phase matrix $\boldsymbol{\mathcal{R}}$ for $\epsilon = 0$. The eigenvalues of $\boldsymbol{\mathcal{R}}\boldsymbol{\mathcal{R}}^H$ can be found as $\lambda_1 = 2 + \sqrt{2 + 2\cos(\theta)}$ and $\lambda_2 = 2 - \sqrt{2 + 2\cos(\theta)}$, where θ is a uniform random variable in the interval $[0, 2\pi)$. Note that $\lambda_1 \in [1, 4]$ with probability 1. Using Theorem 14 and the fact that $\lambda_1 \geq 1$, we can easily see that the optimal $\alpha_1 = 0^-$. Hence, the problem simplifies to determining

$$d^* = \min_{\alpha_2} \ \Gamma(0^-, \alpha_2) + 2 - \alpha_2. \tag{5.21}$$

One can derive the distribution of λ_2 as

$$F_{\lambda_2}(\lambda) = \Pr\{\lambda_2 \leq \lambda\} = \frac{2}{\pi}\cos^{-1}(1 - \frac{\lambda}{2}), \ 0 \leq \lambda \leq 2.$$

Then, the behavior of the $F_{\lambda_2}(\lambda)$ around zero is given as $F_{\lambda_2}(\lambda) \approx \frac{2}{\pi}\sqrt{\lambda}$, as $\lambda \to 0$. The infimum in (5.21) is obtained when $\alpha_2 = 1$, which gives us a fractional value $d^* = 1.5$.

[2]To see why the pdf of $\boldsymbol{\mathcal{R}}$ does not exist, let's look at the special case where $\boldsymbol{\mathcal{R}}$ is 1×1. Here all the probability mass is concentrated on the unit circle. Hence the "pdf" is what is sometimes referred to as an impulse sheet. Viewed in an engineering sense, this pdf is not bounded (hence Theorem 16 does not apply). From the measure theoretic point of view, the measure induced by $\boldsymbol{\mathcal{R}}$ is not absolutely continuous with respect to the Lebesgue measure on the complex plane [53]. Therefore, its Radon-Nikodym derivative (hence its pdf) with respect to Lebesgue measure does not exist.

5.4.4 Uniform distribution on a hypersphere

Let us assume that the k'th column of the $L \times N$ randomization matrix, $\mathbf{r}_k$, is uniformly selected on the surface of a complex/real hypersphere of radius ρ, *i.e.,* $||\mathbf{r}_k|| = \rho$. Note that, in this case, the total power constraint (5.13) is satisfied, *i.e.,*

$$\mathrm{Tr}(\boldsymbol{\mathcal{R}}\boldsymbol{\mathcal{R}}^H) = \rho^2 N < \infty.$$

Similar to uniform phase randomization with $\epsilon = 0$ (Section 5.4.3), the probability density function of $\boldsymbol{\mathcal{R}}$ does not exist in this case. However, we will show through numerical examples that (5.14) is still valid.

Real hypersphere with $N = L = 2$

Let us assume that the columns of the randomization matrix $\boldsymbol{\mathcal{R}}$ are drawn uniformly on a sphere. We can obtain the eigenvalues of $\boldsymbol{\mathcal{R}}\boldsymbol{\mathcal{R}}^T$ as $\lambda_1 = 1+\cos^2(\theta), \lambda_2 = 1 - \cos^2(\theta)$, where $\theta \sim U(0, 2\pi)$. Note that $\lambda_1 \geq 1$ and $\Pr\{\lambda_2 \leq \lambda\} \approx \lambda/(2\pi)$ as $\lambda \rightarrow 0$. Using Theorem 14, the diversity order is

$$d^* = \min_{\alpha_2} \Gamma(0^-, \alpha_2) + 2 - \alpha_2 = 2,$$

where the infimum is obtained when $\alpha_1 = 0^-$ and α_2 is any value.

Complex hypersphere with $N = L = 2$

Let us assume that the columns of the randomization matrix $\boldsymbol{\mathcal{R}}$ are drawn uniformly on complex hypersphere. We obtain the eigenvalues of $\boldsymbol{\mathcal{R}}\boldsymbol{\mathcal{R}}^H$ as $\lambda_1 = 1 + \sqrt{\zeta}/2, \lambda_2 = 1 - \sqrt{\zeta}/2$, where $\zeta \sim F_{24}$ and F_{nm} is the F-distribution. Note that $\lambda_1 \geq 1$. Using Theorem 14, the diversity order obtained is $d^* = 2$, where the infimum obtained when $(\alpha_1, \alpha_2) = (0, 0^-)$.

5.5 Antenna Selection and Discrete Randomization Matrix

The case considered in this section is that where the randomization matrices $\boldsymbol{\mathcal{R}}$ are drawn from discrete distributions. In the next example, we present the random selection matrices.

Example 2 *Let* $\boldsymbol{\mathcal{R}} = [\mathbf{r}_1 \dots \mathbf{r}_N]$ *be a random matrix such that* $\mathbf{r}_i \in Q \triangleq \{\mathbf{e}_i, i = 1 \dots L\}$ *where* $\mathbf{e}_i$ *is the vector of all zeros except the* i*'th position, which is* 1*. Note that the randomized space-time coding, with the selection matrix* $\boldsymbol{\mathcal{R}}$*, corresponds to assigning the columns of a given space-time code matrix at random to each of the nodes. This scheme will be referred as* random antenna selection*. In [36], we analyzed the performance of random antenna selection with an underlying orthogonal space-time code. We showed that this simple method almost meets the ideal performance for* SNR *below a threshold* SNR_t*, which increases with node density. In the following, we extend the results in [36] to more general scenarios.*

When the randomization matrix $\boldsymbol{\mathcal{R}}$ is drawn from a discrete distribution, the probability that the rank of $\boldsymbol{\mathcal{R}}$ is unity, *i.e.,* $\Pr\{\mathrm{rank}(\boldsymbol{\mathcal{R}}\boldsymbol{\mathcal{R}}^H) = 1\}$ is nonzero. In the light of this observation, the following lemma presents the diversity order of this scheme with finite L, N.

Lemma 12 *The randomized space-time coding, with* $\boldsymbol{\mathcal{R}}$ *drawn from a discrete distribution, has diversity order* $d^* = 1$ *for* $N < \infty$*.*

Proof The proof follows from Theorem 14. The diversity order is obtained when $\{\alpha_1 = 0^-, \alpha_i = 1, \forall i = 1\}$.

Lemma 12 states that the maximum diversity that can be achieved with schemes based on randomization matrices drawn from discrete distribution is 1, which is

quite discouraging. This is somewhat misleading as can be shown by studying the diversity order as the number of nodes increases. We now define the *asymptotic diversity order*.

Definition Let $P_e^{(N)}(\mathrm{SNR})$ denote the probability of error of a randomized space-time code utilizing an $L \times N$ randomization matrix $\frac{\boldsymbol{\mathcal{R}}}{\sqrt{N}}$. Then, the *asymptotic probability of error* $P_e^{\infty}(\mathrm{SNR})$ is defined as

$$P_e^{\infty}(\mathrm{SNR}) \triangleq \lim_{N\to\infty} P_e^{(N)}(\mathrm{SNR}).$$

Also, the *asymptotic diversity order* D of this randomized space-time code is defined as

$$D \triangleq \lim_{\mathrm{SNR}\to\infty} \frac{-\log P_e^{\infty}(\mathrm{SNR})}{\log \mathrm{SNR}}.$$

In the asymptotic case, full diversity conditions are more relaxed. The sufficient conditions in order to achieve the asymptotic diversity order $D = L$ are provided in the following theorem. In order to derive the asymptotic probability of error $P_e^{\infty}(\mathrm{SNR})$, we utilize the behavior of effective channel for large N in the proof of next theorem.

Theorem 17 *Let* $\boldsymbol{\mathcal{R}} = [\mathbf{r}_1 \dots \mathbf{r}_N]$ *be an* $L \times N$ *random matrix such that the columns* $\mathbf{r}_i$ *are i.i.d. with zero-mean and covariance* $\boldsymbol{\Sigma}$*. Assume that* $\mathbf{h} \sim \mathcal{N}_c(\mathbf{0}, \boldsymbol{\Sigma}_h)$*, where* $\boldsymbol{\Sigma}_h = diag(\sigma_{h1}^2, \sigma_{h2}^2, \dots, \sigma_{hN}^2)$*. If* $L < \infty$*, then the asymptotic diversity order* $D = L$ *is achieved if the following conditions are satisfied:*

1) $(\boldsymbol{\mathcal{G}}_k - \boldsymbol{\mathcal{G}}_i)$ *is full-rank,*

2) $\boldsymbol{\Sigma}$ *is full-rank, i.e.,* $\det(\boldsymbol{\Sigma}) > 0$.

Proof See Appendix 5.E.

The behavior of the schemes utilizing discrete randomization matrices changes abruptly in the high node asymptote due to Theorem 17. From Lemma 12, we know that as SNR$\rightarrow\infty$, the diversity order of this system is 1 for $N < \infty$. On the other hand, from Theorem 17, in the asymptote that number of nodes goes to infinity, the diversity order $\eta = \min(L, N)$ is achieved. In addition, an interesting observation on the behavior of networks with finite but sufficiently large number of nodes is made. The average error probability curve (in the typical logarithmic scale, versus SNR in dB) exhibits multiple slopes in different SNR ranges. The justification for this behavior is as follows.

Assume that $(\boldsymbol{\mathcal{G}}_k - \boldsymbol{\mathcal{G}}_i)$ is of rank L for any pair of space-time code matrices $\{\boldsymbol{\mathcal{G}}_k, \boldsymbol{\mathcal{G}}_i\}$. Let $\eta = \min(L, N)$. Let $S = \{\sigma_1^2, \sigma_2^2, \ldots, \sigma_\eta^2\}$ be the set of non-negative eigenvalues of $\boldsymbol{\mathcal{R}}\boldsymbol{\mathcal{R}}^H$ ordered such that σ_1^2 is the largest. Let us rewrite the average probability error as a polynomial in 1/SNR (using (5.43) and (5.48)): $P_e \leq \bar{P}_e$, where

$$\bar{P}_e = \sum_{m=1}^{\eta} \underbrace{B_m \, \mathbb{E}\left\{ \prod_{i=\eta-m+1}^{\eta} \sigma_i^{-2} | \mathrm{rank}(\boldsymbol{\mathcal{R}}\boldsymbol{\mathcal{R}}^H) = m \right\}}_{\triangleq C_m} \frac{1}{\mathrm{SNR}^m}, \tag{5.22}$$

where $B_m \triangleq \frac{4^m(|\mathcal{M}|-1)\Pr\{\mathrm{rank}(\boldsymbol{\mathcal{R}}\boldsymbol{\mathcal{R}}^H)=m\}}{|(\boldsymbol{\mathcal{G}}_k-\boldsymbol{\mathcal{G}}_i)^H(\boldsymbol{\mathcal{G}}_k-\boldsymbol{\mathcal{G}}_i)|_{m+}|\boldsymbol{\Sigma}_h|_{m+}}$. The expression (5.22) helps explain the fact that when the number of nodes is finite but *sufficiently* large, the probability of error curve changes its slope, but above a certain SNR threshold, the expected $O(1/\mathrm{SNR})$ behavior is obtained. The breaking points of the curve change and move towards higher SNRs as the number of nodes increases. In fact, depending on the values of $\{C_m\}$, the range of SNR where the term C_m/SNR^m is dominant in the summation (5.22) can be derived as follows:

$$\max_{k>m} \left(\frac{C_m}{C_k}\right)^{\frac{1}{m-k}} << \mathrm{SNR} << \min_{k<m} \left(\frac{C_m}{C_k}\right)^{\frac{1}{m-k}}, \tag{5.23}$$

if $\min_{k<m} (C_m/C_k)^{\frac{1}{m-k}} >> \max_{k>m} (C_m/C_k)^{\frac{1}{m-k}}$ (for $m = 1$, the upper bound is ∞ and for $m = L$, the lower bound is 0). In Section 5.6, we will show this behavior in a numerical example.

The main advantage of choosing columns of $\boldsymbol{\mathcal{R}}$ from a discrete distribution is the simplification in the encoder, since the random selection can be enforced at the data link layer and hence, the scheme can be implemented in logic without any modification of the existing physical layer modem.

Example 3 *(*Frequency Diversity*)*

In [44], the authors propose a protocol where the cooperating nodes introduce intentional delays in order to obtain diversity through an artificially created frequency selective channel. In one version of their protocol, they allow the nodes to randomly select the delays from a pool. This scheme can be reexpressed as a randomized space-time code: Let $\boldsymbol{\mathcal{G}}(\mathbf{s})$ *be a Toeplitz matrix having all the possible shifted replicas of the transmitted signal and the randomization matrix* $\boldsymbol{\mathcal{R}}$ *be the selection matrix. The performance of this scheme under coherent detector is analyzed in Section 5.5. Furthermore, the diversity and coding gains can be attained if the strategy is combined with a coded- OFDM modem that includes a cyclic prefix on the order of the maximum allowed delay dispersion among the cooperative relays (see also [27]).*

5.6 Simulations & Numerical Evaluations

In this section, we present the performance of the proposed *randomized* distributed space-time codes. We obtain the average probability of error through Monte-Carlo methods and validate the conclusions we draw in the analytical sections. We

compare the performance of randomized schemes with the centralized space-time codes for different values of N and L. In the following, we assume the nodes channel gains to the destination are i.i.d., *i.e.,* $h_k \sim \mathcal{N}_c(0,1)$.

In Fig. 5.2, we look at the performance of Alamouti scheme under different randomization methods and compare it with a centralized space-time coding. Here $L = 2$, and

$$\boldsymbol{\mathcal{G}}(\mathbf{s}) = \begin{bmatrix} s_1 & s_2 \\ s_2^* & -s_1^* \end{bmatrix},$$

where $\mathbf{s} = [s_1 \ s_2]$ is the transmitted symbol vector and $s_i = \pm 1$ (BPSK symbols). The randomization is done in four different ways: (i) Complex Gaussian randomization (see Section 5.4.1) (ii) Uniform phase randomization (see Section 5.4.3) (iii) Uniform spherical randomization (see Section 5.4.4) and (iv) Random antenna selection (see Section 5.5 - Example 2). Let $\mathbf{r}_i$ be the i'th column of the randomization matrix $\boldsymbol{\mathcal{R}}$. In uniform phase randomization, each element of $\mathbf{r}_i$ is equal to $e^{j\theta}$ where θ is a random variable uniformly distributed in $[0, 2\pi)$. In the case of Gaussian randomization, $\mathbf{r}_i$'s are zero-mean independent complex Gaussian vectors with covariance $\mathbf{I}$. In the uniform spherical randomization, $\mathbf{r}_i$'s are chosen as zero-mean independent complex Gaussian vectors with covariance $\mathbf{I}$, and then normalized to have the norm $\rho = ||\mathbf{r}_i|| = 1$ [67, 68].

In the centralized Alamouti, half of the nodes choose to serve as the first antenna, and the other half choose to serve as the second antenna (if N is odd, at one of the nodes the power is equally distributed between two antennas). The transmission power of each node is $P_t = \frac{1}{N}$ for the centralized Alamouti, antenna selection, and spherical randomization schemes. For the Gaussian and uniform phase randomization schemes, $P_t = \frac{1}{NL}$.[3] This way the average transmission power of each

[3]The aim of normalization by $1/L$ is to make the comparison fair among differ-

antenna is approximately the same for all schemes, hence the comparison is more fair.

In Fig. 5.2, we plot the average probability of error with respect to SNR $= 1/N_0$ for $N = 2, 3, 4, 10$. From theoretical analysis, for $N = 2$, we know that the Gaussian and spherical randomization schemes have diversity order $d^* = 2$; on the other hand, uniform phase randomization has diversity order $d^* = 1.5$ and the diversity order of the random antenna selection is 1. This is supported by the simulation results. However, for $N = 2$, the performance of the centralized scheme is much better than the decentralized schemes. We also plot the upper bounds to the average probability of error ($\bar{P}_e$, Eqn. 5.43), which are very close to the actual P_e curves. For $N = 3, 4$, the Gaussian, uniform phase, and spherical randomization schemes achieve diversity order 2 similar to the centralized scheme. However, the centralized scheme has a better coding gain. Nevertheless, one can observe that as N increases the performance of the distributed schemes approaches the centralized scheme not only in the diversity order but also in the coding gain.

In Fig. 5.3, we look at the performance of an orthogonal space-time code of order $L = 3$:

$$\boldsymbol{\mathcal{G}}(\mathbf{s}) = \begin{bmatrix} s_1 & 0 & s_2 & -s_3 \\ 0 & s_1 & s_3^* & s_2^* \\ -s_2^* & -s_3 & s_1^* & 0 \end{bmatrix}^t,$$

where $\mathbf{s} = [s_1 \ s_2 \ s_3]$ is the transmitted symbol vector. Note that the rate of this code is 3/4. In the centralized scheme, for $N \geq L$, the nodes are divided into L equal number groups, and if N is not a multiple of L, then at the remaining nodes,

ent randomization schemes; the normalization by $1/N$ is just to cancel the effect of power enhancement due to transmission of N nodes; hence we are able to distinguish the diversity order easily. Note that in general, normalization by $1/L$ should depend on the selected code $\boldsymbol{\mathcal{G}}$.

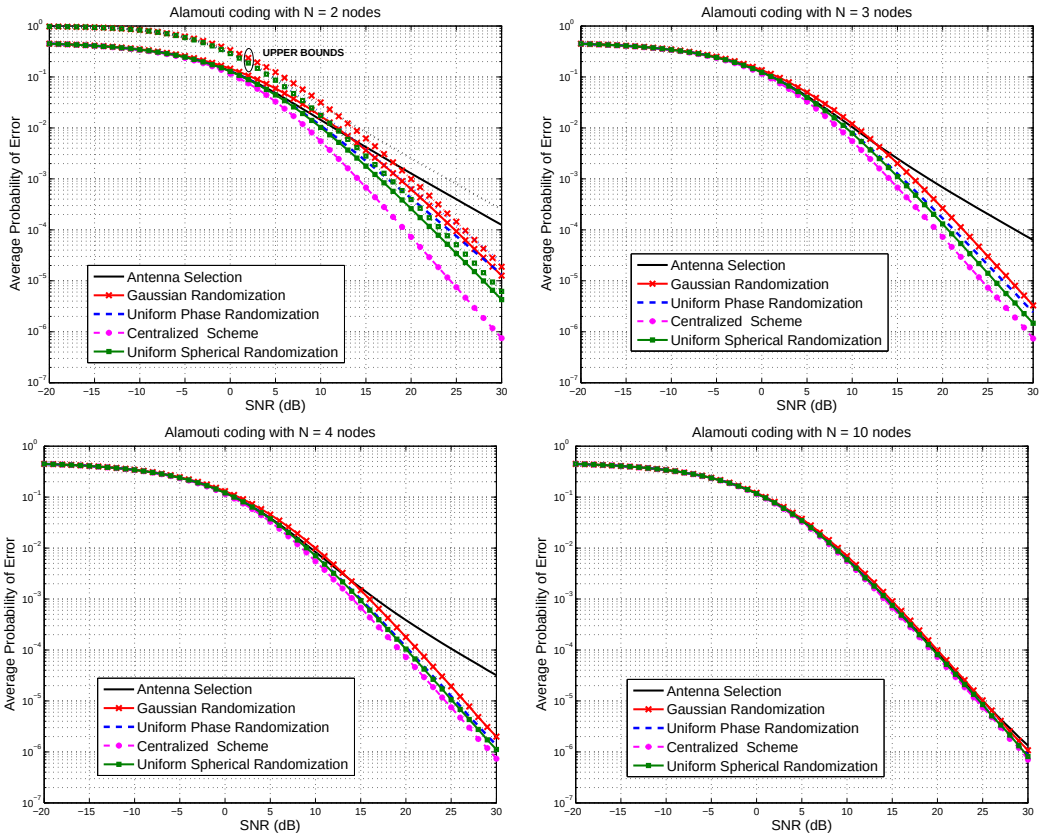

Figure 5.2: Average Probability of Error versus SNR (dB), L = 2: N=2 (upper-left); N=3 (upper-right); N=4 (lower-left); N=10 (lower-right). For $N = 2$, the upper bounds to the average probability of error are drawn for each of the schemes with dotted curves.

the power is distributed equally among the L antennas. If $N < L$, the nodes imitate N of the preselected antennas. Similar to the Alamouti coding, the transmission power of each node is $P_t = \frac{1}{N}$ for the centralized scheme, antenna selection, and spherical randomization schemes, and $P_t = \frac{1}{NL}$ for the Gaussian and uniform phase randomization schemes. In Fig. 5.3, for $N = 2$, the diversity order $d^* = 2$ is achieved by centralized, Gaussian randomization and uniform phase, on the other hand, the antenna selection scheme has the worst performance. For $N = 3$, the

centralized scheme has diversity order $d^* = 3$ and the performance is much better than the decentralized schemes. In addition, the performance of the randomization via continuous distributions (Gaussian, uniform phase and spherical) is considerably superior to the antennas selection scheme. For $N = 4$, the Gaussian, uniform phase, and spherical randomization schemes achieve diversity order 3. Similar to the Alamouti scheme, the performance of all the randomized schemes converges to the performance of centralized space-time coding as N increases.

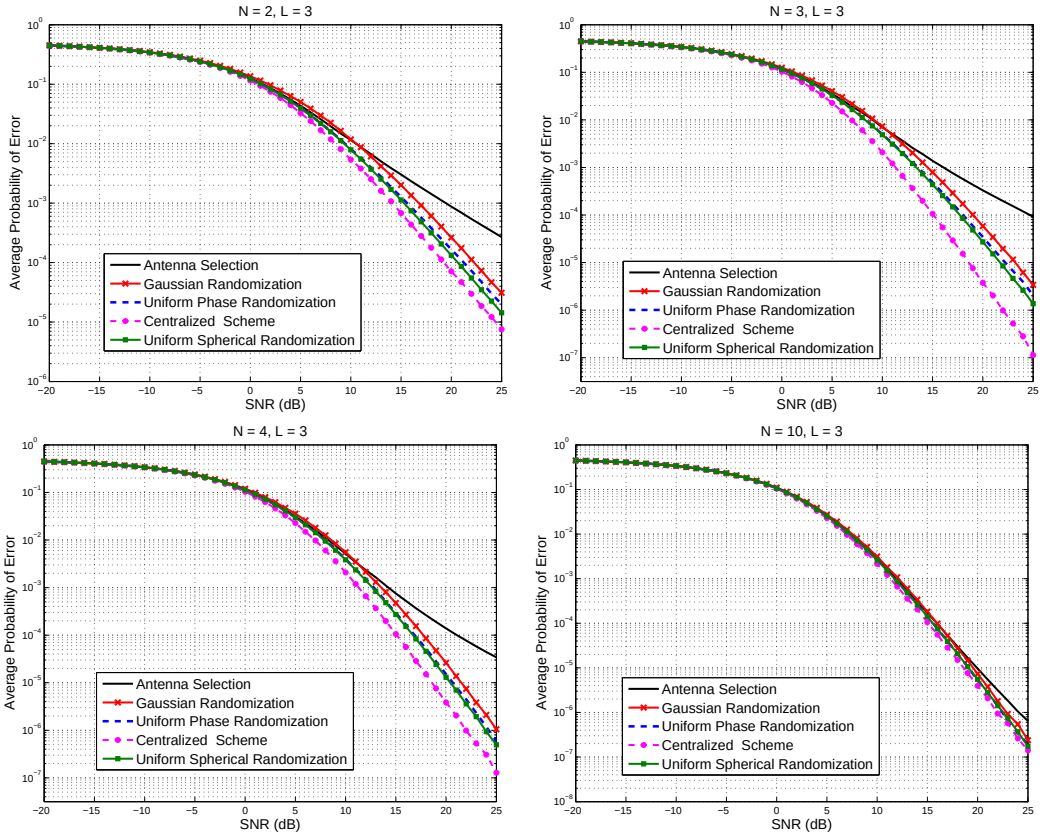

Figure 5.3: Average Probability of Error versus SNR (dB), L = 2: N=2 (upper-left); N=3 (upper-right); N=4 (lower-left); N=10 (lower-right).

In the next experiment, we present the multi-slope behavior of antenna selection scheme with the underlying deterministic Alamouti space-time code. When N is

odd and $L = 2$, the analytical expression of the average error probability simplifies to [36],

$$P_e = \frac{1}{2^N} \sum_{k=0}^{N} \binom{N}{k} \frac{g(k) - g(N-k)}{2k - N}, \tag{5.24}$$

where $g(x) = \frac{x}{2}\left(1 - \sqrt{\frac{x\ \mathrm{SNR}}{x\ \mathrm{SNR}+1}}\right)$. The numerical evaluation of (5.24) for $N = 3, 5, 7, 9, 11$ is displayed in addition to the asymptotic result (centralized scheme performance) in Fig. 5.4.

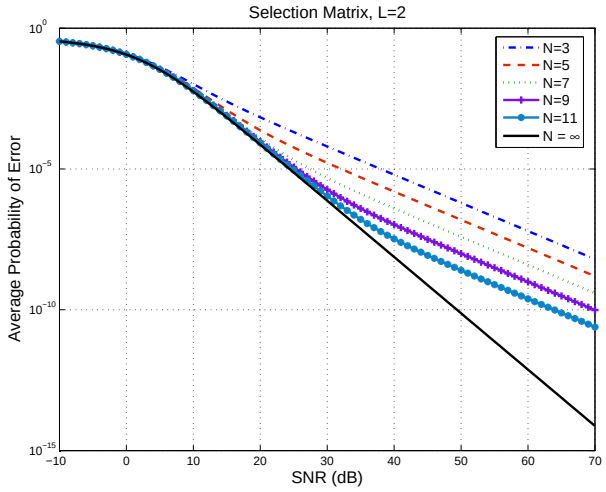

Figure 5.4: Average error probability behavior w.r.t. N

As expected, the P_e curves have a breaking point, which becomes more pronounced as N increases; beyond a certain SNR, they all have the same slope which corresponds to diversity order 1. For SNR values less than a threshold, the diversity order 2 is achieved. This can be clearly seen for $N = 11$ which has a breakpoint around SNR = 35 dB.

Appendix 5.A Proof of Lemma 11

The average probability of error (5.41) can be lower bounded as follows ($\forall \mathbf{s}_k, \mathbf{s}_i \in \mathcal{M}, i \neq k$):

$$\begin{aligned} P_e &\geq \frac{1}{|\mathcal{M}|} \Pr(\mathbf{s}_k \rightarrow \mathbf{s}_i) \\ &\geq \frac{1}{|\mathcal{M}|} \Pr(\mathbf{s}_k \rightarrow \mathbf{s}_i \mid ||\mathbf{Rh}||^2 \leq \frac{1}{\mathrm{SNR}}) \Pr\{||\mathbf{Rh}||^2 \leq \frac{1}{\mathrm{SNR}}\}. \end{aligned} \tag{5.25}$$

In the following, we will assume that $(\boldsymbol{\mathcal{G}}_k - \boldsymbol{\mathcal{G}}_i)$ is of rank L. Let $\lambda_{ik,max}$ be the maximum eigenvalue of the matrix $(\boldsymbol{\mathcal{G}}_k - \boldsymbol{\mathcal{G}}_i)^H(\boldsymbol{\mathcal{G}}_k - \boldsymbol{\mathcal{G}}_i)$. Define $\lambda_{max} \triangleq \max_{i,k} \lambda_{ik,max}$. Let $Q(\cdot) = \int_x^\infty \frac{1}{\sqrt{2}} e^{-u^2/2} du$. Since $Q(\cdot)$ is a decreasing function, the first part of (5.25) is lower bounded as

$$\begin{aligned} &\Pr(\mathbf{s}_k \rightarrow \mathbf{s}_i \mid ||\mathbf{Rh}||^2 \leq \frac{1}{\mathrm{SNR}}) \\ &\qquad = \mathbb{E}\left\{ Q\left(\sqrt{\mathrm{SNR}/2} ||(\boldsymbol{\mathcal{G}}_k - \boldsymbol{\mathcal{G}}_i)\boldsymbol{\mathcal{R}}\mathbf{h}|| \right) \mid ||\mathbf{Rh}||^2 \leq \frac{1}{\mathrm{SNR}} \right\} \\ &\qquad \geq \mathbb{E}\left\{ Q\left(\sqrt{\mathrm{SNR}} \sqrt{\lambda_{max}/2}\ ||\boldsymbol{\mathcal{R}}\mathbf{h}|| \right) \mid ||\mathbf{Rh}||^2 \leq \frac{1}{\mathrm{SNR}} \right\} \\ &\qquad \geq Q\left(\sqrt{\lambda_{max}/2} \right). \end{aligned} \tag{5.26}$$

Then the average probability of error can be lower bounded as

$$P_e \geq \frac{1}{M} Q\left(\sqrt{\lambda_{max}/2} \right) \Pr\{||\boldsymbol{\mathcal{R}}\mathbf{h}||^2 \leq \mathrm{SNR}^{-1}\}. \tag{5.27}$$

The pairwise error probability can be upper bounded as follows for some $\alpha \in (0,1)$:

$$\begin{aligned} \Pr(\mathbf{s}_k \rightarrow \mathbf{s}_i) &= \Pr(\mathbf{s}_k \rightarrow \mathbf{s}_i, ||\boldsymbol{\mathcal{R}}\mathbf{h}||^2 \leq \mathrm{SNR}^{-\alpha}) + \Pr(\mathbf{s}_k \rightarrow \mathbf{s}_i, ||\boldsymbol{\mathcal{R}}\mathbf{h}||^2 > \mathrm{SNR}^{-\alpha}) \\ &\leq \Pr\{||\boldsymbol{\mathcal{R}}\mathbf{h}||^2 \leq \mathrm{SNR}^{-\alpha}\} + \underbrace{\Pr\{\mathbf{s}_k \rightarrow \mathbf{s}_i \mid ||\boldsymbol{\mathcal{R}}\mathbf{h}||^2 > \mathrm{SNR}^{-\alpha}\}}_{\triangleq P_{ki}}. \end{aligned} \tag{5.28}$$

Next, we will upper bound the probability P_{ki}. For the system given by Eqn. 5.3, the conditional pairwise error probability is upper bounded as

$$\Pr\{\mathbf{s}_k \rightarrow \mathbf{s}_i | \boldsymbol{\mathcal{R}}, \mathbf{h}\} \leq \exp(-(\mathrm{SNR}/4)||(\boldsymbol{\mathcal{G}}_k - \boldsymbol{\mathcal{G}}_i)\boldsymbol{\mathcal{R}}\mathbf{h}||^2).$$

Then,

$$P_{ki} \leq \mathbb{E}\{\exp(-\frac{\mathrm{SNR}\lambda_{min,ik}||\boldsymbol{\mathcal{R}}\mathbf{h}||^2)}{4} \mid ||\boldsymbol{\mathcal{R}}\mathbf{h}||^2 > \mathrm{SNR}^{-\alpha}\}, \tag{5.29}$$

where $\lambda_{min,ik}$ is the minimum eigenvalue of $(\boldsymbol{\mathcal{G}}_k - \boldsymbol{\mathcal{G}}_i)^H(\boldsymbol{\mathcal{G}}_k - \boldsymbol{\mathcal{G}}_i)$. The right-hand side of (5.29) converges to zero as SNR$\rightarrow\infty$ since $\alpha \in (0,1)$. Using the union bound, the average probability of error can be upper bounded by the pairwise error probabilities assuming that all source messages $\mathbf{s}_i \in \mathcal{M}$ are equally likely:

$$P_e \leq (|\mathcal{M}| - 1) \max_{i,k} \Pr\{\mathbf{s}_k \rightarrow \mathbf{s}_i\}. \tag{5.30}$$

Using (5.28),(5.29) and (5.30)

$$\begin{aligned} d^* &= \lim_{\mathrm{SNR}\rightarrow\infty} \frac{-\log(P_e)}{\log \mathrm{SNR}} \\ &\geq \lim_{\mathrm{SNR}\rightarrow\infty} \frac{-\log \Pr\{||\boldsymbol{\mathcal{R}}\mathbf{h}||^2 \leq \mathrm{SNR}^{-\alpha}\}}{\log \mathrm{SNR}}. \end{aligned} \tag{5.31}$$

Since (5.31) is valid $\forall\alpha \in (0,1)$, if we take the limit as $\alpha\rightarrow 1$, it is still valid. The lemma follows from this fact and (5.27).

Appendix 5.B Proof of Theorem 14

The argument after the theorem proves Eqn. 5.7. In this appendix we will prove the opposite inequality. Using (5.6) we obtain that

$$\begin{aligned} \Pr\{||\boldsymbol{\mathcal{R}}\mathbf{h}||^2 \leq \frac{1}{\mathrm{SNR}}\} &= \Pr\{\sum_{i=1}^{\eta} \sigma_i^2 |\hat{h}_i|^2 \leq \frac{1}{\mathrm{SNR}}\} \\ &\leq \Pr\{\underbrace{\sigma_1^2|\hat{h}_1|^2 \leq \mathrm{SNR}^{-1}, \ldots, \sigma_\eta^2|\hat{h}_\eta|^2 \leq \mathrm{SNR}^{-1}}_{\triangleq S_\eta}\}. \end{aligned}$$

In the following, we will prove the theorem for $\eta = 2$. Generalization to $\eta > 2$ will be obvious. Let $\gamma \triangleq \mathrm{SNR}$. Let $S_2 = \{\sigma_1^2|\hat{h}_1|^2 \leq \gamma^{-1}, \sigma_2^2|\hat{h}_2|^2 \leq \gamma^{-1}\}$. Let

$P_2 = \Pr\{S_2\}$ and n be a fixed parameter. We can write P_2 as:

$$\begin{aligned} P_2 &= \sum_{i=1}^{n} \underbrace{\Pr\{\gamma^{(i-1)/n-1} \leq |\hat{h}_1|^2 \leq \gamma^{i/n-1}, S_2\}}_{P_{21i}} \\ &\qquad + \underbrace{\Pr\{|\hat{h}_1|^2 \leq \gamma^{-1}, S_2\}}_{P_{22}} + \underbrace{\Pr\{|\hat{h}_1|^2 \geq 1, S_2\}}_{P_{23}}. \end{aligned} \quad (5.32)$$

Using the definitions of P_{21i} and the event S_2, we obtain

$$\begin{aligned} P_{21i} &= \Pr\{\gamma^{(i-1)/n-1} \leq |\hat{h}_1|^2 \leq \gamma^{i/n-1}, \sigma_2^2|\hat{h}_2|^2 \leq \gamma^{-1}, \sigma_1^2 \leq \gamma^{(1-i)/n}\} \\ &\leq \Pr\{|\hat{h}_1|^2 \leq \gamma^{i/n-1}, \sigma_2^2|\hat{h}_2|^2 \leq \gamma^{-1}, \sigma_1^2 \leq \gamma^{(1-i)/n}\}. \end{aligned} \quad (5.33)$$

Similarly, using the definitions of P_{22}, P_{23} and the event S_2, we obtain

$$\begin{aligned} P_{22} &\leq \Pr\{|\hat{h}_1|^2 \leq \gamma^{-1}, \sigma_2^2|\hat{h}_2|^2 \leq \gamma^{-1}\} \\ &= \Pr\{|\hat{h}_1|^2 \leq \gamma^{-1}\} \Pr\{\sigma_2^2|\hat{h}_2|^2 \leq \gamma^{-1}\} \end{aligned} \quad (5.34)$$

and

$$\begin{aligned} P_{23} &= \Pr\{|\hat{h}_1|^2 \geq 1, \sigma_1^2 \leq \gamma^{-1}, \sigma_2^2|\hat{h}_2|^2 \leq \gamma^{-1}\} \\ &\leq \Pr\{\sigma_1^2 \leq \gamma^{-1}\}. \end{aligned} \quad (5.35)$$

Let $P_3 \triangleq \Pr\{\sigma_2^2|\hat{h}_2|^2 \leq \gamma^{-1}\}$. Using similar tricks, we can also upper bound P_3 as

$$\begin{aligned} P_3 &\leq \sum_{j=1}^{n} \Pr\{|\hat{h}_2|^2 \leq \gamma^{j/n-1}, \sigma_2^2 \leq \gamma^{(1-j)/n}\} \\ &\qquad + \Pr\{|\hat{h}_2|^2 \leq \gamma^{-1}\} + \Pr\{\sigma_2^2 \leq \gamma^{-1}\} \end{aligned} \quad (5.36)$$

Let A, B, C, D be four events. Then we know that,

$$\Pr\{A\} \leq \Pr\{B\} + \Pr\{C\} \quad \Rightarrow \quad \Pr\{A, D\} \leq \Pr\{B, D\} + \Pr\{C, D\}. \quad (5.37)$$

Using (5.37), we obtain

$$\begin{aligned} P_{21i} &\leq \sum_{j=1}^{n} \Pr\{|\hat{h}_1|^2 \leq \gamma^{i/n-1}, \sigma_1^2 \leq \gamma^{(1-i)/n}, |\hat{h}_2|^2 \leq \gamma^{j/n-1}, \sigma_2^2 \leq \gamma^{(1-j)/n}\} \\ &\qquad + \Pr\{|\hat{h}_1|^2 \leq \gamma^{i/n-1}, \sigma_1^2 \leq \gamma^{(1-i)/n}, |\hat{h}_2|^2 \leq \gamma^{-1}\} \\ &\qquad + \Pr\{|\hat{h}_1|^2 \leq \gamma^{i/n-1}, \sigma_1^2 \leq \gamma^{(1-i)/n}, \sigma_2^2 \leq \gamma^{-1}\} \end{aligned} \quad (5.38)$$

By using the independence among $\{\hat{h}_i\}$ and between $\hat{h}_i$ and σ_i^2, we obtain

$$\begin{aligned} P_{21i} \;\leq\; & \sum_{j=1}^{n} \Pr\{|\hat{h}_1|^2 \leq \gamma^{i/n-1}\} \Pr\{|\hat{h}_2|^2 \leq \gamma^{j/n-1}\} \Pr\{\sigma_1^2 \leq \gamma^{(1-i)/n}, \sigma_2^2 \leq \gamma^{(1-j)/n}\} \\ & + \Pr\{|\hat{h}_1|^2 \leq \gamma^{i/n-1}\} \Pr\{|\hat{h}_2|^2 \leq \gamma^{-1}\} \Pr\{\sigma_1^2 \leq \gamma^{(1-i)/n}\} \\ & + \Pr\{|\hat{h}_1|^2 \leq \gamma^{i/n-1}\} \Pr\{\sigma_1^2 \leq \gamma^{(1-i)/n}, \sigma_2^2 \leq \gamma^{-1}\} \end{aligned} \tag{5.39}$$

Also,

$$\begin{aligned} P_{22} \;\leq\; & \sum_{j=1}^{n} \Pr\{|\hat{h}_1|^2 \leq \gamma^{-1}\} \Pr\{|\hat{h}_2|^2 \leq \gamma^{j/n-1}, \sigma_2^2 \leq \gamma^{(1-j)/n}\} \\ & + \Pr\{|\hat{h}_1|^2 \leq \gamma^{-1}\} \Pr\{|\hat{h}_2|^2 \leq \gamma^{-1}\} \\ & + \Pr\{|\hat{h}_1|^2 \leq \gamma^{-1}\} \Pr\{\{\sigma_2^2 \leq \gamma^{-1}\} \end{aligned} \tag{5.40}$$

Compute the diversity order of P_2 from Eqn. (5.32) (for both sides). Let $\alpha_1 = (i-1)/n, \alpha_2 = (j-1)/n$. It is true that

$$\lim_{\gamma\to\infty} \frac{\log(\Pr\{A\} + \Pr\{B\})}{\log \gamma} = \min\left(\lim_{\gamma\to\infty} \frac{\log(\Pr\{A\})}{\log \gamma}, \lim_{\gamma\to\infty} \frac{\log(\Pr\{B\})}{\log \gamma} \right).$$

Using this fact, we can P_{22} (Eqn. 5.40),P_{23} (Eqn. 5.35); and hence the diversity order of P_2. Then, consider the asymptote as $n\to\infty$. By further analysis, we can see that

$$\lim_{\gamma\to\infty} \frac{-\log(P_2)}{\log \gamma} \geq \min_{\alpha_1,\alpha_2} \{2 - \alpha_1 - \alpha_2 + \Gamma(\alpha_1, \alpha_2).\}$$

By using similar tricks, we can find the diversity order of P_η as

$$d^* \geq \min_{\boldsymbol{\alpha}} \{\eta - \sum_{i=1}^{\eta} \alpha_i + \Gamma(\alpha_1, \ldots, \alpha_\eta), \}$$

where $0^- \leq \alpha_i \leq 1$.

Appendix 5.C Proof of Theorem 15

Using the union bound, the average probability of error can be upper bounded by the pairwise error probabilities assuming that all source messages $\mathbf{s}_i \in \mathcal{M}$ are

equally likely:

$$P_e \leq \frac{1}{|\mathcal{M}|} \sum_{\mathbf{s}_k \in \mathcal{M}} \sum_{\mathbf{s}_i \in \mathcal{M}, i \neq k} \Pr(\mathbf{s}_k \rightarrow \mathbf{s}_i), \tag{5.41}$$

where $\Pr(\mathbf{s}_k \rightarrow \mathbf{s}_k)$ denotes the probability that a transmitted message $\mathbf{s}_k$ is mistaken for another message $\mathbf{s}_i$. Let $\mathbf{s}_k \in \mathcal{M}$ denote the transmitted symbol. For the system given by Eqn. 5.3, the conditional pairwise error probability is upper bounded as

$$\Pr\{\mathbf{s}_k \rightarrow \mathbf{s}_i | \boldsymbol{\mathcal{R}}, \mathbf{h}\} \leq \exp\left(-\frac{\mathrm{SNR}||(\boldsymbol{\mathcal{G}}_k - \boldsymbol{\mathcal{G}}_i)\boldsymbol{\mathcal{R}}\mathbf{h}||^2}{4}\right). \tag{5.42}$$

Assuming $\mathbf{h} \sim \mathcal{N}_c(\mathbf{0}, \boldsymbol{\Sigma}_h)$ (for a given positive definite Hermitian $\boldsymbol{\Sigma}_h$); using (5.41) and (5.42), the average error probability of coherent detection (averaged over $\{\boldsymbol{\mathcal{R}}, \mathbf{h}\}$) is bounded as,

$$\bar{P}_e \triangleq \mathbb{E}_{\boldsymbol{\mathcal{R}}} \left\{ \frac{|\mathcal{M}| - 1}{\min_{(i,k)} \det(\mathbf{I} + \mathrm{SNR}/4 \ \mathbf{A}_{ik}\boldsymbol{\mathcal{R}}\boldsymbol{\Sigma}_h\boldsymbol{\mathcal{R}}^H)} \right\}. \tag{5.43}$$

where $\mathbf{A}_{ik} \triangleq (\boldsymbol{\mathcal{G}}_k - \boldsymbol{\mathcal{G}}_i)^H(\boldsymbol{\mathcal{G}}_k - \boldsymbol{\mathcal{G}}_i)$. Assume conditions C1 is satisfied, and $\boldsymbol{\mathcal{R}}\boldsymbol{\Sigma}_h\boldsymbol{\mathcal{R}}^H$ is of rank d with probability 1. We will upper bound $\bar{P}_e$ (5.43) for the proof. In the following, we assume that we are given a realization $\boldsymbol{\mathcal{R}}$ of rank $d \leq \min(L, N)$, then the final result follows by averaging over all such realizations.

Under the given conditions, we know that $\boldsymbol{\mathcal{R}}^H\mathbf{A}_{ik}\boldsymbol{\mathcal{R}}$ has non-negative real eigenvalues. Then,

$$\det(\mathbf{I} + \mathrm{SNR}/4 \ \mathbf{A}_{ik}\boldsymbol{\mathcal{R}}\boldsymbol{\Sigma}_h\boldsymbol{\mathcal{R}}^H) \geq |\mathrm{SNR}/4 \ \mathbf{A}_{ik}\boldsymbol{\mathcal{R}}\boldsymbol{\Sigma}_h\boldsymbol{\mathcal{R}}^H|_{d+}. \tag{5.44}$$

Let $\boldsymbol{\mathcal{R}}\boldsymbol{\Sigma}_h\boldsymbol{\mathcal{R}}^H = \mathbf{Q}\mathbf{S}\mathbf{Q}^H$ be the eigenvalue decomposition of $\boldsymbol{\mathcal{R}}\boldsymbol{\Sigma}_h\boldsymbol{\mathcal{R}}^H$ where $\mathbf{Q}\mathbf{Q}^H = \mathbf{Q}^H\mathbf{Q} = \mathbf{I}$ and $\mathbf{S} = \mathrm{diag}(\lambda_1, \ldots, \lambda_d, 0, \ldots, 0)$ such that $\lambda_1 \geq \lambda_2 \ldots \geq \lambda_d > 0$. Define $L \times d$ semi-unitary matrix $\mathbf{U}$ as $\mathbf{U} = (q_{ik})_{i=1\ldots L, k=1\ldots d}$ where $\mathbf{Q} = (q_{ik})_{i=1\ldots L, k=1\ldots L}$.

Notice that $\mathbf{U}^H\mathbf{U} = \mathbf{I}$. Let $\Lambda = \text{diag}(\lambda_1, \ldots, \lambda_d)$, then

$$\begin{aligned} |\text{SNR}/4\ \mathbf{A}_{ik}\boldsymbol{\mathcal{R}}\boldsymbol{\Sigma}_h\boldsymbol{\mathcal{R}}^H|_{d+} &= |\text{SNR}/4\ \mathbf{A}_{ik}\mathbf{U}\boldsymbol{\Lambda}\mathbf{U}^H|_{d+} \\ &= |\text{SNR}/4\ \mathbf{U}^H\mathbf{A}_{ik}\mathbf{U}\boldsymbol{\Lambda}|_{d+}. \end{aligned} \tag{5.45}$$

We know that $d \times d$ matrix $\mathbf{U}^H\mathbf{A}_{ik}\mathbf{U}$ is of rank d [69, Section 0.4.5(c), page 13]. Furthermore, the eigenvalues of $\mathbf{U}^H\mathbf{A}_{ik}\mathbf{U}$ and the eigenvalues of $\mathbf{A}_{ik}$ have an inequality relation [69, Section 4.3.16, page 190]. That is, let $\lambda_n(\mathbf{C})$ denote the n'th smallest eigenvalue of a matrix $\mathbf{C}$, then $\lambda_n(\mathbf{A}_{ik}) \leq \lambda_n(\mathbf{U}^H\mathbf{A}_{ik}\mathbf{U}),\ n = 1 \ldots d$. Using this result,

$$\begin{aligned} |\text{SNR}/4\ \mathbf{U}^H\mathbf{A}_{ik}\mathbf{U}\boldsymbol{\Lambda}|_{d+} &= (\text{SNR}/4)^d|\mathbf{U}^H\mathbf{A}_{ik}\mathbf{U}|_{d+}\ |\boldsymbol{\Lambda}|_{d+} \\ &\geq (\text{SNR}/4)^d|\mathbf{A}_{ik}|_{d+}\ |\boldsymbol{\Lambda}|_{d+} \\ &= (\text{SNR}/4)^d|\mathbf{A}_{ik}|_{d+}\ |\boldsymbol{\mathcal{R}}\boldsymbol{\Sigma}_h\boldsymbol{\mathcal{R}}^H|_{d+} \end{aligned} \tag{5.46}$$

We know that the positive eigenvalues of $\boldsymbol{\mathcal{R}}\boldsymbol{\Sigma}_h\boldsymbol{\mathcal{R}}^H$ are the same as the positive eigenvalues of $\boldsymbol{\mathcal{R}}^H\boldsymbol{\mathcal{R}}\boldsymbol{\Sigma}_h$. Using similar techniques to the derivation of (5.46), we obtain

$$|\boldsymbol{\mathcal{R}}\boldsymbol{\Sigma}_h\boldsymbol{\mathcal{R}}^H|_{d+} \geq |\boldsymbol{\mathcal{R}}\boldsymbol{\mathcal{R}}^H|_{d+}|\boldsymbol{\Sigma}_h|_{d+}. \tag{5.47}$$

Using (5.44), (5.45), (5.46) and (5.47), we obtain

$$\det(\mathbf{I} + \text{SNR}/4\ \mathbf{A}_{ik}\boldsymbol{\mathcal{R}}\boldsymbol{\Sigma}_h\boldsymbol{\mathcal{R}}^H) \geq (\text{SNR}/4)^d|\mathbf{A}_{ik}|_{d+}\ |\boldsymbol{\Sigma}_h|_{d+}\ |\boldsymbol{\mathcal{R}}\boldsymbol{\mathcal{R}}^H|_{d+}. \tag{5.48}$$

Then the proof follows by letting $d = \eta = \min(N, L)$.

Appendix 5.D Proof of Theorem 16

In the following we will first assume that $L \neq N$. Consider a complex random matrix $\boldsymbol{\mathcal{R}}(L \times N, L < N)$ with the probability density function $p(\boldsymbol{\mathcal{R}})$, then the

density of the matrix $\boldsymbol{\mathcal{R}}\boldsymbol{\mathcal{R}}^H$ is called the generalized Wishart density [70]. The following formula allows us to compute the probability density function of $\boldsymbol{\mathcal{R}}\boldsymbol{\mathcal{R}}^H$ from the probability density function of $\boldsymbol{\mathcal{R}}$. The formula is the generalization of Theorem 1.3.1 in [70] to the complex random matrices.

Let Γ be the set of unitary $N \times N$ matrices and μ the normalized Haar measure on it [4], $\boldsymbol{\mathcal{R}}$ a rectangular random $L \times N$ matrix ($L \leq N$) with the probability density $p(\boldsymbol{\mathcal{R}})$. Let Λ be the set of Hermitian positive definite matrices. Then the probability density function (pdf) of $\boldsymbol{\mathcal{R}}\boldsymbol{\mathcal{R}}^H$ is equal to

$$f_{\boldsymbol{\mathcal{R}}\boldsymbol{\mathcal{R}}^H}(\mathbf{Z}) = \frac{1}{c_{L,N}} \int_{\Gamma} p(\sqrt{\mathbf{Z}}\tilde{\mathbf{U}}) \det(\mathbf{Z})^{N-L} \mu(d\mathbf{U}), \tag{5.49}$$

where $L \times L$ matrix $\mathbf{Z} \in \Lambda$, $\mathbf{U} = (u_{ik}) \in \Gamma$, $\tilde{\mathbf{U}} = (u_{ik})_{i=1\ldots L,\ k=1\ldots N}$,

$$c_{L,N} = \pi^{L(L-1)/2 - LN} \prod_{k=1}^{L} (N-k)!. \tag{5.50}$$

By using the formula for the pdf of $\boldsymbol{\mathcal{R}}\boldsymbol{\mathcal{R}}^H$, we conclude that $\mathbb{E}\{\det(\boldsymbol{\mathcal{R}}\boldsymbol{\mathcal{R}}^H)^{-1}\} < \infty$ if and only if the integral

$$I \triangleq \int_{\Lambda} \int_{\Gamma} p(\sqrt{\mathbf{Z}}\tilde{\mathbf{U}}) \det(\mathbf{Z})^{N-L-1} \mu(d\mathbf{U}) d\mathbf{Z} \tag{5.51}$$

is finite. The notation $d\mathbf{Z}$ refers to the Lebesgue measure on the set of $L \times L$ dimensional matrices. The proof of the theorem follows from bounding the integral (5.51). Remember that the density $p(\cdot)$ is bounded by a constant, say c_1. Therefore, the righthand side of (5.51) is bounded as

$$\int_{\Lambda} \int_{\Gamma} p(\sqrt{\mathbf{Z}}\tilde{\mathbf{U}}) \det(\mathbf{Z})^{N-L-1} \mu(d\mathbf{U}) d\mathbf{Z} \leq c_1 \int_{\Lambda} \int_{\Gamma} \det(\mathbf{Z})^{N-L-1} \mu(d\mathbf{U}) d\mathbf{Z}. \tag{5.52}$$

[4] The μ can be viewed as the uniform distribution on Γ. More formally, a measure μ on Γ is called a Haar measure if $\mu(UA) = \mu(A)$ holds $\forall U \in \Gamma$ and measurable set $A \subset \Gamma$, where UA is the set of all matrices of the form Ua where $a \in A$. Haar measure μ on Γ is called normalized if $\mu(\Gamma) = 1$.

Since $\mu(\cdot)$ is the normalized Haar measure,

$$\int_{\Lambda}\int_{\Gamma} \det(\mathbf{Z})^{N-L-1}\mu(d\mathbf{U})d\mathbf{Z} = \int_{\Lambda} \det(\mathbf{Z})^{N-L-1}d\mathbf{Z}. \tag{5.53}$$

For a Hermitian positive definite matrix $\mathbf{Z}$, $\mathrm{Tr}(\mathbf{Z}) \leq P_T \Rightarrow \det(\mathbf{Z}) \leq P_T^L < \infty$. Furthermore, if $N \geq L+1$, the exponent of $\det(\mathbf{Z})$ in (5.53) is non-negative. Then using the constraint $\mathrm{Tr}(\mathbf{Z}) \leq P_T$ on the integration domain Λ,

$$\int_{\Lambda} \det(\mathbf{Z})^{N-L-1}d\mathbf{Z} = \int_{\mathrm{Tr}(\mathbf{Z})\leq P_T} \det(\mathbf{Z})^{N-L-1}d\mathbf{Z} \leq P_T^{L(N-L-1)} \int_{\mathrm{Tr}(\mathbf{Z})\leq P_T} d\mathbf{Z}. \tag{5.54}$$

Note that for a Hermitian positive-definite matrix $\mathbf{Z}$, $\mathrm{Tr}(\mathbf{Z}) \leq P_T \Rightarrow ||\mathbf{Z}||_F \leq P_T$, where $||\mathbf{Z}||_F$ is the Frobenious norm of $\mathbf{Z}$. Then,

$$\int_{\mathrm{Tr}(\mathbf{Z})\leq P_T} d\mathbf{Z} \leq \int_{||\mathbf{Z}||_F\leq P_T} d\mathbf{Z} = \frac{\pi^{N^2/2}P_T^{N^2}}{\Gamma(N^2/2+1)}, \tag{5.55}$$

where $\Gamma(z) = \int_0^{\infty} t^{z-1}e^{-t}dt$. The final integration amounts to finding a volume of N^2 dimensional sphere. By combining (5.52), (5.53), (5.54) and (5.55), we obtain

$$I \leq c_1 P_T^{L(N-L-1)} \frac{\pi^{N^2/2}P_T^{N^2}}{\Gamma(N^2/2+1)} < \infty.$$

Hence, $\mathbb{E}\{\det(\boldsymbol{\mathcal{R}}^H\boldsymbol{\mathcal{R}})^{-1}\} < \infty$. Similar to the above derivation, we can easily show that If $L \geq N+1$, then $\mathbb{E}\{\det(\boldsymbol{\mathcal{R}}^H\boldsymbol{\mathcal{R}})^{-1}\} < \infty$. Hence, the result 5.14 follows.

For $N = L$, we expect that $N-1 \leq d^* \leq N$. We know that $d^* \leq N$ (a conclusion that can be drawn from Theorem 14). The fact that $d^* > N-1$ for $N = L$ can be proved as follows: Consider the randomized code obtained using an $L' \times N'$ dimensional randomization matrix $\boldsymbol{\mathcal{R}}$ such that $L' = N$ and $N' = N-1$. We know that such a system has diversity order $N-1$ (using Eqn. 5.14). Adding 1 more node to a system would never decrease the diversity order; hence the diversity order of the randomized space-time code with $N \times N$ dimensional randomization matrix is at least $N-1$.

Appendix 5.E Proof of Theorem 17

The effective channel vector $\tilde{\mathbf{h}} = \boldsymbol{\mathcal{R}}\mathbf{h}$ is conditionally Gaussian with zero mean and covariance $\boldsymbol{\mathcal{R}}\boldsymbol{\Sigma}_h\boldsymbol{\mathcal{R}}^H$. In the following, we provide the statistics of $\tilde{\mathbf{h}}$ as $N\to\infty$. Denote (i,j)'th element of $\boldsymbol{\mathcal{R}}$ by r_{ij}. Define $\mathbf{Z}_k = [h_k r_{1k}, h_k r_{2k}, \ldots, h_k r_{Lk}]^t$ for $k = 1 \ldots N$. We can rewrite $\tilde{\mathbf{h}}$ in terms of the random vectors $\mathbf{Z}_k$, i.e. $\tilde{\mathbf{h}} = [\tilde{h}_1 \tilde{h}_2 \ldots \tilde{h}_L]^t = \sum_{k=1}^{N} \mathbf{Z}_k$.

In the following, first we derive the mean and variance of $\mathbf{Z}_k$ and then by using the multivariate central limit theorem [71, pp. 20] as $N\to\infty$, we show that $\frac{\mathbf{h}}{\sqrt{N}}$ converges in distribution to a Gaussian random variable. We know that $\boldsymbol{\mathcal{R}}$ is a random matrix independent of $\mathbf{h}$, then the mean of $\mathbf{Z}_k$ is $\mathbb{E}\{\mathbf{Z}_k\} = \mathbf{0}$, and the covariance matrix is $\boldsymbol{\Sigma}_k = \mathbb{E}\{\mathbf{Z}_k\mathbf{Z}_k^H\} = \sigma_k^2\boldsymbol{\Sigma}$. Since $\mathbf{Z}_k$'s are independent, using the multivariate central limit theorem, we can conclude that

$$\frac{\tilde{\mathbf{h}}}{\sqrt{N}} = \frac{1}{\sqrt{N}} \sum_{k=1}^{N} \mathbf{Z}_k \to^d \mathcal{N}(\mathbf{0}, \tilde{\boldsymbol{\Sigma}}) \text{ as } N\to\infty, \tag{5.56}$$

where $\tilde{\boldsymbol{\Sigma}} = \boldsymbol{\Sigma} \lim_{N\to}(\sum_{i=1}^{N} \sigma_{hi}^2/N)$. Now we can prove the theorem using (5.56). We know that

$$\begin{aligned} \frac{1}{|\mathcal{M}|}\mathbb{E}\left\{Q\left(\frac{||(\boldsymbol{\mathcal{G}}_k - \boldsymbol{\mathcal{G}}_i)\boldsymbol{\mathcal{R}}\mathbf{h}||}{\sqrt{N}\sqrt{2N_0}}\right)\right\} &\leq P_e^N(\text{SNR}) \\ &\leq (|\mathcal{M}|-1)\mathbb{E}\left\{Q\left(\frac{||(\boldsymbol{\mathcal{G}}_k - \boldsymbol{\mathcal{G}}_i)\boldsymbol{\mathcal{R}}\mathbf{h}||}{\sqrt{N}\sqrt{2N_0}}\right)\right\}. \end{aligned} \tag{5.57}$$

Eqn. 5.56 tells that as $N\to\infty$, $\frac{\boldsymbol{\mathcal{R}}\mathbf{h}}{\sqrt{N}} \xrightarrow{d} \mathcal{N}(\mathbf{0}, \tilde{\boldsymbol{\Sigma}})$. The *continuous mapping theorem* [53] states that for any continuous and bounded function $h(\cdot)$ and random variables X_n, X, if $X_n \xrightarrow{d} X$, then $\mathbb{E}\{h(X_n)\}\to\mathbb{E}\{h(X)\}$. By taking the limit in (5.57), we can deduce that as $N\to\infty$, the randomized space-time code $\boldsymbol{\mathcal{G}}(\mathbf{s})\boldsymbol{\mathcal{R}}$ is equivalent to a deterministic space-time code $\boldsymbol{\mathcal{G}}(\mathbf{s})\tilde{\boldsymbol{\Sigma}}^{1/2}$ and hence, it provides diversity order L when both $\boldsymbol{\Sigma}$ and $\boldsymbol{\mathcal{G}}$ are full-rank L.

Chapter 6

Conclusion

In this dissertation, we proposed distributed schemes for cooperative networks and utilized continuum approximation of random networks in order to analyze the behavior of cooperative networks. To the best of our knowledge, continuum analysis of cooperative *multi-hop* networks has not been done previously for any cooperative protocol.

In Chapter 2, we analyzed the behavior of a wireless network with cooperative transmissions for a single source-destination pair. The analysis is based on the idea of continuum approximation, which models networks with high node density. We believe that the techniques used in this thesis can be useful in the analysis of other cooperative protocols. The accuracy of the continuum approximation is verified by simulations. The interesting conclusion drawn from the analysis is that there exists a phase transition in the propagation of the message, which is a function of the node powers and the reception threshold. In Chapter 3, we analyzed the behavior of a wireless network with cooperative broadcasting. Interestingly, similar to the point-to-point scenario, there exists a phase transition in the propagation of the message.

In Chapter 4, we studied the power efficiency of cooperative broadcast. The optimal power allocation problem for cooperative broadcast is of high complexity, and it is hard to draw conclusions for general network topologies and channel models. Similarly, in this chapter, we approximated dense networks with a continuum of nodes which allowed us to determine the behavior of optimal power density and total power expenditure for dense large-scale networks. We also proposed practical, energy efficient and distributed schemes that achieve almost optimal performance for large-scale networks. We compared the total power expenditure of distributed cooperative protocols with multi-hop non-cooperative transmission.

In Chapter 5, we proposed a decentralized space-time coding for distributed networks. Our scheme is based on independent randomization done at each node. We analyzed its performance and proposed different designs that achieve the diversity order ($\min(N, L)$) when the number of nodes N is different than the number of antennas L in the underlying space-time code. For $N = L$, we presented examples where the diversity order is fractional. In addition, we showed that the randomized schemes achieve the performance of a centralized space-time code in terms of coding gain as the number of nodes increases.

Bibliography

[1] A. Sendonaris, E. Erkip, and B. Aazhang, "User cooperation diversity. part 1: System description; part 2: Implementation aspects and performance analysis," *IEEE Trans. Commun.*, vol. 51, pp. 1927 – 1948, Nov. 2003.

[2] A. Sendonaris, E. Erkip, and B. Aazhang, "Increasing uplink capacity via user cooperation diversity," in *Proc. of IEEE Inter. Symp. on Inform. Theory (ISIT)*, p. 156, 16-21 Aug. 1998.

[3] J. N. Laneman, D. N. C. Tse, , and G. W. Wornell, "Cooperative diversity in wireless networks: Efficient protocols and outage behavior," *IEEE Trans. Inform. Theory*, vol. 50, pp. 3062 – 3080, Dec. 2004.

[4] T. M. Cover and A. E. Gamal, "Capacity theorems for the relay channel," *IEEE Trans. on Information Theory*, vol. 25, Sep. 1979.

[5] G. Kramer, M. Gastpar, and P. Gupta, "Cooperative strategies and capacity theorems for relay networks," *IEEE Trans. Inform. Theory*, vol. 51, pp. 3037 – 3063, Sep. 2005.

[6] A. Stefanov and E. Erkip, "Cooperative coding for wireless networks," *IEEE Transactions on Communications*, vol. 52, Sep. 2004.

[7] A. Nosratinia, T. E. Hunter, and A. Hedayat, "Cooperative communication in wireless networks," *2004*, vol. 42, pp. 74–80, Oct.

[8] P. Gupta and P. R. Kumar, "The capacity of wireless networks," *IEEE Trans. Inform. Theory*, vol. 46, pp. 388–404, march 2000.

[9] M. Gastpar and M. Vetterli, "On the capacity of wireless networks: The relay case," in *Proc. of Twenty-First Annual Joint Conf. of the IEEE Computer and Commun. Societies (INFOCOM)*, vol. 3, p. 1577=1586, 23-27 June 2002.

[10] J. N. Laneman and G. W. Wornell, "Distributed space-time-coded protocols for exploiting cooperative diversity in wireless networks," *IEEE Trans. Inform. Theory*, vol. 49, pp. 2415–2525, Oct. 2003.

[11] S. Shakkottai, R. Srikant, and N. Shroff, "Unreliable sensor grids: Coverage, connectivity and diameter," *Twenty-Second Annual Joint Conference of the IEEE Computer and Communications Societies (INFOCOM)*, vol. 2, pp. 1073–1083, 30 March - 3 April 2003.

[12] P. Jacquet, "Geometry of information propagation in massively dense ad hoc networks," in *ACM MobiHoc'04*, pp. 157–162, May 2004.

[13] J. E. Wieselthier, G. D. Nguyen, and A. Ephremides, "Energy-efficient broadcast and multicast trees in wireless networks," *Mob. Netw. Appl.*, vol. 7, no. 6, pp. 481–492, 2002.

[14] B. Williams and T. Camp, "Comparison of broadcasting techniques for mobile ad hoc networks," in *ACM Proc. on MOBIHOC*, June 2002.

[15] J. Boyer, D. D. Falconer, and H. Yanikomeroglu, "Multihop diversity in wireless relaying channels," *IEEE Trans. Commun.*, vol. 52, pp. 1820 – 1830, Oct. 2004.

[16] I. Maric and R. D. Yates, "Cooperative multihop broadcast for wireless networks," *IEEE J. Select. Areas Commun.*, vol. 22, pp. 1080 – 1088, Aug. 2004.

[17] A. Scaglione and Y.-W.Hong, "Opportunistic large arrays:cooperative transmission in wireless multihop adhoc networks to reach far distances," *IEEE Trans. Signal Processing*, vol. 51, pp. 2082 – 2092, Aug. 2003.

[18] P. Viswanath, D. Tse, , and R. Laroia, "Opportunistic beamforming using dump antennas," *IEEE Trans. Inform. Theory*, vol. 48, June 2002.

[19] Y.-W. Hong and A. Scaglione, "Energy-efficient broadcasting with cooperative transmission in wireless sensor networks," *IEEE Trans. on Wireless Comm.*, to appear.

[20] Y.-W. Hong and A. Scaglione, "Energy-efficient broadcasting with cooperative transmission in wireless sensory ad hoc networks," in *Proc. of Allerton Conf. on Commun., Contr. and Comput. (ALLERTON)*, Oct. 2003.

[21] A. Khandani, J. Abounadi, E. Modiano, and L. Zhang, "Cooperative routing in wireless networks," in *Proc. of Allerton Conf. on Commun., Contr. and Comput. (ALLERTON)*, 2003.

[22] S. Cui, *Cross-layer Optimization in Energy-constrained Networks*. PhD thesis, Stanford University, Stanford, CA, June 2005.

[23] X. Li, M. Chen, and W. Liu, "Application of stbc-encoded cooperative transmissions in wireless sensor networks," *IEEE Signal Processing Letters*, vol. 12, pp. 134 – 137, Feb. 2005.

[24] B. Sirkeci-Mergen, A. Scaglione, and G. Mergen, "Asymptotic analysis of multi-stage cooperative broadcast in wireless networks," *Joint special issue of the IEEE Transactions on Information Theory and IEEE/ACM Trans. On Networking*, June 2006.

[25] V. Tarokh, N. Seshadri, and A. Calderbank, "Space-time codes for high data rate wireless communication: performance criterion and code construction," *IEEE Trans. Inform. Theory*, vol. 44, pp. 744–765, March 1998.

[26] P. A. Anghel, G. Leus, and M. Kaveh, "On the performance of distributed space-time coding systems with one and two non-regenerative relays," *IEEE Transactions on Wireless Communications*, vol. 5, pp. 682– 692, March 2006.

[27] S. Barbarossa and G. Scutari, "Distributed space-time coding for multihop networks," in *Proc. of IEEE Proc. of IEEE International Conference on Communications*, vol. 2, pp. 916 – 920, 20-24 June 2004.

[28] S. Barbarossa and G. Scutari, "Distributed space-time coding strategies for wideband multihop networks: regenerative vs. non-regenerative relays," in *Proc. of IEEE Inter. Conf. on Acoustics, Speech, and Signal Process. (ICASSP)*, vol. 4, pp. 501–504, 17-21 May 2004.

[29] J. Mietzner, R. Thobaben, and P. A. Hoeher, "Analysis of the expected error performance of cooperative wireless networks employing distributed space-time codes," in *Proc. IEEE Global Telecomm. Conf. (Globecom 2004)*, vol. 5, pp. 2854 – 2858, 29 Nov. - 3 Dec. 2004.

[30] Y. Hua, Y. Mei, and Y. Chang, "Parallel wireless mobile relays with space-time modulations," in *Statistical Signal Processing, 2003 IEEE Workshop*, pp. 375 – 378, 28 Sept.- 1 Oct. 2003.

[31] Y. Chang and Y. Hua, "Application of space-time linear block codes to parallel wireless relays in mobile ad hoc networks," in *Signals, Systems and Computers, 2003 The Thrity-Seventh Asilomar Conference*, vol. 1, pp. 1002 – 1006, Nov. 2003.

[32] T. Wang, Y.Yao, and G. B. Giannakis, "Non-coherent distributed space-time processing for multiuser cooperative transmissions," *to appear in IEEE Transactions on Wireless Communications*, 2006.

[33] T. Ho, R. Koetter, M. Médard, D. R. Karger, and M. Effros, "The benefits of coding over routing in a randomized setting," in *Proc. of IEEE Inter. Symp. on Inform. Theory (ISIT)*, p. 442, 29 June-4 July 2003.

[34] P. A. Chou, Y. Wu, and K. Jain, "Practical network coding," in *41st Allerton Conf. Communication, Control and Computing*, Oct. 2003.

[35] D. Tse and P. Viswanath, *Fundamentals of Wireless Communication*. Cambridge University Press, 2005.

[36] B. Sirkeci-Mergen and A. Scaglione, "Randomized distributed space-time coding for cooperative communication in self-organized networks," in *Proc. of IEEE Workshop on Signal Process. Advances in Wireless Commun. (SPAWC)*, pp. 500–504, June 2005.

[37] R. U. Nabar, F. W. Kneubuhler, and H. Bölcskei, "Performance limits of amplify-and-forward based fading relay channel," in *Proc. of IEEE Inter. Conf. on Acoustics, Speech, and Signal Process. (ICASSP)*, vol. 4, pp. 565–568, 17-21 May 2004.

[38] P. A. Anghel and M. Kaveh, "Exact symbol error probability of a cooperative network in a rayleigh-fading environment," *IEEE Trans. Wireless Commun.*, vol. 3, Sep. 2004.

[39] J. Boyer, D. D. Falconer, and H. Yanikomeroglu, "A theoretical characterization of the multihop wireless communications channel with diversity," in *Global Telecommunications Conference*, vol. 2, pp. 841 – 845, 2001.

[40] A. Ribeiro, X. Cai, and G. B. Giannakis, "Symbol error probabilities for general cooperative links," *IEEE Trans. on Wireless Comm.*, vol. 4, pp. 1264 – 1273, May 2005.

[41] A. Khisti, U. Erez, and G. Wornell, "A capacity theorem for cooperative multicasting in large wireless networks," in *Proc. of Allerton Conf. on Commun., Contr. and Comput. (ALLERTON)*, 2004.

[42] O. Dousse and P. Thiran, "Connectivity vs. capacity in dense ad hoc networks," in *Proc. of 23rd Annual Joint Conf. of the IEEE Computer and Commun. Societies (Infocom)*, vol. 1, 7-11 March 2004.

[43] Y.-C. Cheng and T. Robertazzi, "Critical connectivity phenomena in multihop radio models," *IEEE Trans. on Communications*, vol. 37, July 1989.

[44] S. Wei, D. Goeckel, and M. Valenti, "Asynchronous cooperative diversity," in *Proc. of 2004 Conference on Information Sciences and Systems (CISS)*, March 2004.

[45] H. E. Gamal and D. Aktas, "Distributed space-time filtering for cooperative wireless networks," in *Proc. IEEE Global Telecomm. Conf. (Globecom 2003)*, vol. 4, pp. 1826 – 1830, 1-5 Dec. 2003.

[46] S. Yiu, R. Schober, and L. Lampe, "Distributed space-time block coding," *accepted for publication in IEEE Trans. on Communication*, 2006.

[47] Y. Hua, Y. Mei, and Y. Chang, "Wireless-antennas making wireless communications perform like wireline communications," in *IEEE Topical Conference on Wireless Communication Technology*, pp. 47–73, 15-17 Oct. 2003.

[48] Y. Jing and B. Hassibi, "Wireless networks, diversity and space-time codes," in *Proc. of IEEE Information Theory Workshop*, pp. 463 – 468, 24-29 Oct. 2004.

[49] Y. Jing and B. Hassibi, "Distributed space-time coding in wireless relay networks-part 1: basic diversity results, - part 2:tighter upper bounds and a more general case," *submitted to IEEE Trans. On Wireless Communications*, July 2004.

[50] T. S. Rappaport, *Wireless Communications Principles and Practice*. second edition ed.

[51] A. Jovicic, P. Viswanath, and S. R. Kulkarni, "Upper bounds to transport capacity of wireless networks," *IEEE Transactions on Information Theory*, vol. 50, no. 11, pp. 2555–2565, 2004.

[52] R. L. Devaney, *An Introduction to Chaotic Dynamical Systems*. Addison-Wesley Publishing Company, Inc., 2nd ed., 1989.

[53] P. Billingsley, *Probability and Measure*. John Wiley & Sons, Inc., 3 ed., 1995.

[54] B. Sirkeci-Mergen and A. Scaglione, "Message propagation in a cooperative network with asynchronous receptions," in *Proc. of IEEE Inter. Conf. on Acoustics, Speech, and Signal Process. (ICASSP)*, vol. 3, pp. 377–380, 18-23 March 2005.

[55] V. N. Vapnik, *Statistical Learning Theory*. 1998.

[56] V. N. Vapnik and A. Y. Chervonenkis, "On the uniform convergence of relative frequencies of events to their probabilities," *Theory Probab. Appl.*, vol. 16, pp. 264–280, 1971.

[57] J. W. Brown and R. V. Churchill, *Complex Variables and Applications*. McGraw-Hill International Editions, 6 ed., 1996.

[58] J. G. Proakis, *Digital Communications*. McGraw Hill Higher Education, 2000.

[59] B. Sirkeci-Mergen and A. Scaglione, "Randomized space-time coding for distributed cooperative communication," in *to appear in Proc. of IEEE Proc. of IEEE Inter. Conf. on Comm. (ICC)*, 2006.

[60] W. V. Lovitt, *Linear Integral Equations*. Dover Phoenix Editions, 2005.

[61] P. Linz, *Analytical and Numerical Methods for Volterra Equations*. Siam Studies in Applied Mathematics, 1985.

[62] S. Verdu, "Spectral efficiency in the wideband regime," *IEEE Trans. on Inform. Theory*, vol. 48, Jun. 2002.

[63] B. Sirkeci-Mergen and A. Scaglione, "On the power efficiency of cooperative broadcast in dense wireless networks," *submitted to IEEE Journal on Selected Areas in Communications (JSAC): Special issue on Cooperative Communications and Networking.*

[64] A. Scaglione, B. Sirkeci-Mergen, S. Geirhofer, and L. Tong, "Randomized distributed multi-antenna systems in multi-path channels," in *submitted to 14th European Signal Processing Conference - EUSIPCO 2006*, Sep. 2006.

[65] A. M. Tulino and S. Verdú, *Random Matrix Theory and Wireless Communications.* now Publishers Inc., 2004.

[66] A. Edelman, *Eigenvalues and Condition Numbers of Random Matrices.* PhD thesis, Massachusetts Institute of Technology (MIT), May 1989.

[67] G. Marsaglia, "Choosing a point from the surface of a sphere," *Ann. Math. Stat.*, vol. 43, 1972.

[68] M. E. Muller, "A note on a method for generating points uniformly on n-dimensional spheres," *Comm. Assoc. Comp. Mach.*, vol. 2, 1959.

[69] R. A. Horn and C. R. Johnson, *Matrix Analysis.* Cambridge University Press, 1985.

[70] V. Girko, *Theory of Random Determinants.* Kluwer Academic Publishers, 1990.

[71] A. W. van der Vaart, *Asymptotic statistics.* Cambridge University Press, 1998.